January 2005 • NREL/SR-500-36346

Subcontractor Report

Design and Experimental Results for the S825 Airfoil

Period of Performance: 1998 – 1999

D.M. Somers
Airfoils, Inc.
State College, Pennsylvania

National Renewable Energy Laboratory
1617 Cole Boulevard, Golden, Colorado 80401-3393
303-275-3000 • www.nrel.gov

Operated for the U.S. Department of Energy
Office of Energy Efficiency and Renewable Energy
by Midwest Research Institute • Battelle

Contract No. DE-AC36-99-GO10337

January 2005 • NREL/SR-500-36346

Design and Experimental Results for the S825 Airfoil

Period of Performance: 1998 – 1999

D.M. Somers
Airfoils, Inc.
State College, Pennsylvania

NREL Technical Monitor: Jim Tangler

Prepared under Subcontract No. AAF-4-14289-01

National Renewable Energy Laboratory
1617 Cole Boulevard, Golden, Colorado 80401-3393
303-275-3000 • www.nrel.gov

Operated for the U.S. Department of Energy
Office of Energy Efficiency and Renewable Energy
by Midwest Research Institute • Battelle

Contract No. DE-AC36-99-GO10337

Table of Contents

Abstract 1
Introduction 1
Symbols 2
Airfoil Design 4
    Objectives and Constraints 4
    Philosophy 5
    Execution 7
Experimental Procedure 8
    Wind Tunnel 8
    Model 8
    Wake-Survey Probe 8
    Instrumentation 9
    Methods 9
    Tests 9
Discussion of Results 10
    Experimental Results 10
    Comparison of Theoretical and Experimental Results 12
Concluding Remarks 13
Acknowledgments 13
References 14

List of Tables

Table I. Airfoil Design Specifications 17
Table II. S825 Airfoil Coordinates 18
Table III. Model Orifice Locations 19-20
Table IV. Roughness Location and Size 21

List of Figures

Figure 1: S825 airfoil shape 22
Figure 2: NASA Langley Low-Turbulence Pressure Tunnel 23
Figure 3: Sketch of model and wake-survey probe mounted in test section 24
Figure 4: Wake-survey probe 25
Figure 5: Pressure distributions for R = 2 x 10^6 with transition free ..... 26 – 59
Figure 6: Section characteristics with transition free, fixed, and rough ..... 60 – 64
Figure 7: Effects of Reynolds number on section characteristics ..... 65 – 67
Figure 8: Variation of maximum lift coefficient with Reynolds number 68

Figure 9: Variation of change in maximum lift coefficient due to leading edge-roughness with Reynolds number 69
Figure 10: Variation of profile-drag coefficient at $c_l = 0.4$ with Reynolds number 70
Figure 11: Comparison of theoretical and experimental pressure distributions ..... 71 – 73
Figure 12: Comparison of theoretical and experimental section characteristics with transition free ..... 74 – 78
Figure 13: Comparison of theoretical and experimental section characteristics with transition fixed ..... 79 – 83

ABSTRACT

A 17-percent-thick, natural-laminar-flow airfoil, the S825, for the 75-percent blade radial station of 20- to 40-meter, variable-speed and variable-pitch (toward feather), horizontal-axis wind turbines has been designed and analyzed theoretically and verified experimentally in the NASA Langley Low-Turbulence Pressure Tunnel. The two primary objectives of high maximum lift, relatively insensitive to roughness, and low profile drag have been achieved. The airfoil exhibits a rapid, trailing-edge stall, which does not meet the design goal of a docile stall. The constraints on the pitching moment and the airfoil thickness have been satisfied. Comparisons of the theoretical and experimental results generally show good agreement.

INTRODUCTION

The majority of the airfoils in use on horizontal-axis wind turbines today were originally developed for aircraft. The design requirements for these airfoils, primarily National Advisory Committee for Aeronautics (NACA) and National Aeronautics and Space Administration (NASA) airfoils (refs. 1–6), are significantly different from those for wind-turbine airfoils (ref. 7). Accordingly, several families of airfoils have been designed specifically for horizontal-axis wind-turbine applications, as shown in the following table.

Diameter	Type	Thickness Category	Airfoil			Reference
			Primary	Tip	Root	
2–10 m	Variable speed Variable pitch	Thick	—	S822	S823	13
10–20 m	Variable speed Variable pitch	Thin	S801	S802 S803	S804	8
	Stall regulated	Thin	S805 S805A	S806 S806A	S807 S808	8
	Stall regulated	Thick	S819	S820	S821	12
20–30 m	Stall regulated	Thick	S809	S810	S811	9
	Stall regulated	Thick	S812	S813	S814 S815	9 and 10
20–40 m	Variable speed Variable pitch	—	S825	S826	S814 S815	10 and 14
30–50 m	Stall regulated	Thick	S816	S817	S818	11
40–50 m	Stall regulated	Thick	S827	S828	S818	11 and 15

An overview of all these airfoil families is given in reference 16.

The airfoil designed under the present study is intended for the primary (75-percent) blade radial station of 20- to 40-meter, variable-speed and variable-pitch (toward feather), horizontal-axis wind turbines. To complement the design effort (ref. 14), an investigation was conducted in the NASA Langley Low-Turbulence Pressure Tunnel (LTPT) (refs. 17 and 18) to obtain the basic, low-speed, two-dimensional aerodynamic characteristics of the airfoil. The results have been compared with predictions from the method of references 19 and 20.

The specific tasks performed under this study are described in National Renewable Energy Laboratory (NREL) Subcontract Numbers AAF-4-14289-01 and AAM-8-17232-01. The design specifications for the airfoil are outlined in the first subcontract's Statement of Work. These specifications were later refined during discussions with James L. Tangler of NREL.

SYMBOLS

Values are given in both SI and U.S. Customary Units. Measurements and calculations were made in U.S. Customary Units.

C_p pressure coefficient, $\frac{p_l - p_\infty}{q_\infty}$

c airfoil chord, mm (in.)

c_c section chord-force coefficient, $\oint C_p \, d\left(\frac{z}{c}\right)$

c_d section profile-drag coefficient, $\int_{\text{Wake}} c_d' \, d\left(\frac{h}{c}\right)$

c_d' point drag coefficient (ref. 21)

c_l section lift coefficient, $c_n \cos\alpha - c_c \sin\alpha$

c_m section pitching-moment coefficient about quarter-chord point, $-\oint C_p \left(\frac{x}{c} - 0.25\right) d\left(\frac{x}{c}\right) + \oint C_p \left(\frac{z}{c}\right) d\left(\frac{z}{c}\right)$

c_n section normal-force coefficient, $-\oint C_p \, d\left(\frac{x}{c}\right)$

h	vertical height in wake profile, mm (in.)
L.	lower surface
p	static pressure, Pa (lbf/ft^2)
q	dynamic pressure, Pa (lbf/ft^2)
R	Reynolds number based on free-stream conditions and airfoil chord
S.	boundary-layer separation location, x_S/c
T.	boundary-layer transition location, x_T/c
t	airfoil thickness, mm (in.)
U.	upper surface
x	airfoil abscissa, mm (in.)
y	model span station, y = 0 at midspan, mm (in.)
z	airfoil ordinate, mm (in.)
α	angle of attack relative to x-axis, deg
Δc_d	change in uncorrected section profile-drag coefficient, 0.0350/deg
$\Delta c_{l,max}$	change in maximum section lift coefficient due to leading-edge roughness, $-\frac{(c_{l,\max})_{free} - (c_{l,\max})_{fixed\ or\ rough}}{(c_{l,\max})_{free}}$, percent

Subscripts:

fixed	transition fixed
free	transition free
l	local point on airfoil
last	last wake measurement
ll	lower limit of low-drag range

max	maximum
min	minimum
rough	rough
S	separation
T	transition
u	uncorrected for wind-tunnel boundary effects
ul	upper limit of low-drag range
0	zero lift
∞	free-stream conditions

Abbreviations:

LTPT	NASA Langley Low-Turbulence Pressure Tunnel
NACA	National Advisory Committee for Aeronautics
NASA	National Aeronautics and Space Administration

AIRFOIL DESIGN

OBJECTIVES AND CONSTRAINTS

The design specifications for the airfoil are contained in table I. Two primary objectives are evident from the specifications. The first objective is to achieve a maximum lift coefficient of at least 1.40 for the corresponding Reynolds number of 2×10^6. A requirement related to this objective is that the maximum lift coefficient not decrease significantly with transition fixed near the leading edge on both surfaces. In addition, the airfoil should exhibit docile stall characteristics. The second objective is to obtain low profile-drag coefficients over the range of lift coefficients from 0.40 to 1.20.

Two major constraints were placed on the design of this airfoil. First, the zero-lift pitching-moment coefficient must be no more negative than −0.15. Second, the airfoil thickness must equal 17-percent chord.

PHILOSOPHY

Given the above objectives and constraints, certain characteristics of the design are apparent. The following sketch illustrates a drag polar that meets the goals for this design.

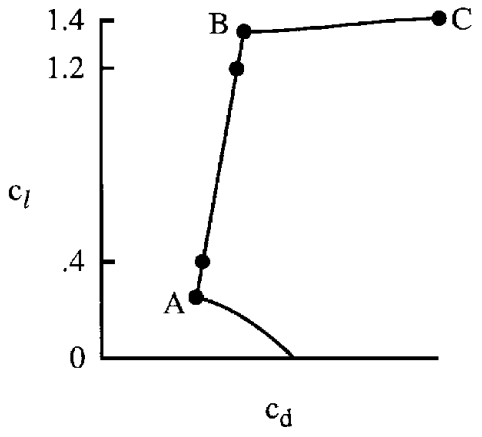

Sketch 1

The desired airfoil shape can be traced to the pressure distributions that occur at the various points in sketch 1. Point A is the lower limit of the low-drag, lift-coefficient range. The lift coefficient at point A is 0.15 lower than the objective specified in table I. The difference is intended as a margin against such contingencies as manufacturing tolerances, operational deviations, three-dimensional effects, and inaccuracies in the theoretical method. A similar margin is also desirable at the upper limit of the low-drag range, point B, although this margin is constrained by the proximity of the upper limit to the maximum lift coefficient. The profile-drag coefficient at point B is not as low as at point A, unlike the polars of many laminar-flow airfoils where the drag coefficient within the laminar bucket is nearly constant. This characteristic is related to the elimination of significant (drag-producing) laminar separation bubbles on the upper surface. (See ref. 22.) The small increase in profile-drag coefficient with increasing lift coefficient is relatively inconsequential because the ratio of the profile drag to the total drag of the wind-turbine blade decreases with increasing lift coefficient. The profile-drag coefficient increases very rapidly outside the low-drag range because boundary-layer transition moves quickly toward the leading edge with increasing (or decreasing) lift coefficient. This feature results in a leading edge that produces a suction peak at higher lift coefficients, which ensures that transition on the upper surface will occur very near the leading edge. Thus, the maximum lift coefficient, point C, occurs with turbulent flow along the entire upper surface and, therefore, should be relatively insensitive to roughness at the leading edge.

Because the large airfoil thickness allows a wider low-drag range to be achieved than specified, the lower limit of the low-drag range should be below point A.

From the preceding discussion, the pressure distributions along the polar can be deduced. The pressure distribution at point A should look something like sketch 2.

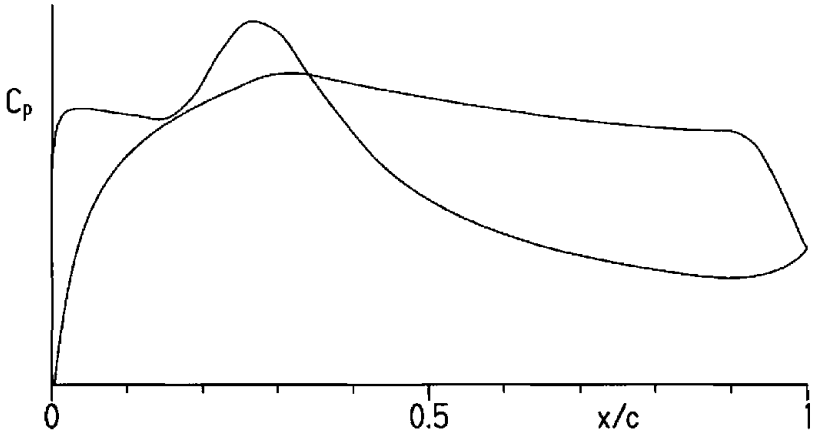

Sketch 2

To achieve low drag, a favorable pressure gradient is desirable along the upper surface to about 30-percent chord. Aft of this point, a short region having a shallow, adverse pressure gradient ("transition ramp") promotes the efficient transition from laminar to turbulent flow (ref. 23). The transition ramp is followed by a concave pressure recovery. The specific pressure recovery employed represents a compromise between maximum lift, drag, pitching moment, and stall characteristics. The steep, adverse pressure gradient aft of about 90-percent chord is a "separation ramp," proposed by F. X. Wortmann,[1] which confines turbulent separation to a small region near the trailing edge. By constraining the movement of the separation point at high angles of attack, high lift coefficients can be achieved with little drag penalty. This feature has the added benefit of promoting docile stall characteristics. (See ref. 24.)

A generally favorable pressure gradient is desirable along the lower surface to about 30-percent chord to achieve low drag. The specific pressure gradients employed along the forward portion of the lower surface increase the loading in the leading-edge region while maintaining low drag at the lower lift coefficients. The forward loading serves to balance, with respect to the pitching-moment constraint, the aft loading, both of which contribute to the achievement of a high maximum lift coefficient and low profile-drag coefficients. This region is followed by a curved transition ramp (ref. 22) that is longer than the one on the upper surface. The ramp is followed by a concave pressure recovery, which exhibits lower drag and has less tendency to separate than the corresponding linear or convex pressure recovery (ref. 23). The pressure recovery must begin relatively far forward to alleviate separation at lower lift coefficients, especially with transition fixed near the leading edge.

---

[1]Director, Institute for Aerodynamics and Gas Dynamics, University of Stuttgart, Germany.

The amounts of pressure recovery on the upper and lower surfaces are determined by the airfoil-thickness and pitching-moment constraints.

At point B, the pressure distribution should look like sketch 3.

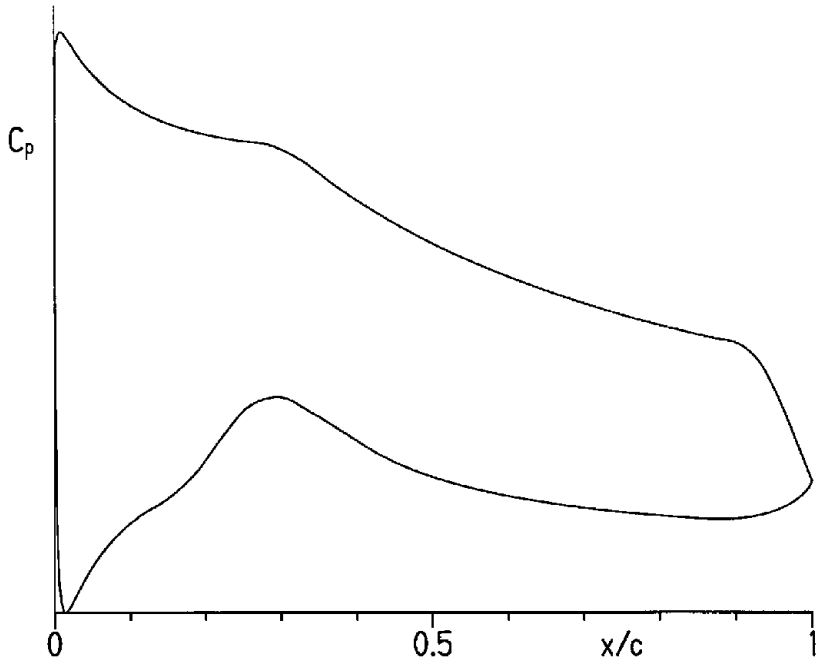

Sketch 3

No suction spike exists at the leading edge. Instead, a rounded peak occurs just aft of the leading edge. Transition is essentially imminent over the entire forward portion of the upper surface. This feature allows a wider low-drag range to be achieved and higher lift coefficients to be reached without significant separation. It also causes transition to move very quickly toward the leading edge with increasing lift coefficient, which leads to the roughness insensitivity of the maximum lift coefficient.

EXECUTION

Given the pressure distributions previously discussed, the design of the airfoil is reduced to the inverse problem of transforming the pressure distributions into an airfoil shape. The Eppler Airfoil Design and Analysis Code (refs. 19 and 20) was used because of its unique capability for multipoint design and because of confidence gained during the design, analysis, and experimental verification of many other airfoils. (See refs. 25–28, for example.)

The airfoil is designated the S825. The airfoil shape is shown in figure 1 and the coordinates are contained in table II. The airfoil thickness is 17-percent chord, which satisfies the design constraint.

EXPERIMENTAL PROCEDURE

WIND TUNNEL

The NASA Langley Low-Turbulence Pressure Tunnel (LTPT) (refs. 17 and 18) is a closed-throat, single-return tunnel (fig. 2) that can be operated at stagnation pressures from 100 to 1000 kPa (1 to 10 atm). The unit Reynolds number can be varied from 1×10^6 to 49×10^6 per meter (0.3×10^6 to 15×10^6 per foot); the Mach number can be varied from 0.05 to 0.47. The turbulence level in the test section is generally below 0.05 percent for unit Reynolds numbers up to 13×10^6 per meter (4×10^6 per foot) at Mach numbers up to 0.15 (ref. 29).

The test section is 91.44 cm (36.00 in.) wide by 228.6 cm (90.00 in.) high. Hydraulically actuated circular plates provide positioning and attachment for the two-dimensional model (fig. 3). The plates, about 86 cm (34 in.) in diameter, are flush with the tunnel sidewalls and rotate with the model. The axis of rotation coincided approximately with the midchord of the model, which was mounted horizontally between the plates. The gaps between the model and the plates were sealed.

MODEL

The aluminum, wind-tunnel model was fabricated by Advanced Technologies, Incorporated, Newport News, Virginia, using a numerically controlled milling machine. The model had a chord of 457.15 mm (17.998 in.) and a span of 91.14 cm (35.88 in.). Upper- and lower-surface orifices were located to one side of midspan at the staggered positions listed in table III. All the orifices were 0.51 mm (0.020 in.) in diameter with their axes perpendicular to the surface. The surface of the model had been polished to ensure an aerodynamically smooth finish. The measured model contour was within 0.1 mm (0.004 in.) of the prescribed shape.

WAKE-SURVEY PROBE

A total- and static-pressure, wake-survey probe (fig. 4) was mounted from the tunnel strut (fig. 3). The probe was positioned spanwise at the tunnel centerline. A traverse mechanism incrementally positioned the probe vertically. The tip of the probe was located 1.84 chord downstream of the trailing edge of the model.

INSTRUMENTATION

Measurements of the pressures on the model and in the wake were made by an electronically scanned, pressure-transducer system. Basic tunnel pressures were measured with precision quartz manometers. Data were obtained and recorded by an electronic data-acquisition system.

METHODS

The pressures measured on the model were reduced to standard pressure coefficients and numerically integrated to obtain section normal- and chord-force coefficients and section pitching-moment coefficients about the quarter-chord point. Section profile-drag coefficients were computed from the wake total and static pressures by the method of reference 21.

Standard, low-speed, wind-tunnel boundary corrections (ref. 30) have been applied to the data. The wake-survey-probe total-pressure-tube displacement correction (ref. 21) has been taken into account.

At angles of attack beyond stall, the unsteadiness of the flow and the large height of the wake made wake surveys impractical. Accordingly, at these angles of attack, the uncorrected profile-drag coefficient was set to $(c_{d,last})_u + \Delta c_d\,(\alpha_u - (\alpha_{last})_u)$, where Δc_d was determined from data presented in reference 31. Typically, the value of $(c_{d,last})_u$ was about 0.1.

TESTS

The model was tested at Reynolds numbers based on airfoil chord of 1×10^6, 2×10^6, 3×10^6, 4×10^6, and 6×10^6 and a Mach number of 0.1 with transition free (smooth) and with transition fixed by roughness at 2-percent chord on the upper surface and 5-percent chord on the lower surface. The grit roughness was sized using the method of reference 32 and sparsely distributed along 3-mm (0.1-in.) wide strips applied to the model with lacquer. (See table IV.) The model was also tested with a grit roughness equivalent to NACA standard roughness (ref. 4), which was applied to the model with lacquer and sparsely distributed from the leading edge to an arc length of 8-percent chord on the upper and lower surfaces. The grit size, nominally 0.211 mm (0.0083 in.), was scaled from the NACA standard-roughness grit size by the ratio of the model chords used: 457.2 mm (18.00 in.) in the present investigation and 609.6 mm (24.00 in.) in the NACA tests.

Starting from 0°, the angle of attack was increased and then decreased to determine hysteresis. The angle of attack was then decreased from 0° until the lift coefficient became negative.

DISCUSSION OF RESULTS

EXPERIMENTAL RESULTS

Pressure Distributions

The pressure distributions at various angles of attack for the design Reynolds number of 2×10^6 with transition free are shown in figure 5. At an angle of attack of 0.00° (fig. 5(a)), a short laminar separation bubble is barely discernible on the upper surface around 50-percent chord. A more obvious, short laminar separation bubble is evident on the lower surface around 35-percent chord. As the angle of attack is increased, the bubble on the upper surface moves forward, whereas the bubble on the lower surface moves slightly aft. At an angle of attack of 5.04° (fig. 5(f)), which corresponds to the upper limit of the low-drag, lift-coefficient range, the bubble on the upper surface has almost disappeared. As the angle of attack is increased further, transition moves rapidly forward and turbulent, trailing-edge separation occurs on the upper surface. The amount of separation increases with increasing angle of attack. The maximum lift coefficient occurs at an angle of attack of 13.10° (fig. 5(n)). As the angle of attack is increased further, the separation point moves rapidly forward to about mid-chord and then slowly migrates further forward. At an angle of attack of 20.03° (fig. 5(u)), the flow around the leading edge is still attached.

As the angle of attack is decreased from 20.03°, the pressure distributions (figs. 5(v)–5(bb)) are essentially identical to the ones that occur with increasing angle of attack (figs. 5(n)–5(t)). Thus, no hysteresis occurs with respect to separation on the upper surface.

As the angle of attack is decreased from −1.03° (fig. 5(cc)), the laminar separation bubble on the lower surface moves slightly forward, whereas the bubble on the upper surface moves aft. At an angle of attack of −5.04° (fig. 5(gg)), which corresponds to the lower limit of the low-drag range, the bubble on the lower surface has almost disappeared.

Section Characteristics

Reynolds number effects.- The section characteristics with transition free, transition fixed, and the scaled, NACA standard roughness ("rough") are shown in figure 6. For the design Reynolds number of 2×10^6 with transition free (fig. 6(b)), the maximum lift coefficient is 1.56, which satisfies the design objective of $c_{l,max} \geq 1.40$. The airfoil exhibits a rapid, trailing-edge stall, which does not meet the design goal of docile stall characteristics. No hysteresis occurs for angles of attack beyond stall. Low profile-drag coefficients are exhibited over the range of lift coefficients from 0.05 to 1.10. Thus, the lower limit of the low-drag, lift-coefficient range is well below the design objective of $c_{l,ll} = 0.40$, although the upper limit of the low-drag range is also below the design objective of $c_{l,ul} = 1.20$, primarily to meet other, more important goals. The drag coefficient at the specified lower limit of the low-drag range ($c_l = 0.40$) is 0.0068, which satisfies the design objective of $c_{d,min} \leq 0.0080$. The zero-lift pitching-moment coefficient is −0.15, which satisfies the design constraint of $c_{m,0} \geq -0.15$.

The effects of Reynolds number on the section characteristics with transition free, transition fixed, and rough are summarized in figure 7. The zero-lift angle of attack, approximately $-5.4°$ with transition free, is relatively unaffected by Reynolds number. In general, the lift-curve slope, the maximum lift coefficient, the sharpness of the stall, the lower limit of the low-drag range, and the magnitude of the pitching-moment coefficients increase with increasing Reynolds number; the upper limit and the width of the low-drag range and the drag coefficients decrease.

Effect of roughness.- The effect of fixing transition on the section characteristics is shown in figure 6. In general, the lift-curve slope, the maximum lift coefficient, and the magnitudes of the zero-lift angle of attack and the pitching-moment coefficients decrease with transition fixed. These results are primarily a consequence of the boundary-layer displacement effect, which decambers the airfoil because the displacement thickness is greater with transition fixed than with transition free. In addition, the lift-curve slope and the maximum lift coefficient decrease with transition fixed because the roughness induces earlier trailing-edge separation, particularly at higher angles of attack. The maximum lift coefficient for the design Reynolds number of 2×10^6 (fig. 6(b)) is 1.52, a reduction of less than 3 percent from that with transition free. Thus, one of the most important design goals has been achieved. The drag coefficients are, of course, adversely affected by the roughness. For many conditions, the Reynolds number, based on local velocity and boundary-layer momentum thickness, at the roughness location is too low to support turbulent flow. Accordingly, to force transition, the roughness must be so large that it increases the momentum thickness, which abnormally decreases the lift coefficients and the magnitude of the pitching-moment coefficients and increases the drag coefficients. Conversely, at low lift coefficients, the roughness on the upper surface, which was sized for higher lift coefficients, was frequently too small to force transition, resulting in improperly low drag coefficients.

The effect of the scaled, NACA standard roughness on the section characteristics is shown in figure 6. The effect is more severe than that of fixing transition. The maximum lift coefficient for the design Reynolds number of 2×10^6 (fig. 6(b)) is 1.34, a reduction of 14 percent from that with transition free. It should be remembered that the effect of roughness is proportional to the ratio of the roughness height to the boundary-layer thickness. Because the height of the scaled, NACA standard roughness and the airfoil chord are constant, the effect of this roughness generally increases with increasing Reynolds number (because increasing Reynolds number results in decreasing boundary-layer thickness).

The variation of maximum lift coefficient with Reynolds number is shown in figure 8. The maximum lift coefficient increases with increasing Reynolds number. The rate of increase is similar with transition free and transition fixed but lower with the scaled, NACA standard roughness.

The variation of the change in maximum lift coefficient due to roughness with Reynolds number is shown in figure 9. The magnitude of the change due to fixing transition is relatively small (< 3 percent) and exhibits no definite trend with Reynolds number. The magnitude of the change due to the scaled, NACA standard roughness is an order of magnitude larger and generally increases with increasing Reynolds number.

The variation of profile-drag coefficient at a lift coefficient of about 0.4 (i.e., approximately the specified lower limit of the low-drag range) with Reynolds number is shown in figure 10. The drag coefficient generally decreases with increasing Reynolds number. (The drag coefficient for a Reynolds number of 1×10^6 with transition fixed is too low probably because the roughness on the upper surface failed to force transition at this lift coefficient.)

COMPARISON OF THEORETICAL AND EXPERIMENTAL RESULTS

Pressure Distributions

The comparison of the theoretical and experimental pressure distributions at various lift coefficients is shown in figure 11. The theoretical pressure distributions are inviscid and incompressible; the experimental pressure distributions were obtained for a Reynolds number of 2×10^6 and a Mach number of 0.1 with transition free. It should be noted that the theoretical lift coefficient is calculated from the lift-curve slope and the angle of attack relative to the zero-lift line, whereas the experimental lift coefficient is derived from the integrated pressure distribution. (See refs. 19–21.) Thus, the theoretical and experimental pressure distributions at a given lift coefficient do not necessarily have identical areas.

Although the pressure coefficients at the lift coefficient that corresponds approximately to the specified lower limit of the low-drag range (fig. 11(a)) do not match exactly, the pressure gradients agree well except where laminar separation bubbles are present and near the trailing edge. The bubbles are not modeled in the pressure distributions predicted by the method of references 19 and 20. At the lift coefficient that corresponds approximately to the specified upper limit of the low-drag range (fig. 11(b)), the decambering viscous effects are more apparent and the discrepancies include small differences in the pressure gradients. At the measured maximum lift coefficient (fig. 11(c)), the agreement is poor primarily because the effect of the upper-surface, trailing-edge separation on the pressure distribution is not modeled in the theory.

Section Characteristics

The comparison of the theoretical and experimental section characteristics with transition free is shown in figure 12. The magnitude of the zero-lift angle of attack is overpredicted. The lift-curve slope is predicted relatively accurately. The maximum lift coefficient is increasingly underpredicted with increasing Reynolds number. It should be noted that the maximum lift coefficient computed by the method of references 19 and 20 is not always realistic. Accordingly, an empirical criterion has been applied to the computed results. This criterion assumes that the maximum lift coefficient has been reached if the drag coefficient of the upper surface is greater than $0.0160\,(2 \times 10^6/R)^{1/7}$ or if the length of turbulent separation on the upper surface is greater than 0.1000c. The upper limit of the low-drag range, the drag coefficients within the low-drag range, and the magnitude of the pitching-moment coefficients are overpredicted. The lower limit of the low-drag range is underpredicted. Thus, the width of the low-drag range is overpredicted.

The comparison of the theoretical and experimental section characteristics with transition fixed is shown in figure 13. The predicted zero-lift angle of attack, lift-curve slope, maximum lift coefficient, and pitching-moment coefficients show the same tendencies as with transition free. The agreement between the predicted and measured drag coefficients is poor at low lift coefficients, probably because the roughness on the upper surface failed to force transition at these lift coefficients.

CONCLUDING REMARKS

A 17-percent-thick, natural-laminar-flow airfoil, the S825, for the 75-percent blade radial station of 20- to 40-meter, variable-speed and variable-pitch (toward feather), horizontal-axis wind turbines has been designed and analyzed theoretically and verified experimentally in the NASA Langley Low-Turbulence Pressure Tunnel. The two primary objectives of high maximum lift coefficient, relatively insensitive to leading-edge roughness, and low profile-drag coefficients have been achieved. The airfoil exhibits a rapid, trailing-edge stall, which does not meet the design goal of docile stall characteristics. The constraints on the zero-lift pitching-moment coefficient and the airfoil thickness have been satisfied. Comparisons of the theoretical and experimental results generally show good agreement.

ACKNOWLEDGMENTS

The assistance of the staff of NASA Langley Research Center is gratefully acknowledged.

REFERENCES

1. Jacobs, Eastman N.; Ward, Kenneth E.; and Pinkerton, Robert M.: The Characteristics of 78 Related Airfoil Sections from Tests in the Variable-Density Wind Tunnel. NACA Rep. 460, 1933.

2. Jacobs, Eastman N.; and Pinkerton, Robert M.: Tests in the Variable-Density Wind Tunnel of Related Airfoils Having the Maximum Camber Unusually far Forward. NACA Rep. 537, 1935.

3. Jacobs, Eastman N.; Pinkerton, Robert M.; and Greenberg, Harry: Tests of Related Forward-Camber Airfoils in the Variable-Density Wind Tunnel. NACA Rep. 610, 1937.

4. Abbott, Ira H.; Von Doenhoff, Albert E.; and Stivers, Louis S., Jr.: Summary of Airfoil Data. NACA Rep. 824, 1945. (Supersedes NACA WR L-560.)

5. Abbott, Ira H.; and Von Doenhoff, Albert E.: Theory of Wing Sections. Dover Publ., Inc., c.1959.

6. McGhee, Robert J.; Beasley, William D.; and Whitcomb, Richard T.: NASA Low- and Medium-Speed Airfoil Development. NASA TM-78709, 1979.

7. Tangler, J. L.; and Somers, D. M.: Status of the Special-Purpose Airfoil Families. SERI/TP-217-3264, Dec. 1987.

8. Somers, Dan M.: The S801 through S808 Airfoils. Airfoils, Inc., 1987. [Proprietary to NREL]

9. Somers, Dan M.: The S809 through S813 Airfoils. Airfoils, Inc., 1988. [Proprietary to NREL]

10. Somers, Dan M.: The S814 and S815 Airfoils. Airfoils, Inc., 1992. [Proprietary to NREL]

11. Somers, Dan M.: The S816, S817, and S818 Airfoils. Airfoils, Inc., 1992. [Proprietary to NREL]

12. Somers, Dan M.: The S819, S820, and S821 Airfoils. Airfoils, Inc., 1993. [Proprietary to NREL]

13. Somers, Dan M.: The S822 and S823 Airfoils. Airfoils, Inc., 1993. [Proprietary to NREL]

14. Somers, Dan M.: The S825 and S826 Airfoils. Airfoils, Inc., 1995. [Proprietary to NREL]

15. Somers, Dan M.: The S827 and S828 Airfoils. Airfoils, Inc., 1995. [Proprietary to NREL]

16. Tangler, J. L.; and Somers, D. M.: NREL Airfoil Families for HAWTs. NREL/TP-442-7109, Jan. 1995.

17. Von Doenhoff, Albert E.; and Abbott, Frank T., Jr.: The Langley Two-Dimensional Low-Turbulence Pressure Tunnel. NACA TN 1283, 1947.

18. McGhee, Robert J.; Beasley, William D.; and Foster, Jean M.: Recent Modifications and Calibration of the Langley Low-Turbulence Pressure Tunnel. NASA TP-2328, 1984.

19. Eppler, Richard: Airfoil Design and Data. Springer-Verlag (Berlin), 1990.

20. Eppler, Richard: Airfoil Program System "PROFIL98." User's Guide. Richard Eppler, c.1998.

21. Pankhurst, R. C.; and Holder, D. W.: Wind-Tunnel Technique. Sir Isaac Pitman & Sons, Ltd. (London), 1965.

22. Eppler, Richard; and Somers, Dan M.: Airfoil Design for Reynolds Numbers Between 50,000 and 500,000. Proceedings of the Conference on Low Reynolds Number Airfoil Aerodynamics, UNDAS-CP-77B123, Univ. of Notre Dame, June 1985, pp. 1–14.

23. Wortmann, F. X.: Experimental Investigations on New Laminar Profiles for Gliders and Helicopters. TIL/T.4906, British Minist. Aviat., Mar. 1960. (Translated from Z. Flugwissenschaften, Bd. 5, Heft 8, Aug. 1957, S. 228–243.)

24. Maughmer, Mark D.; and Somers, Dan M.: Design and Experimental Results for a High-Altitude, Long-Endurance Airfoil. J. Aircr., vol. 26, no. 2, Feb. 1989, pp. 148–153.

25. Somers, Dan M.: Design and Experimental Results for the S805 Airfoil. NREL/SR-440-6917, Jan. 1997.

26. Somers, Dan M.: Design and Experimental Results for the S809 Airfoil. NREL/SR-440-6918, Jan. 1997.

27. Somers, Dan M.: Design and Experimental Results for the S814 Airfoil. NREL/SR-440-6919, Jan. 1997.

28. Somers, Dan M.: Subsonic Natural-Laminar-Flow Airfoils. Natural Laminar Flow and Laminar Flow Control, R. W. Barnwell and M. Y. Hussaini, eds., Springer-Verlag New York, Inc., 1992, pp. 143–176.

29. Wlezien, R. W.; Spencer, S. A.; and Grubb, J. P.: Comparison of Flow Quality in Subsonic Pressure Tunnels. AIAA Paper 94-2503, June 1994.

30. Allen, H. Julian; and Vincenti, Walter G.: Wall Interference in a Two-Dimensional-Flow Wind Tunnel, With Consideration of the Effect of Compressibility. NACA Rep. 782, 1944. (Supersedes NACA WR A-63.)

31. Critzos, Chris C.; Heyson, Harry H.; and Boswinkle, Robert W., Jr.: Aerodynamic Characteristics of NACA 0012 Airfoil Section at Angles of Attack From 0° to 180°. NACA TN 3361, 1955.

32. Braslow, Albert L.; and Knox, Eugene C.: Simplified Method for Determination of Critical Height of Distributed Roughness Particles for Boundary-Layer Transition at Mach Numbers From 0 to 5. NACA TN 4363, 1958.

TABLE I.– AIRFOIL DESIGN SPECIFICATIONS

Parameter	Objective/Constraint
Blade radial station	0.75
Reynolds number R	2×10^6
Maximum lift coefficient $c_{l,max}$	≥ 1.40
Lower limit of low-drag, lift-coefficient range $c_{l,ll}$	0.40
Upper limit of low-drag, lift-coefficient range $c_{l,ul}$	1.20
Minimum profile-drag coefficient $c_{d,min}$	≤ 0.0080
Zero-lift pitching-moment coefficient $c_{m,0}$	≥ -0.15
Airfoil thickness t/c	17%

TABLE II.– S825 AIRFOIL COORDINATES

Upper Surface		Lower Surface	
x/c	z/c	x/c	z/c
0.00001	0.00030	0.00014	–0.00143
.00028	.00224	.00081	–.00307
.00129	.00543	.00197	–.00477
.00721	.01481	.00650	–.00920
.01766	.02500	.01819	–.01650
.03250	.03549	.03502	–.02381
.05161	.04596	.05670	–.03093
.07479	.05616	.08297	–.03780
.10185	.06588	.11351	–.04443
.13251	.07494	.14790	–.05114
.16643	.08315	.18480	–.05834
.20324	.09032	.22231	–.06499
.24253	.09625	.25997	–.06891
.28387	.10060	.29879	–.06869
.32709	.10296	.34011	–.06415
.37230	.10329	.38475	–.05600
.41930	.10195	.43307	–.04520
.46763	.09920	.48499	–.03306
.51676	.09525	.53974	–.02082
.56616	.09029	.59631	–.00935
.61526	.08450	.65355	.00060
.66350	.07806	.71026	.00854
.71028	.07112	.76514	.01410
.75503	.06385	.81692	.01713
.79720	.05636	.86437	.01757
.83624	.04878	.90608	.01553
.87165	.04117	.94062	.01168
.90294	.03351	.96717	.00727
.92994	.02560	.98566	.00342
.95294	.01758	.99646	.00088
.97208	.01022	1.00000	.00000
.98695	.00450		
.99661	.00108		
1.00000	.00000		

TABLE III.- MODEL ORIFICE LOCATIONS

[c = 457.15 mm (17.998 in.)]

Upper Surface		Lower Surface	
x/c	y, mm (in.)	x/c	y, mm (in.)
0.00061	152.1 (5.988)	0.00197	205.1 (8.075)
.00187	153.2 (6.033)	.00437	203.7 (8.019)
.00428	154.0 (6.062)	.00622	202.7 (7.979)
.00648	155.0 (6.104)	.00816	202.1 (7.958)
.00846	156.3 (6.155)	.01181	200.9 (7.908)
.01240	157.2 (6.190)	.01556	199.7 (7.864)
.01630	158.5 (6.240)	.01979	198.6 (7.820)
.02036	159.4 (6.276)	.02623	197.6 (7.780)
.02655	160.6 (6.323)	.03170	196.5 (7.737)
.03209	161.5 (6.359)	.03977	195.6 (7.701)
.04018	162.3 (6.391)	.04932	194.8 (7.670)
.05019	163.5 (6.436)	.06136	193.6 (7.620)
.06237	164.6 (6.479)	.07746	192.0 (7.560)
.07826	166.1 (6.540)	.09926	190.2 (7.489)
.10014	167.8 (6.608)	.12450	188.3 (7.413)
.12033	169.7 (6.682)	.14973	186.2 (7.331)
.14004	171.4 (6.750)	.17467	184.2 (7.250)
.16018	173.2 (6.817)	.20006	182.0 (7.165)
.18027	174.9 (6.888)	.22470	180.1 (7.089)
.19984	176.8 (6.959)	.24953	177.9 (7.006)
.22017	178.7 (7.034)	.25992	176.9 (6.966)
.23997	180.5 (7.106)	.27007	176.1 (6.931)
.26029	182.2 (7.174)	.28991	173.9 (6.847)
.28015	183.9 (7.242)	.29999	172.9 (6.809)
.30008	185.7 (7.311)	.30980	172.0 (6.770)
.30978	186.7 (7.349)	.32003	170.8 (6.726)
.32027	187.6 (7.386)	.32997	169.7 (6.680)
.32983	188.7 (7.430)	.34020	168.7 (6.643)
.34006	189.7 (7.469)	.34996	167.7 (6.603)
.35000	190.8 (7.511)	.36045	166.6 (6.561)
.36013	191.7 (7.548)	.37023	165.5 (6.517)
.37004	192.8 (7.592)	.38040	164.5 (6.475)
.38014	193.8 (7.629)	.38978	163.7 (6.446)
.39013	194.7 (7.664)	.39989	162.6 (6.402)
.40010	195.8 (7.710)	.41029	161.5 (6.359)
.41000	196.9 (7.752)	.42038	160.4 (6.316)
.41998	197.9 (7.791)	.43005	159.5 (6.278)
.42998	198.9 (7.830)	.44047	158.4 (6.237)

TABLE III.- Concluded

[c = 457.15 mm (17.998 in.)]

Upper Surface		Lower Surface	
x/c	y, mm (in.)	x/c	y, mm (in.)
.44007	200.0 (7.874)	.45039	157.4 (6.197)
.45011	200.8 (7.907)	.47010	158.3 (6.231)
.46027	201.9 (7.947)	.50064	159.7 (6.289)
.47000	202.9 (7.989)	.54973	161.7 (6.366)
.48022	204.1 (8.034)	.60014	164.0 (6.457)
.49019	205.1 (8.075)	.64995	166.2 (6.543)
.50016	205.9 (8.107)	.70012	168.3 (6.627)
.51044	207.2 (8.158)	.75050	170.6 (6.716)
.52007	208.0 (8.188)	.79984	172.6 (6.795)
.53029	209.1 (8.234)	.84958	174.7 (6.876)
.54022	210.2 (8.274)	.90005	176.8 (6.963)
.55011	211.1 (8.313)	.91981	177.6 (6.991)
.57025	209.9 (8.265)	.93969	178.6 (7.032)
.60019	207.8 (8.182)	.95936	179.5 (7.068)
.70030	201.2 (7.920)	.97990	180.4 (7.103)
.75015	197.8 (7.788)	.99020	180.9 (7.123)
.80022	194.7 (7.665)	.99947	181.4 (7.143)
.85035	191.5 (7.541)		
.88040	189.5 (7.459)		
.90021	188.2 (7.408)		
.92002	186.9 (7.358)		
.94024	185.4 (7.301)		
.96018	184.2 (7.250)		
.98054	182.8 (7.199)		
.99054	182.3 (7.178)		

TABLE IV.- ROUGHNESS LOCATION AND SIZE

Reynolds Number	Upper Surface			Lower Surface		
	x/c	Grit Number	Nominal Size, mm (in.)	x/c	Grit Number	Nominal Size, mm (in.)
1×10^6	0.02	90	0.178 (0.0070)	0.05	54	0.351 (0.0138)
2×10^6		180	0.089 (0.0035)		80	0.211 (0.0083)
3×10^6		220	0.074 (0.0029)		100	0.150 (0.0059)
4×10^6						
6×10^6					180	0.089 (0.0035)

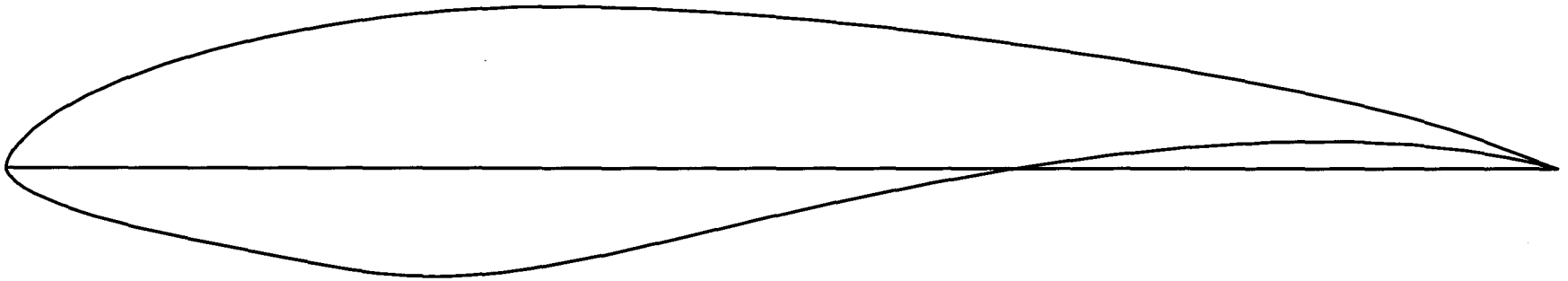

Figure 1.- S825 airfoil shape.

Low-Turbulence Pressure Tunnel

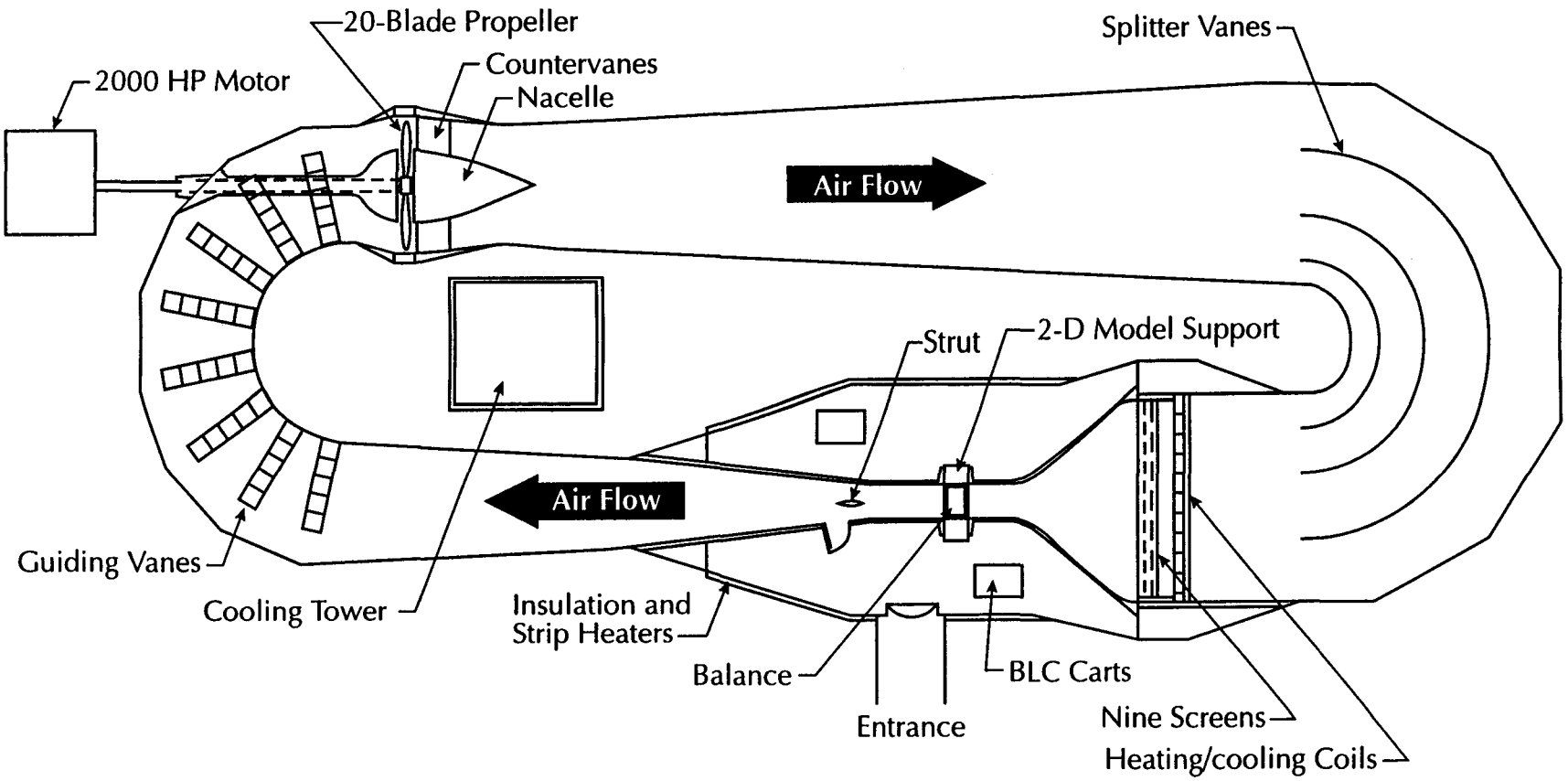

Figure 2.- NASA Langley Low-Turbulence Pressure Tunnel.

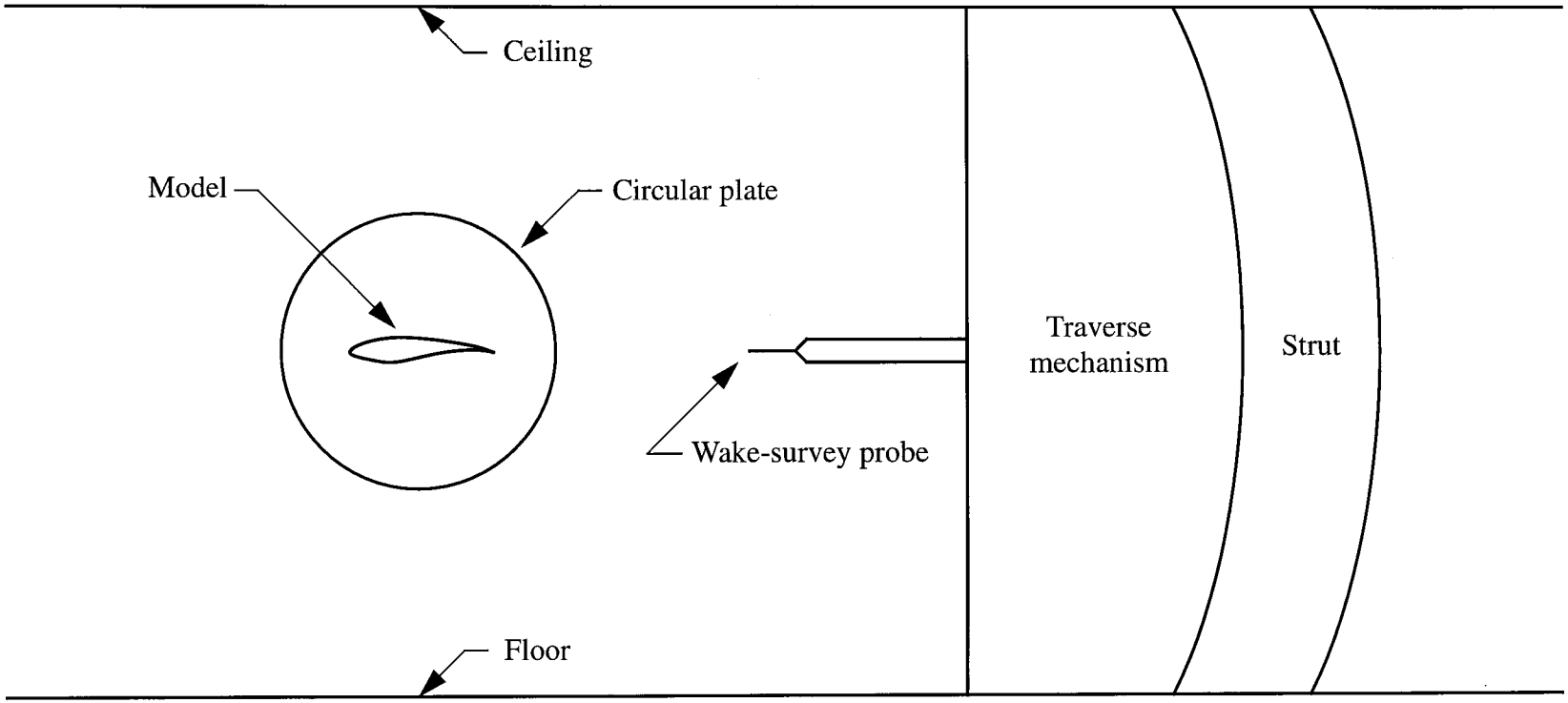

Figure 3.- Sketch of model and wake-survey probe mounted in test section.

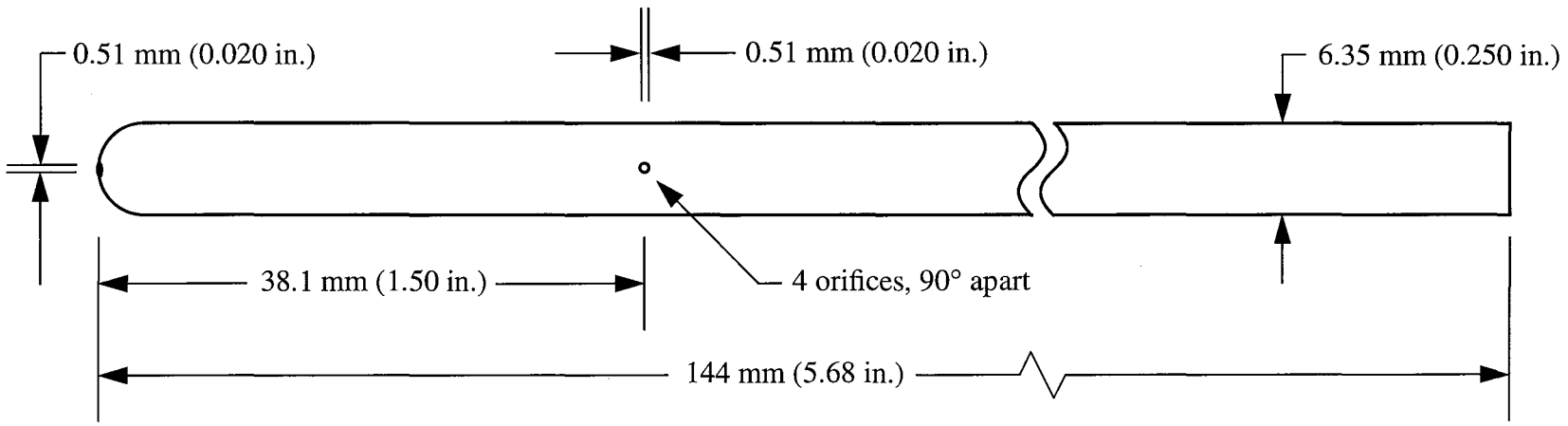

Figure 4.- Wake-survey probe.

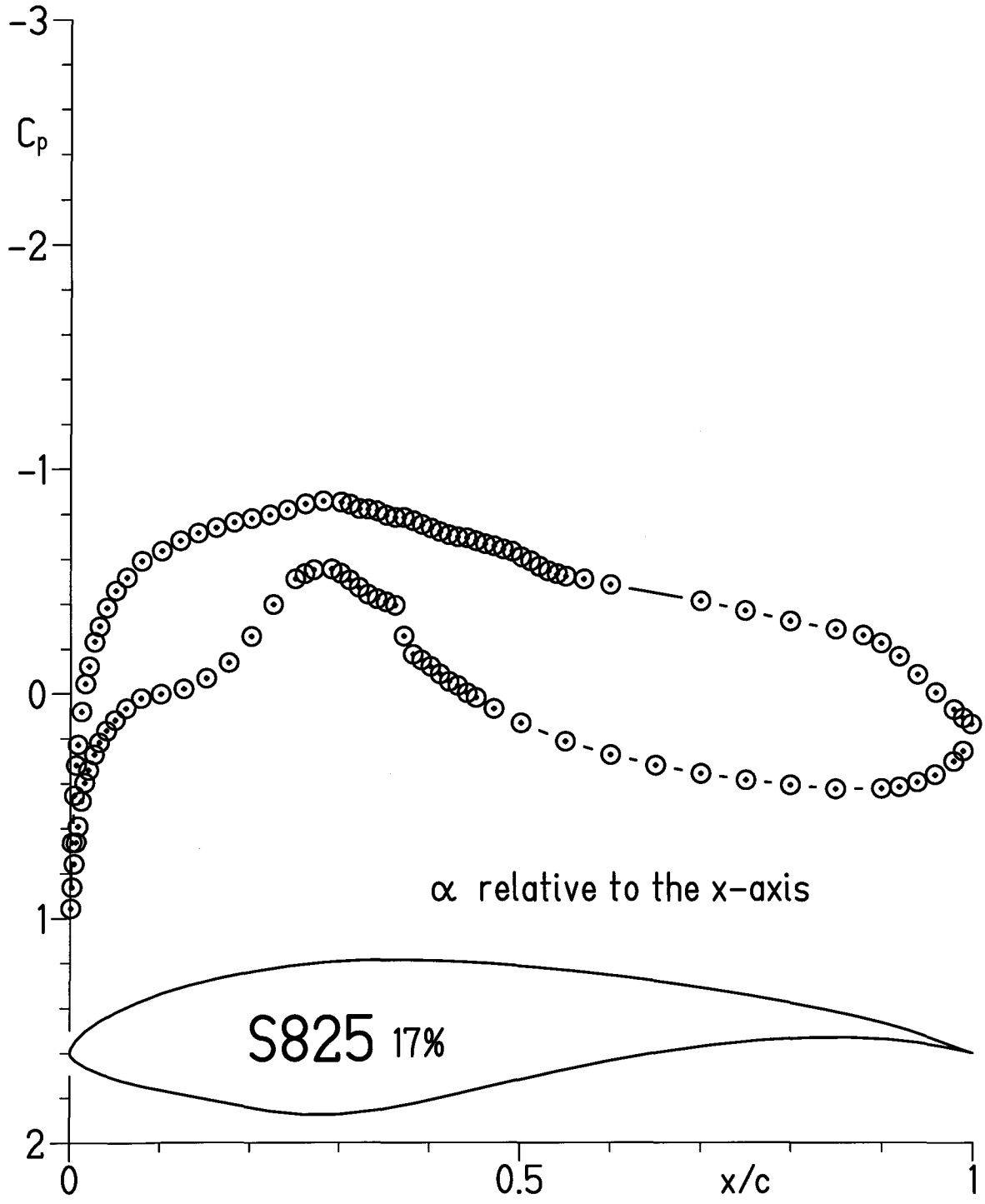

(a) $\alpha = 0.00°$.

Figure 5.- Pressure distributions for $R = 2 \times 10^6$ with transition free.

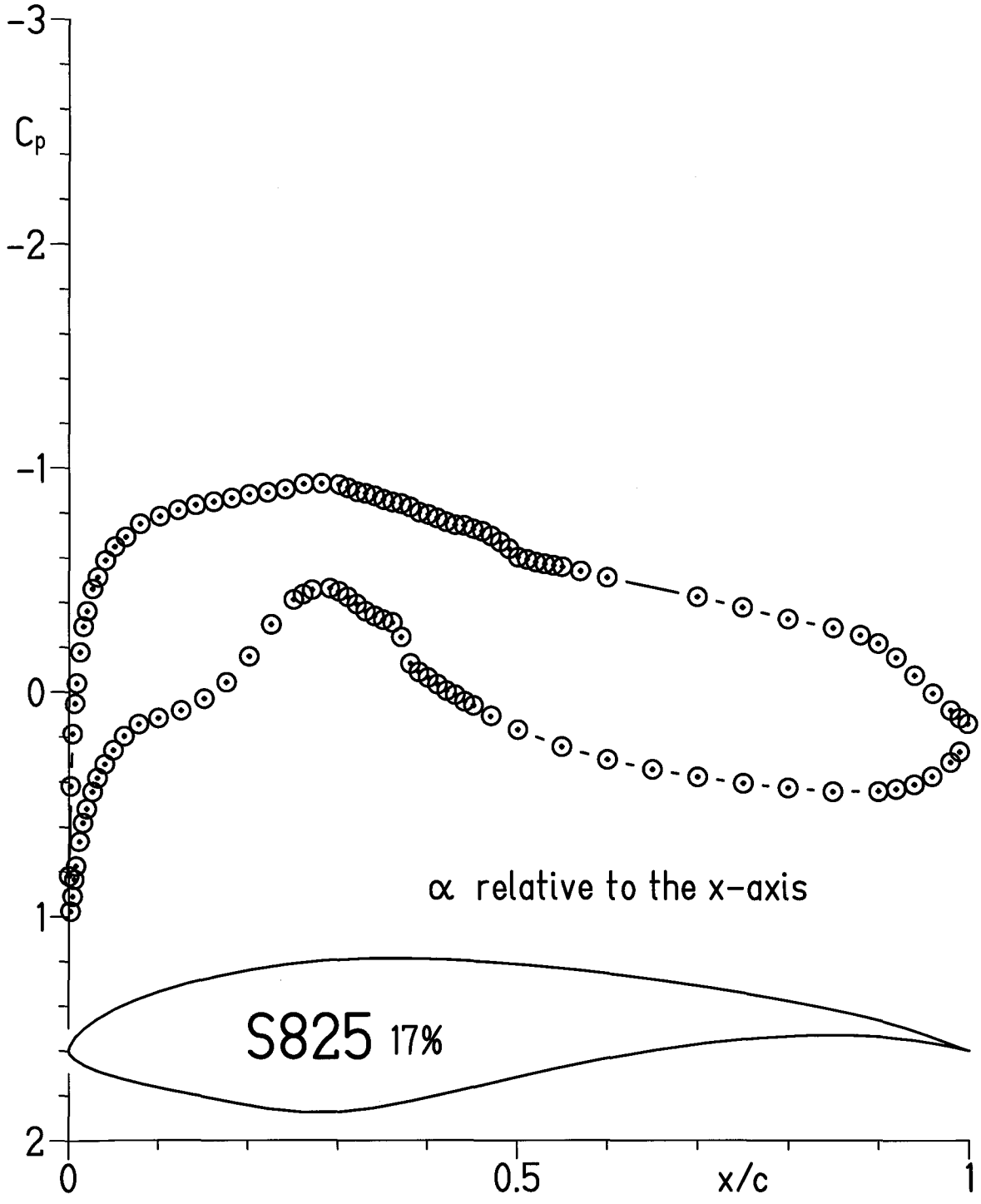

(b) $\alpha = 1.01°$.

Figure 5.- Continued.

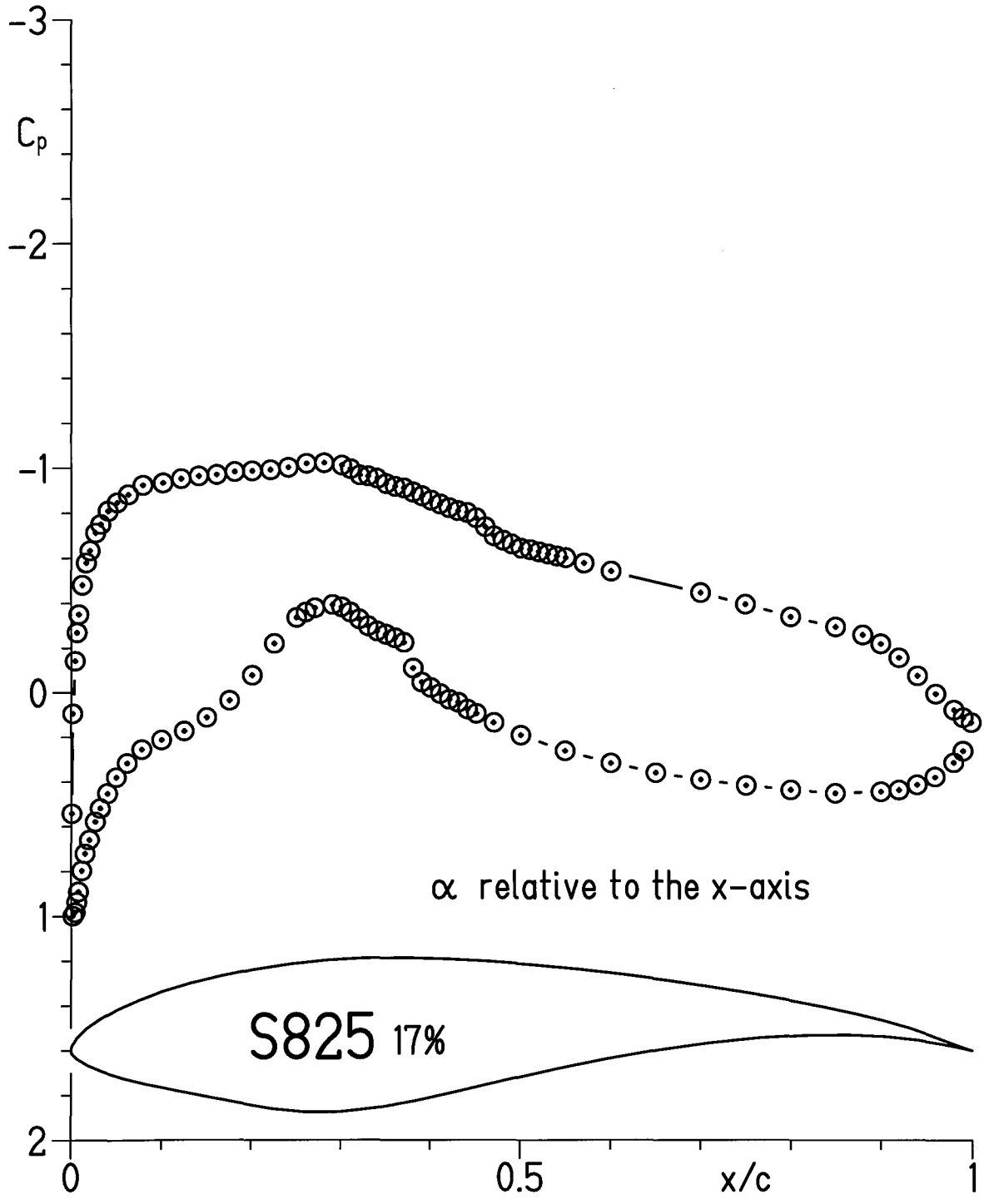

(c) $\alpha = 2.01°$.

Figure 5.- Continued.

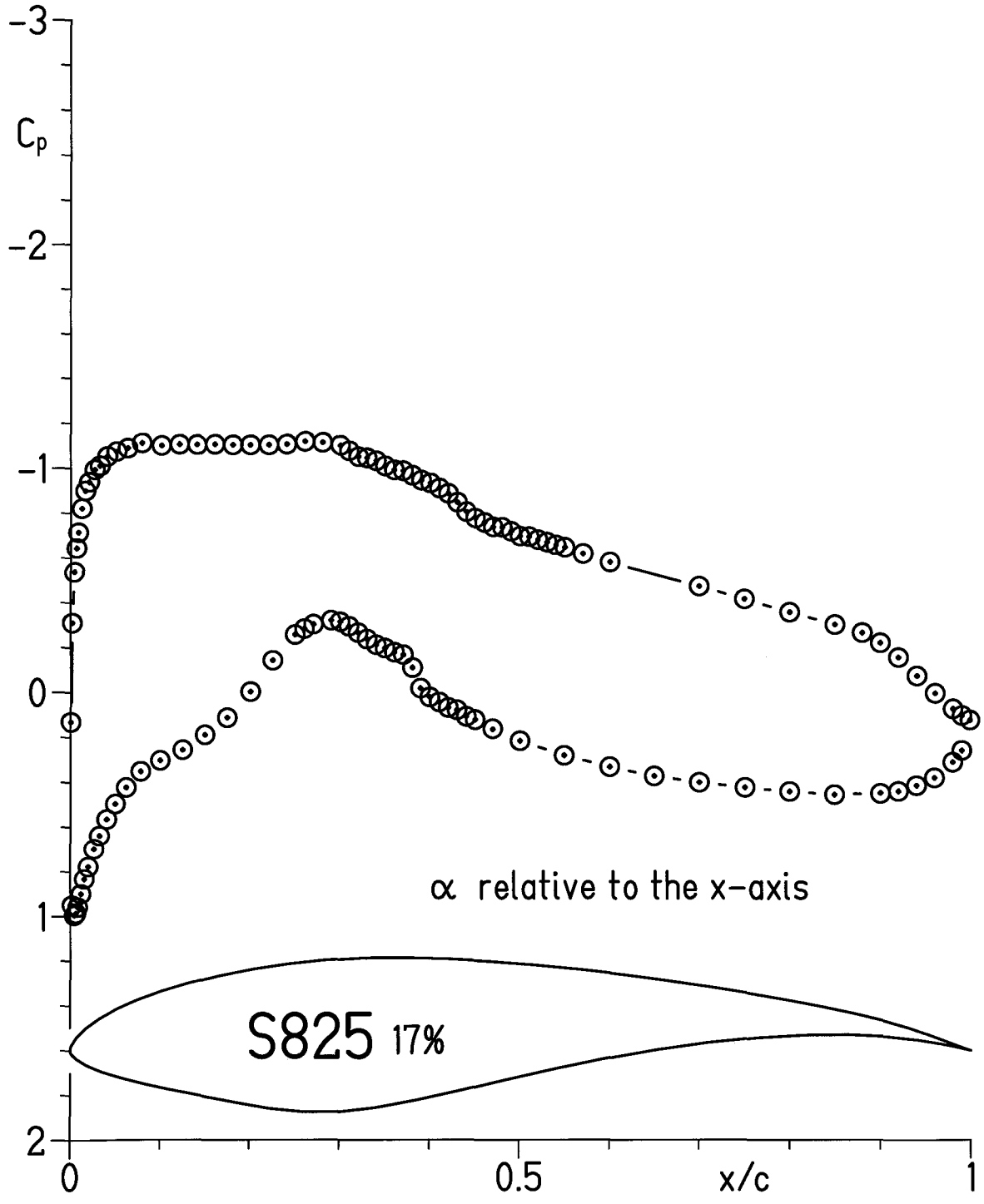

(d) $\alpha = 3.05°$.

Figure 5.- Continued.

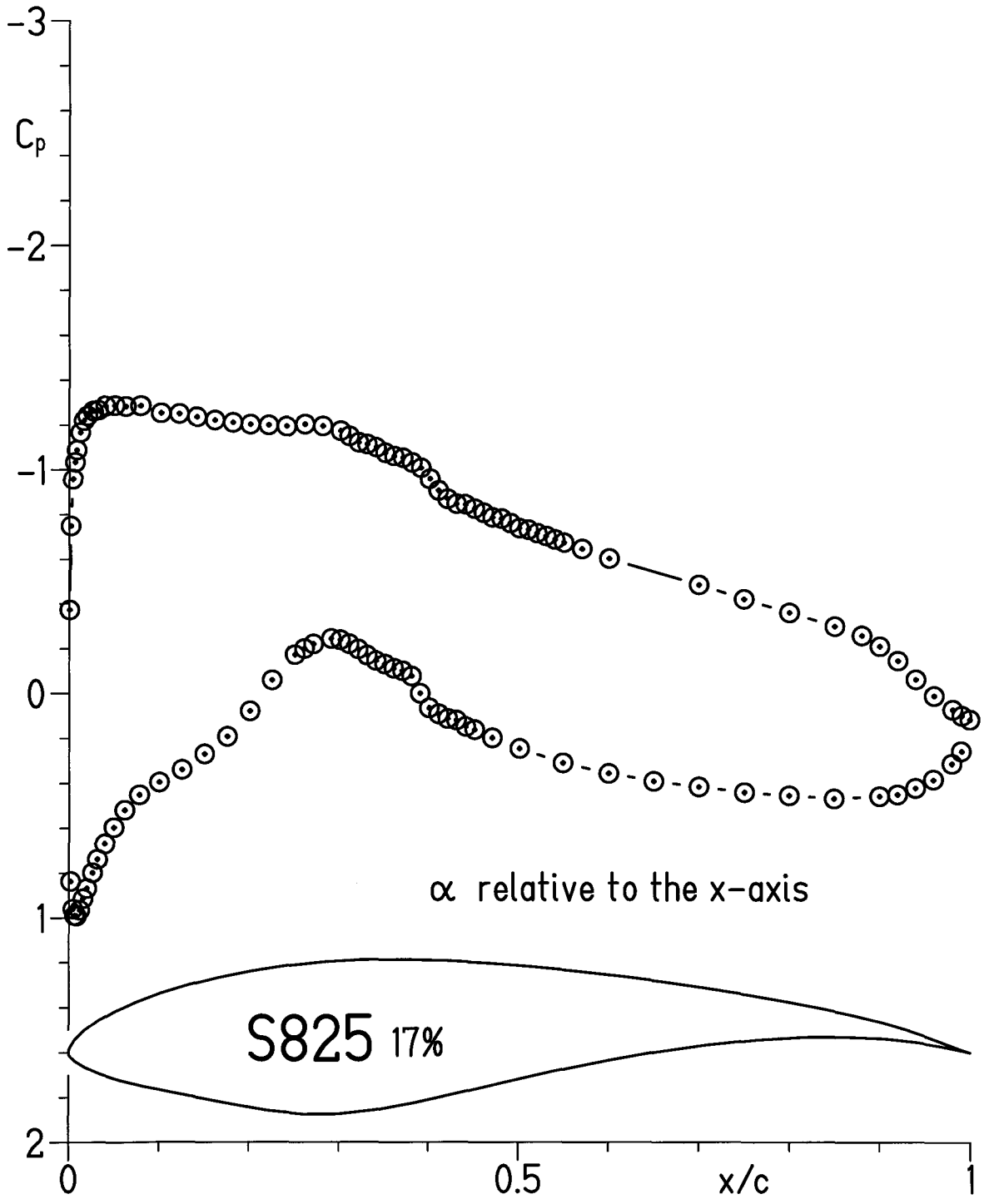

(e) $\alpha = 4.04°$.

Figure 5.- Continued.

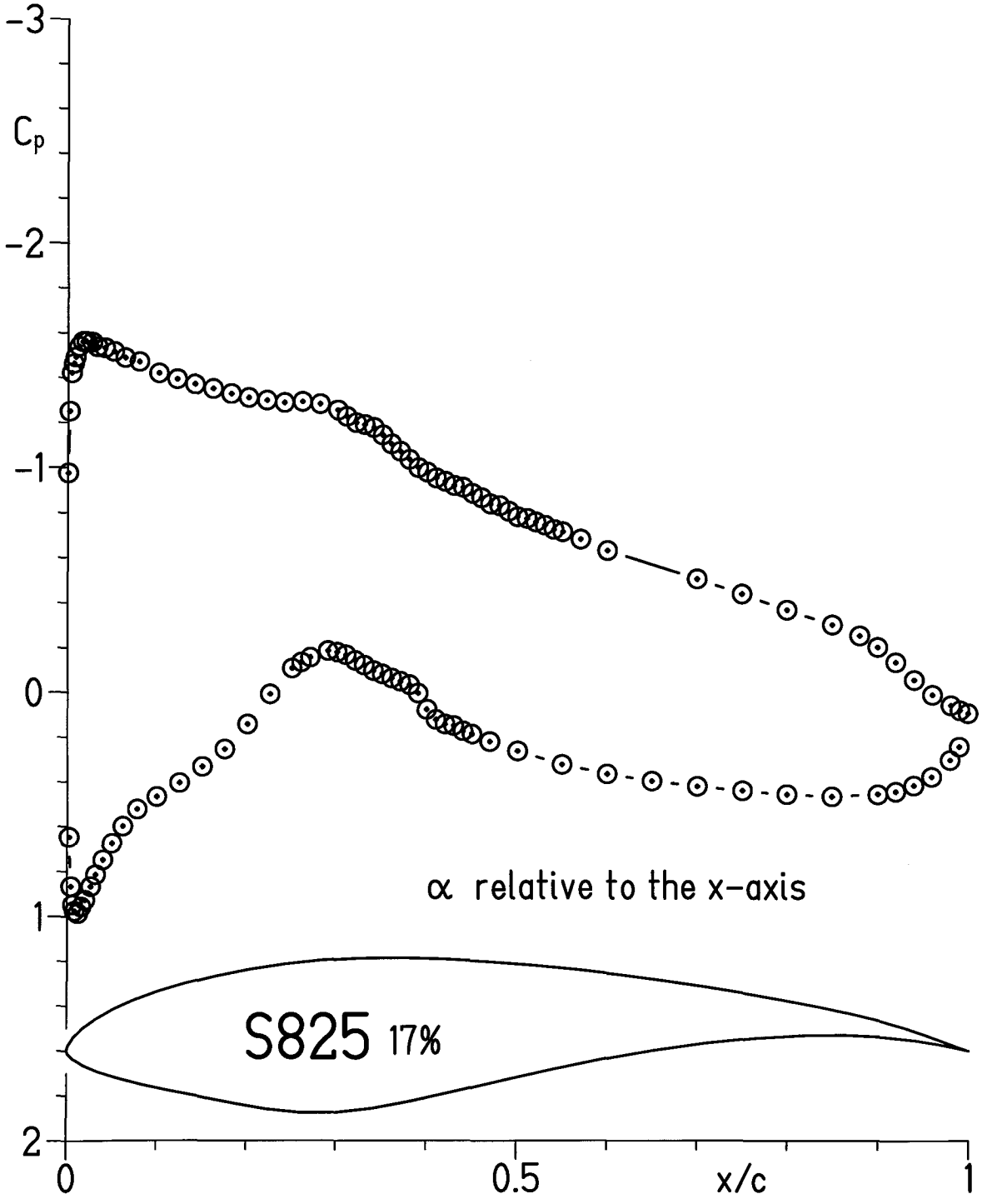

(f) $\alpha = 5.04°$.

Figure 5.- Continued.

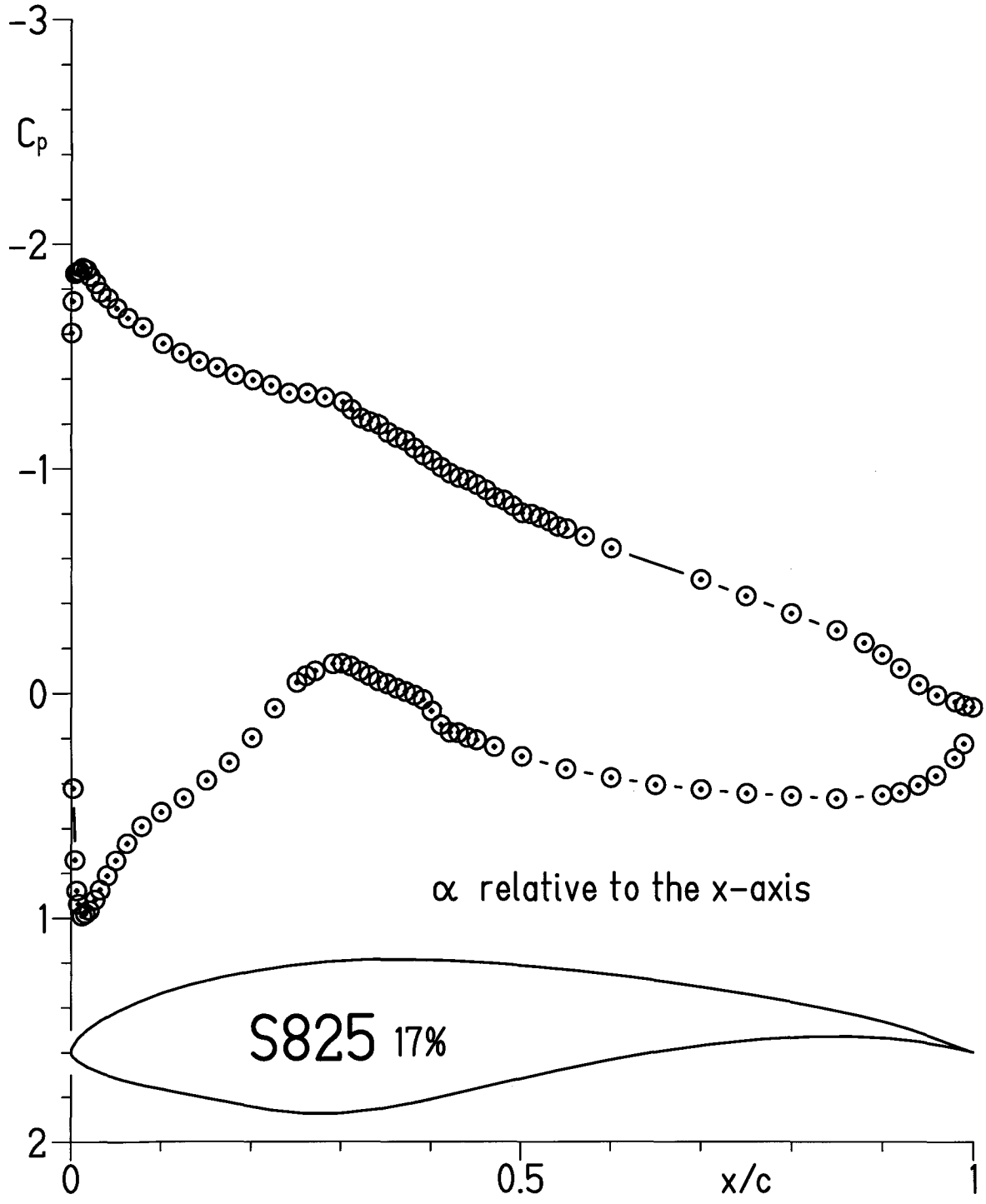

(g) $\alpha = 6.04°$.

Figure 5.- Continued.

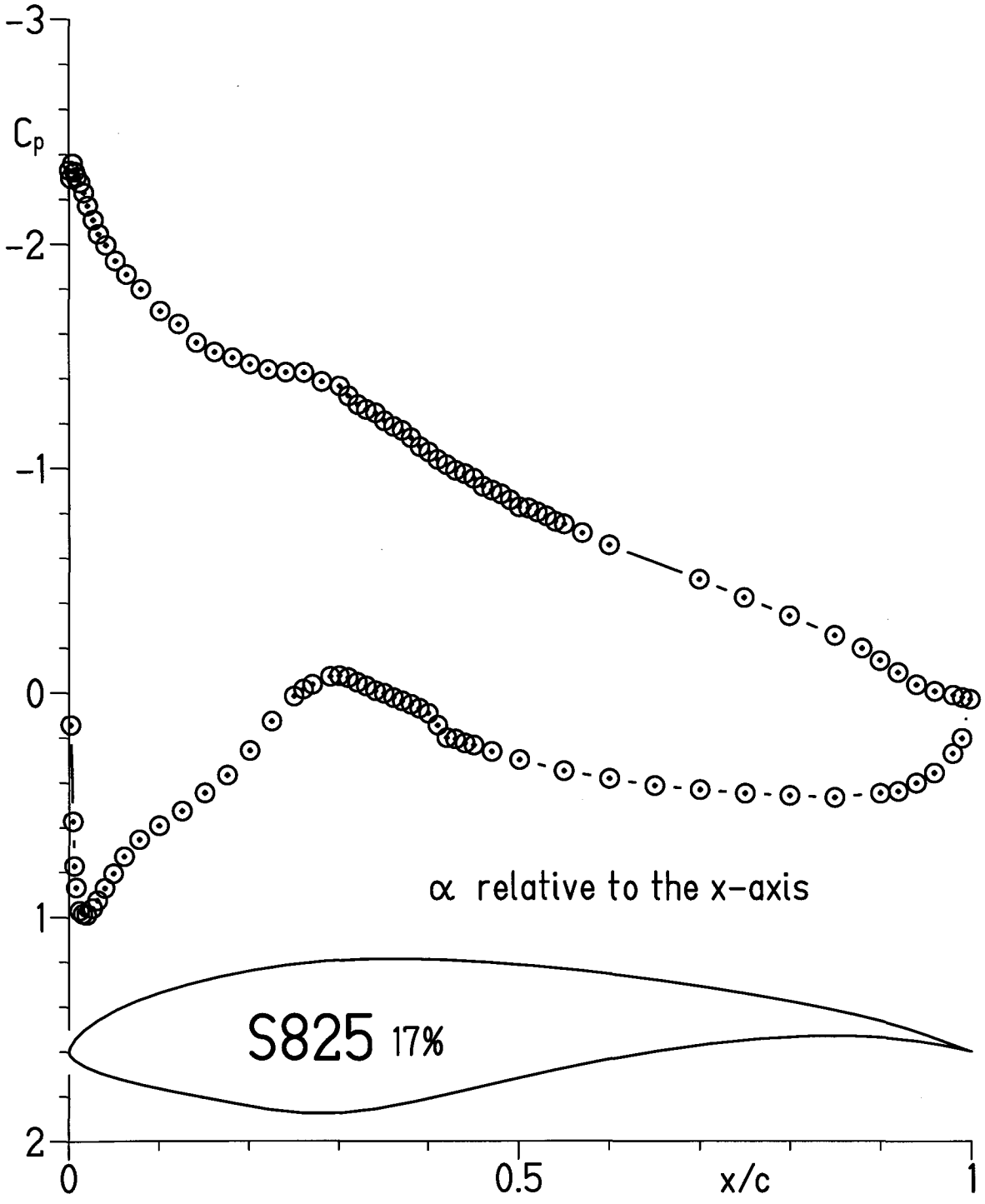

(h) $\alpha = 7.06°$.

Figure 5.- Continued.

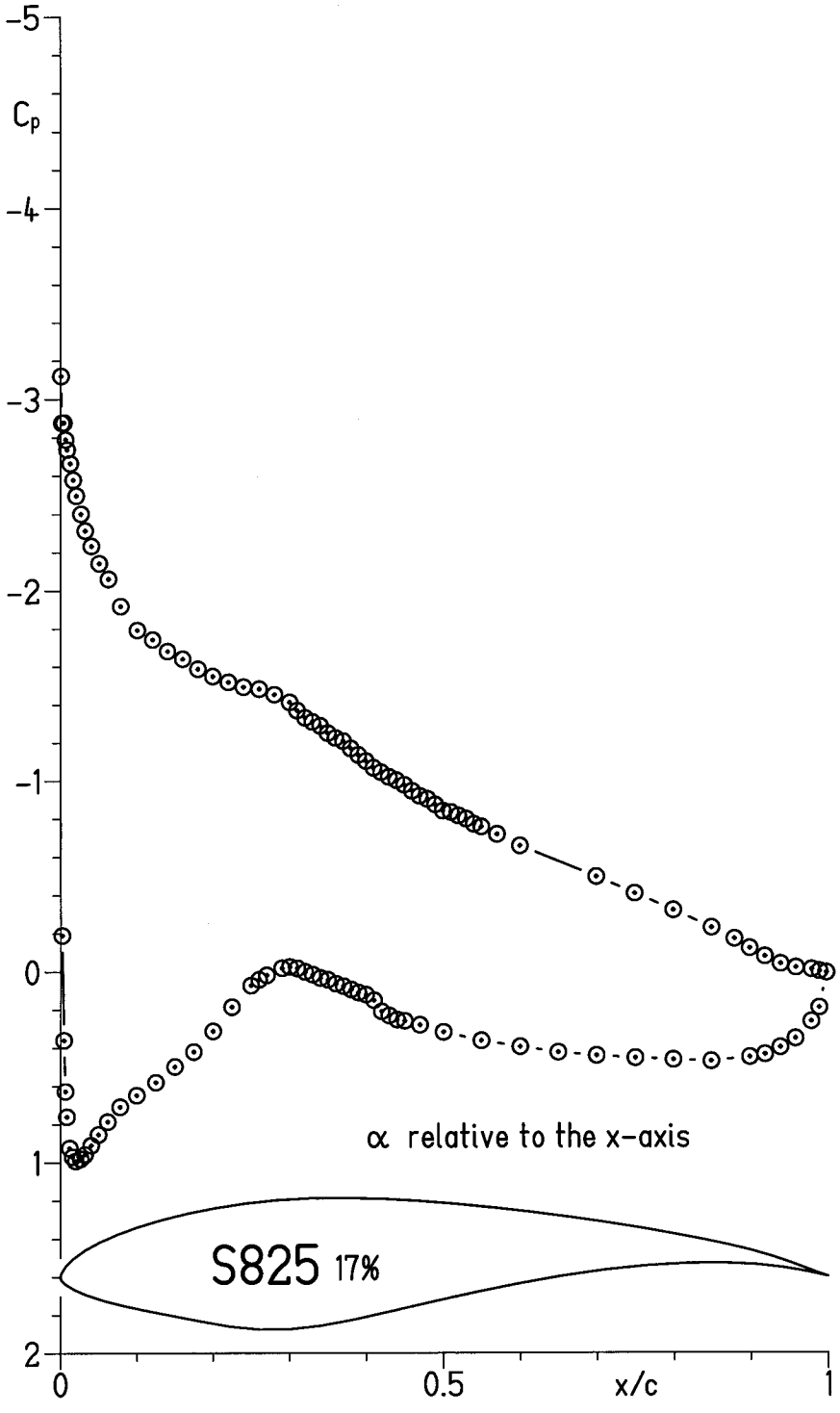

(i) $\alpha = 8.06°$.

Figure 5.- Continued.

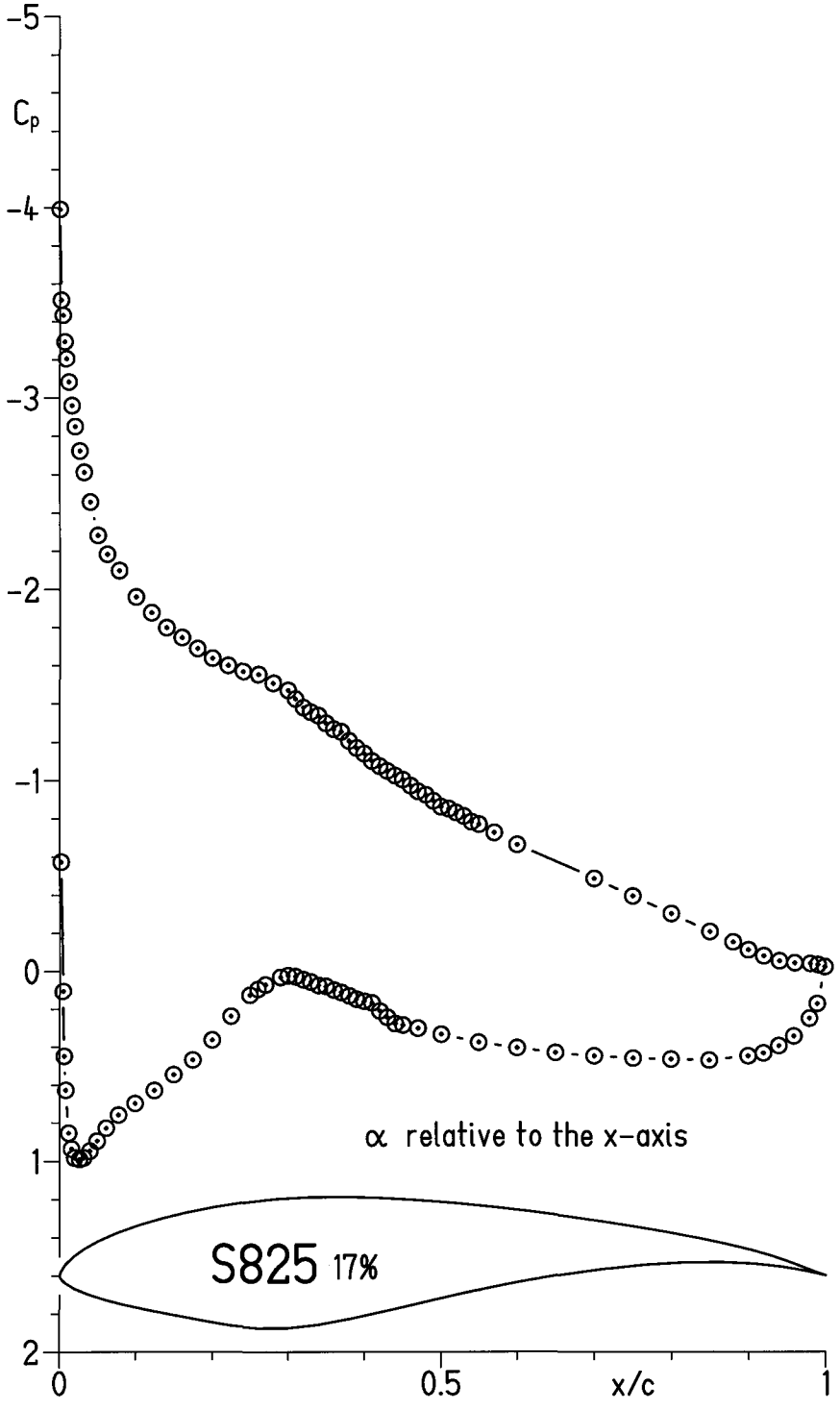

(j) $\alpha = 9.06°$.

Figure 5.- Continued.

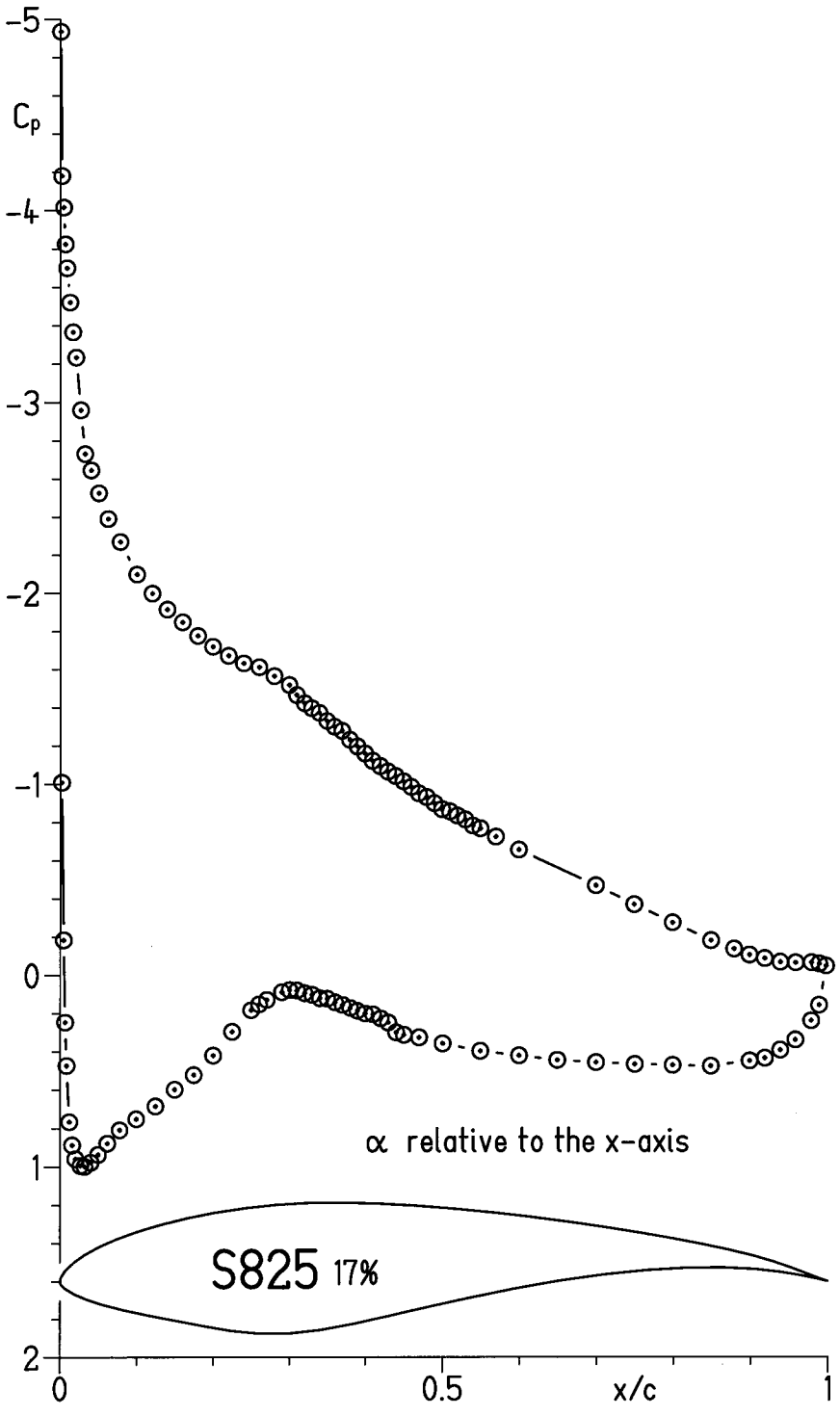

(k) $\alpha = 10.09°$.

Figure 5.- Continued.

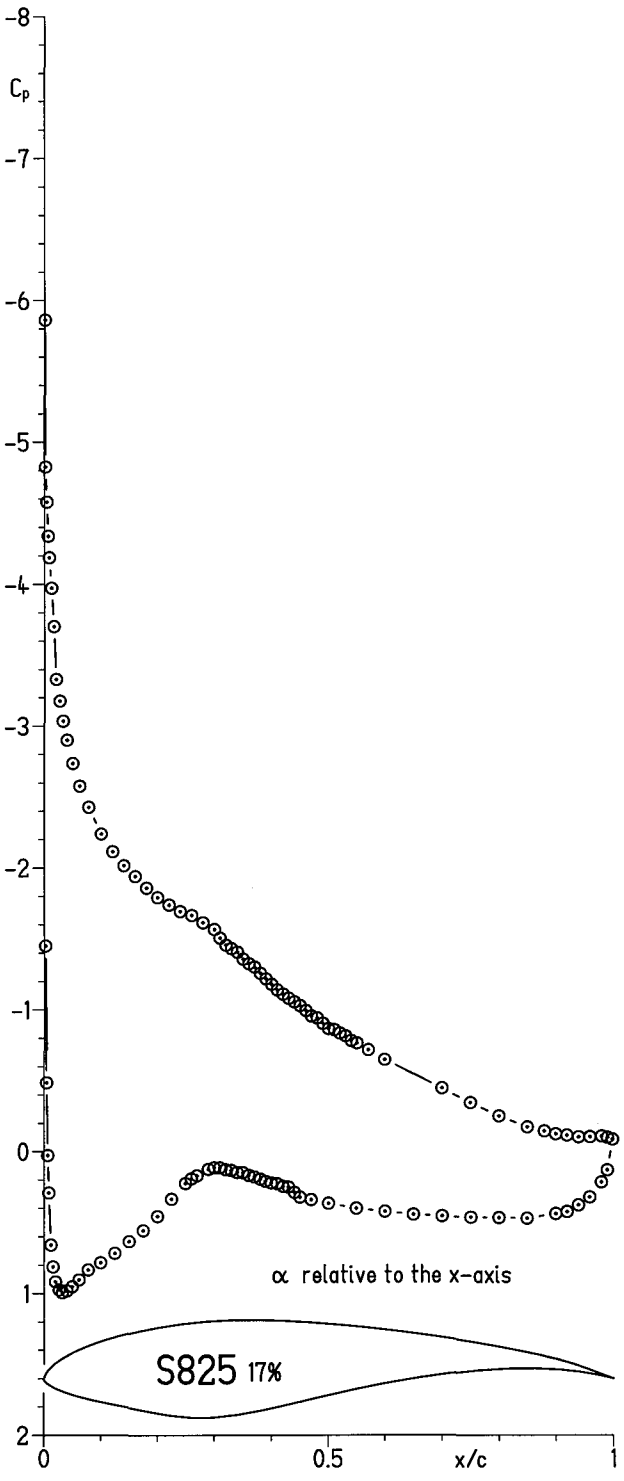

(l) $\alpha = 11.08°$.

Figure 5.- Continued.

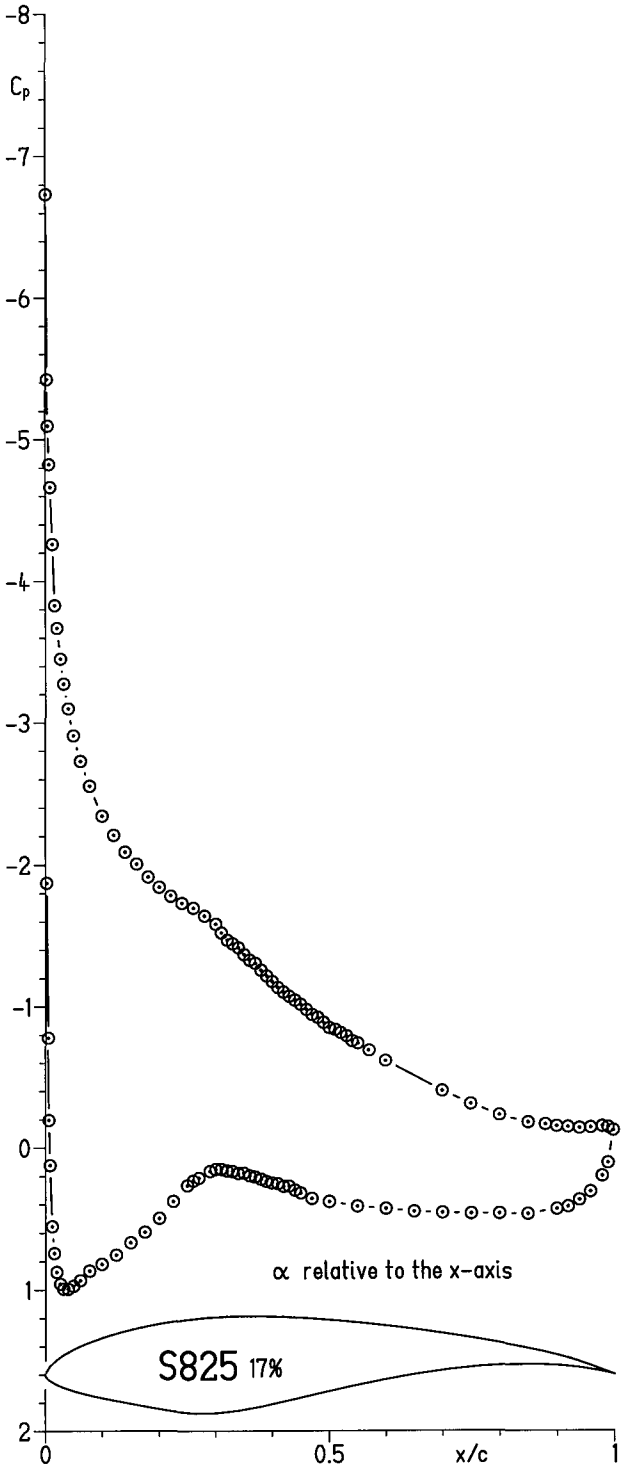

(m) $\alpha = 12.08°$.

Figure 5.- Continued.

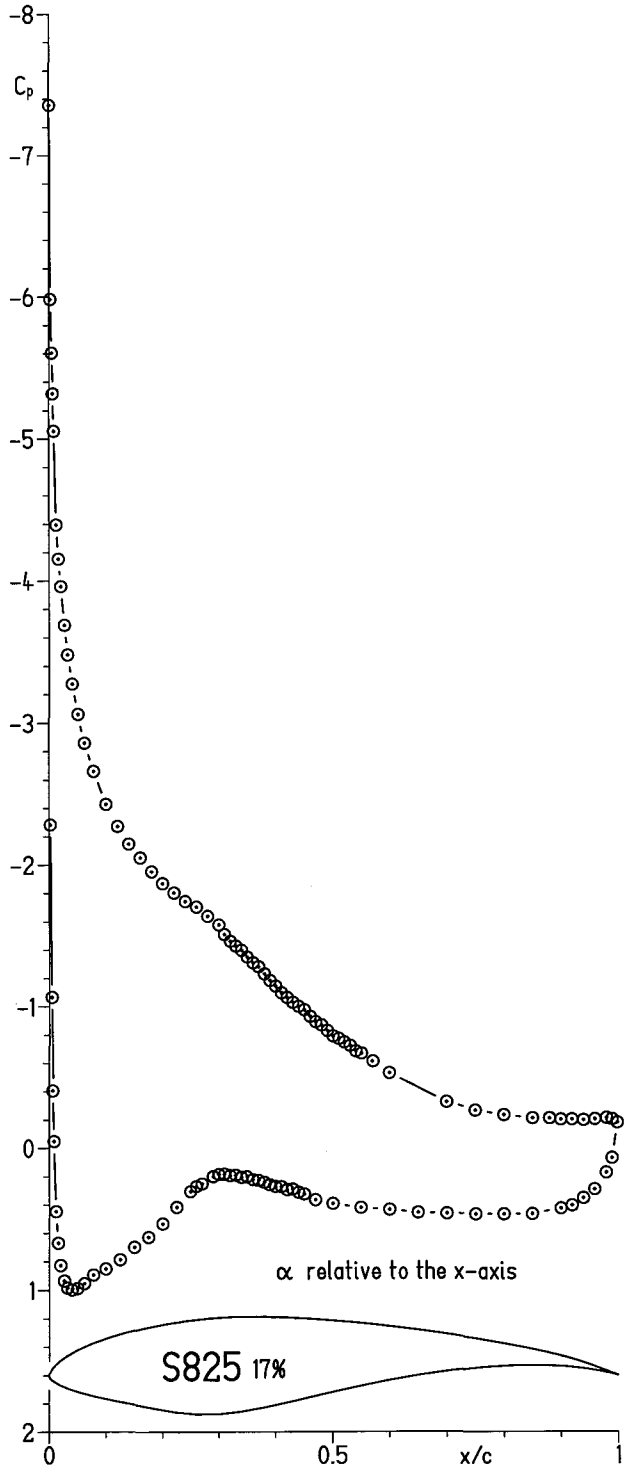

(n) $\alpha = 13.10°$.

Figure 5.- Continued.

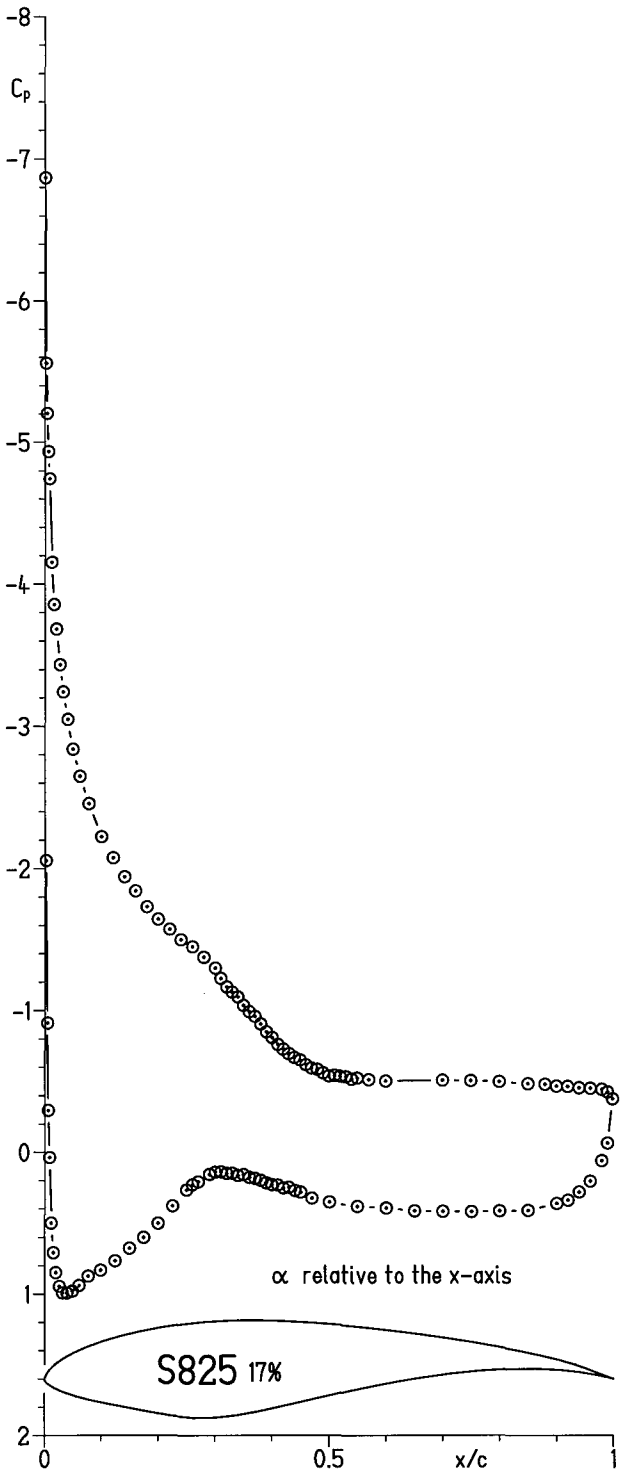

(o) $\alpha = 14.09°$.

Figure 5.- Continued.

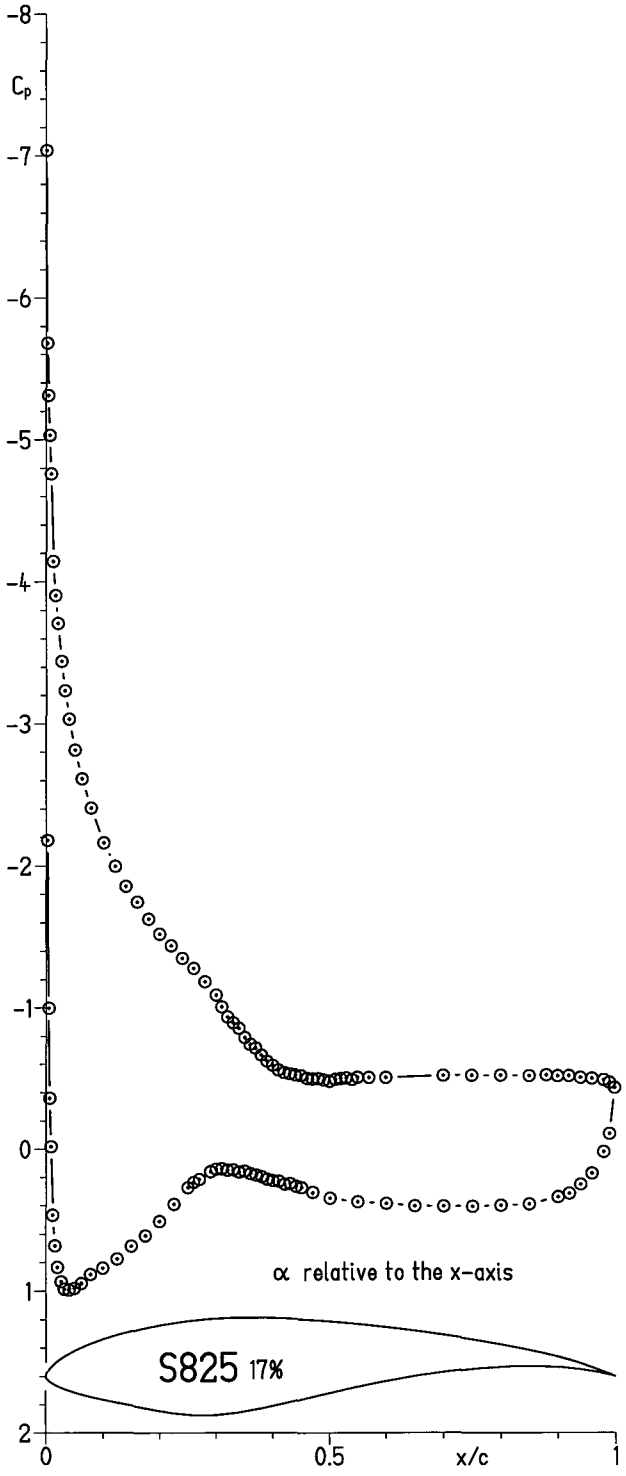

(p) $\alpha = 15.07°$.

Figure 5.- Continued.

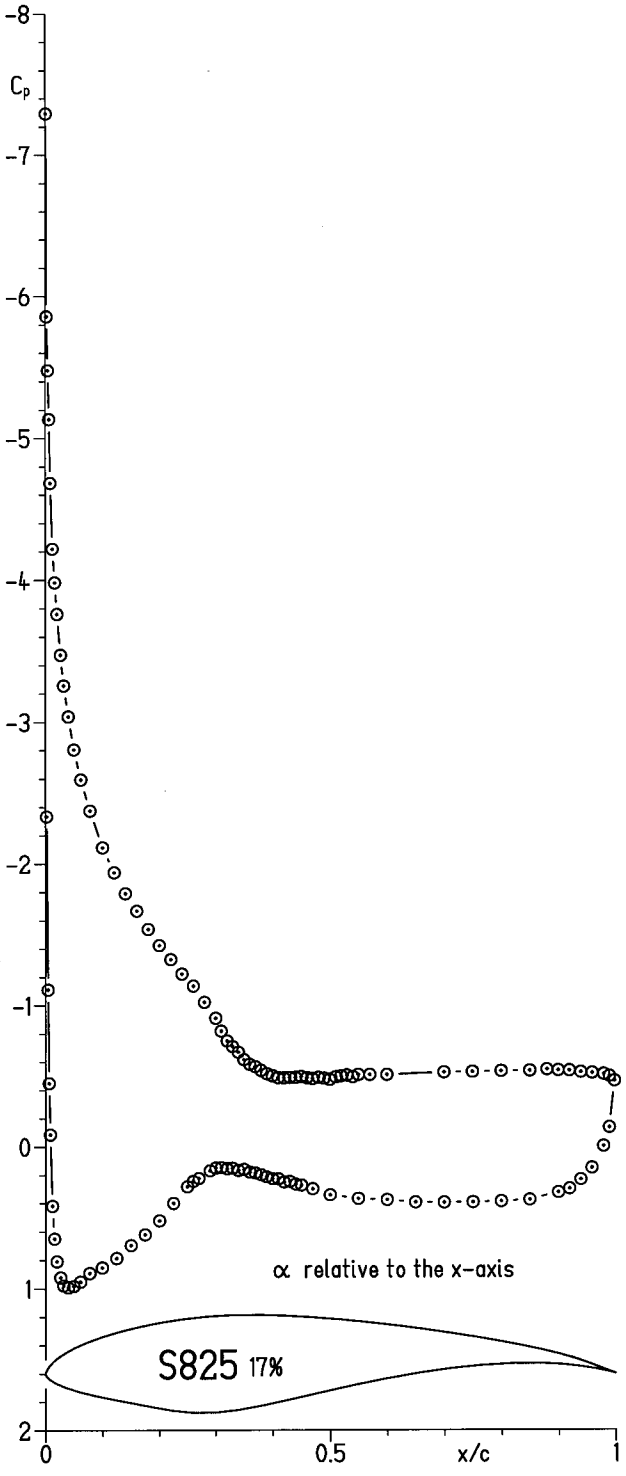

(q) $\alpha = 16.06°$.

Figure 5.- Continued.

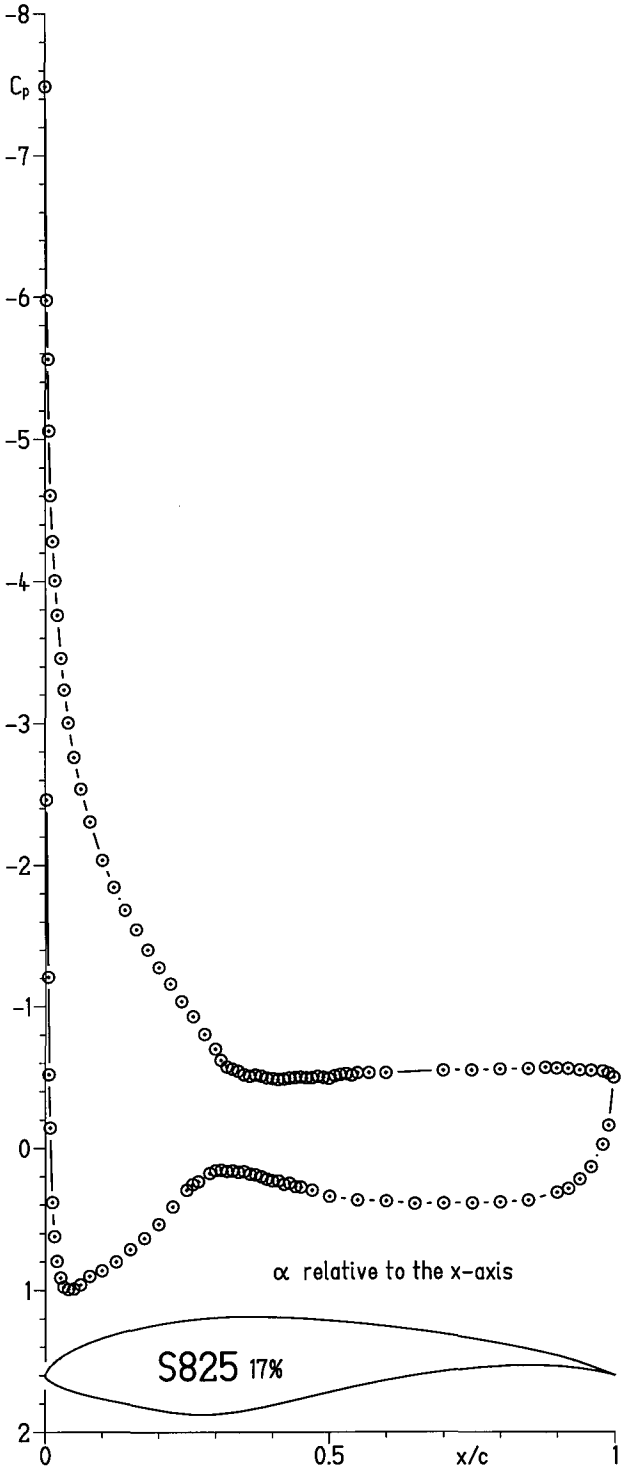

(r) $\alpha = 17.06°$.

Figure 5.- Continued.

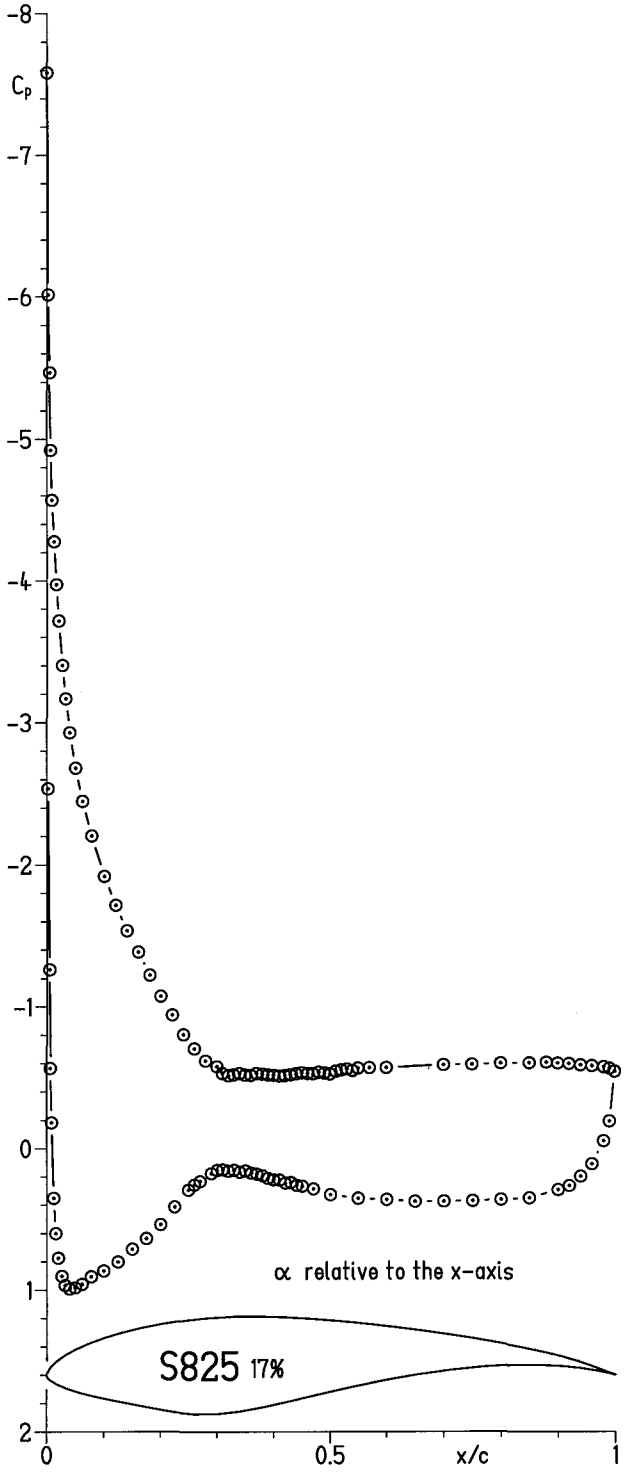

(s) $\alpha = 18.06°$.

Figure 5.- Continued.

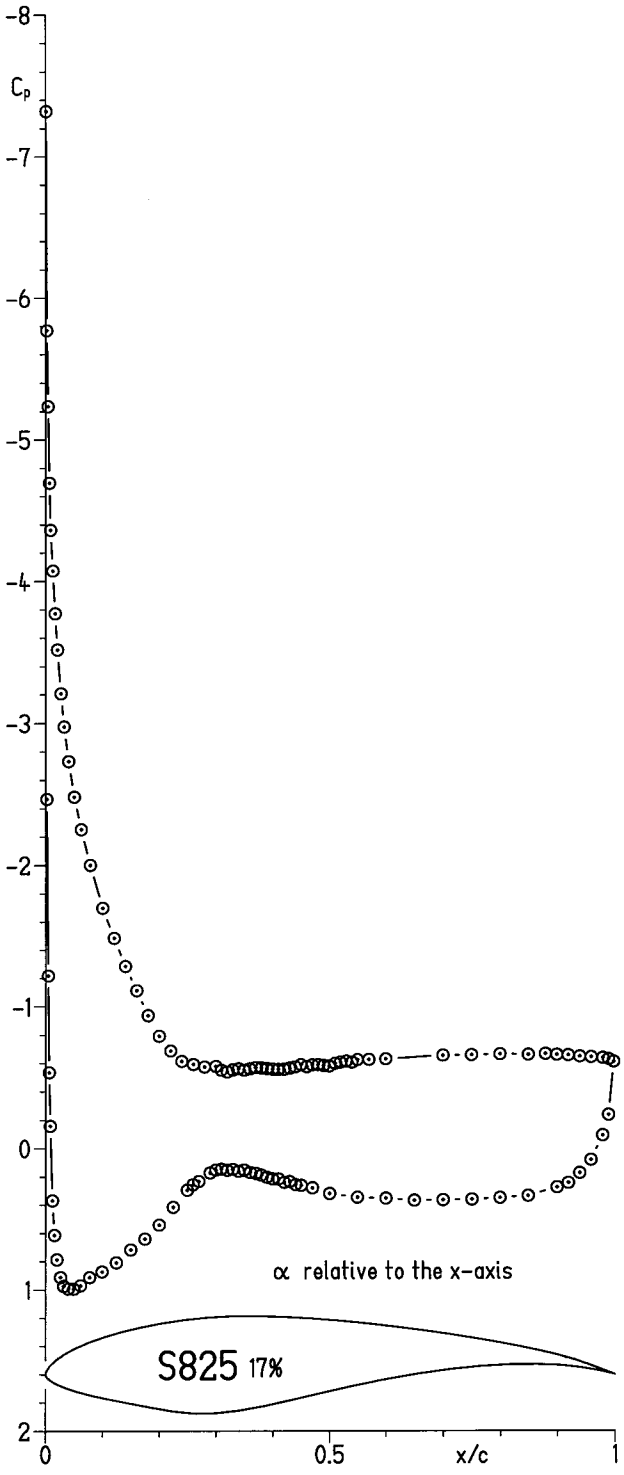

(t) $\alpha = 19.05°$.

Figure 5.- Continued.

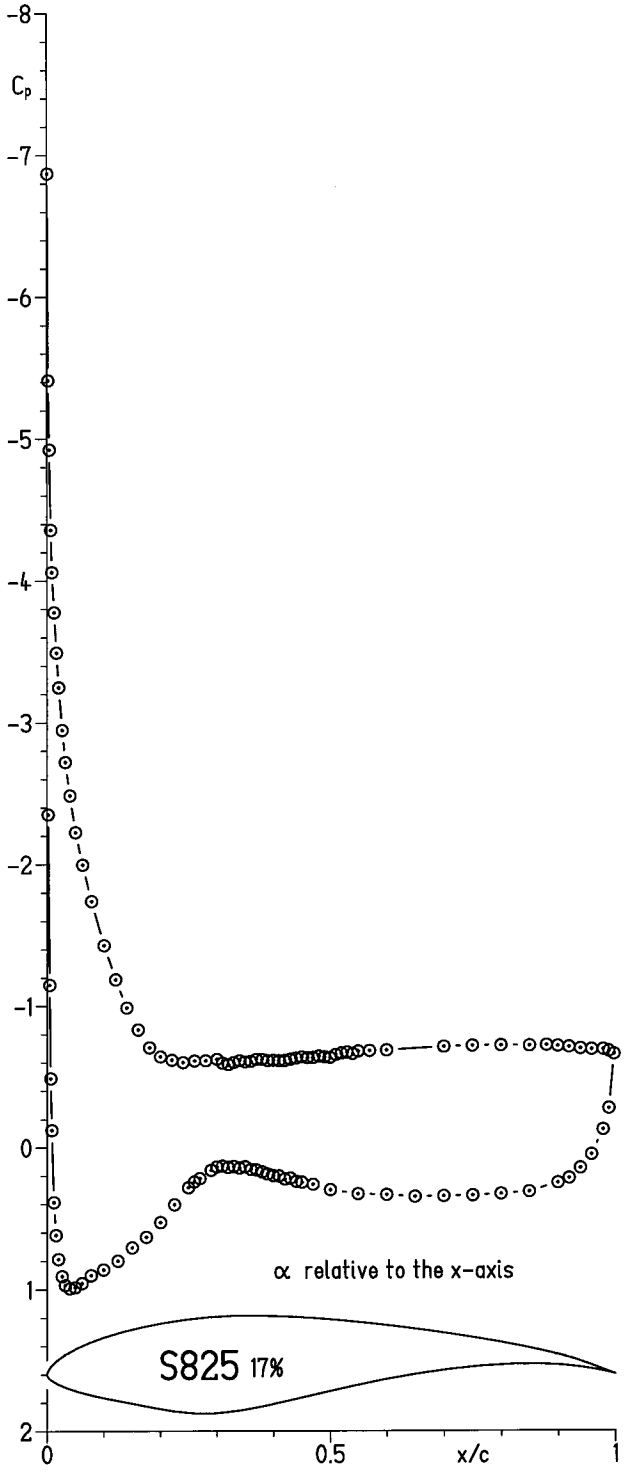

(u) $\alpha = 20.03°$.

Figure 5.- Continued.

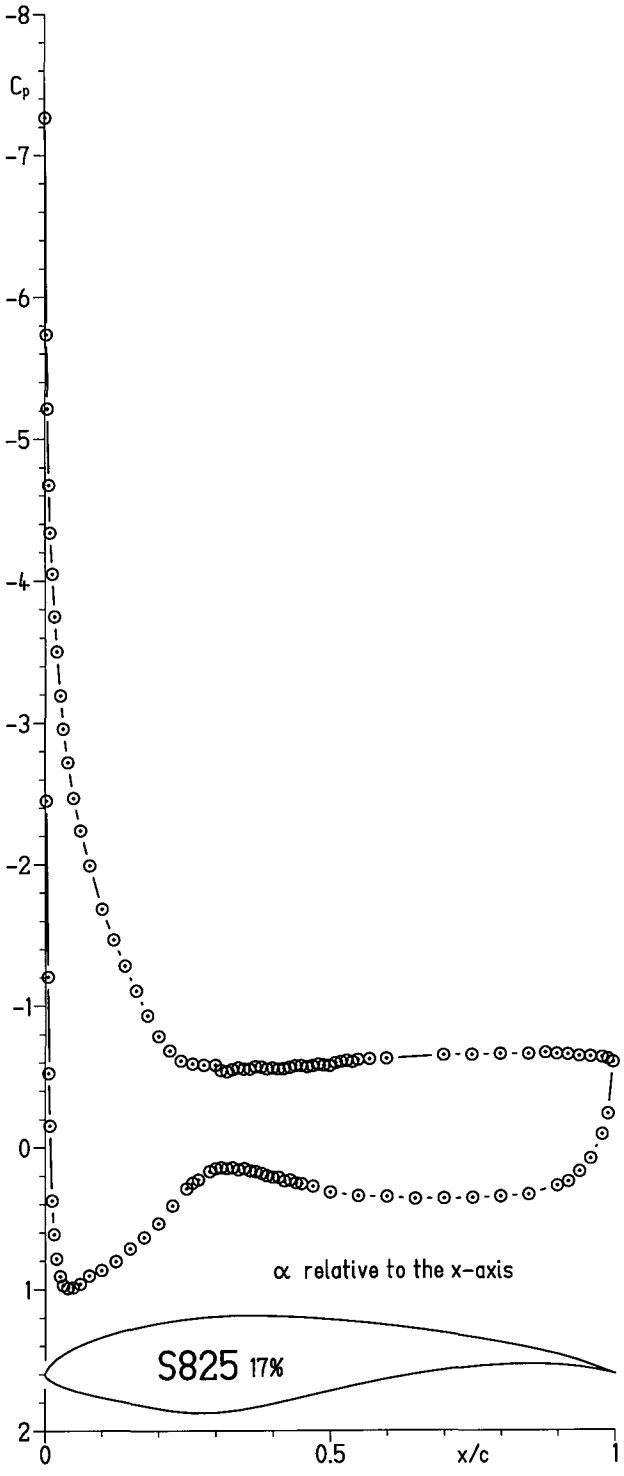

(v) $\alpha = 19.05°$.

Figure 5.- Continued.

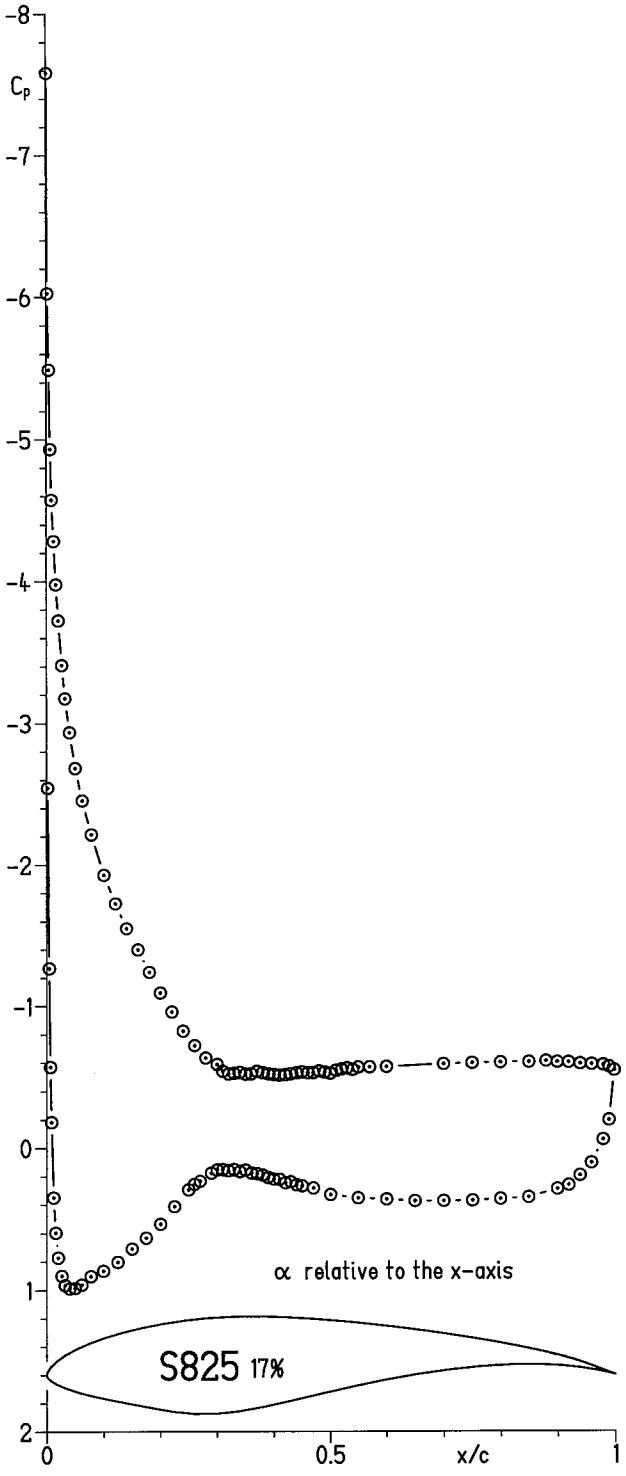

(w) $\alpha = 18.05°$.

Figure 5.- Continued.

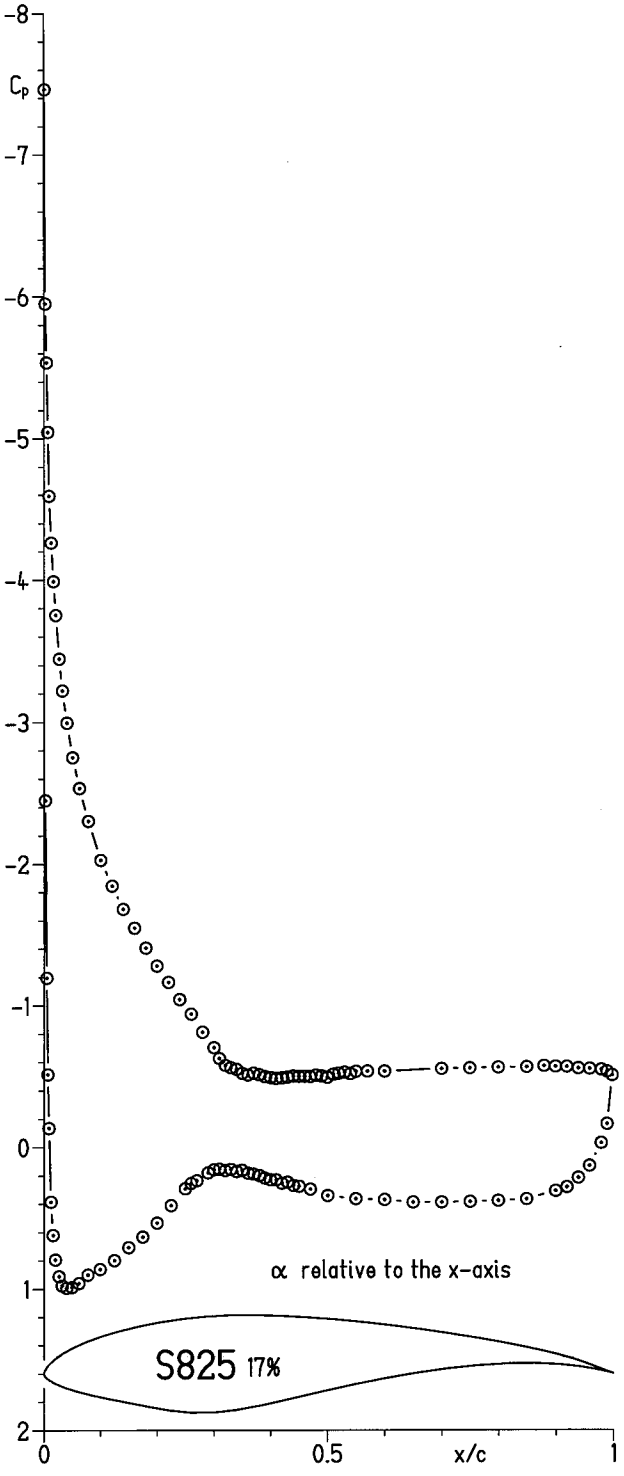

(x) $\alpha = 17.05°$.

Figure 5.- Continued.

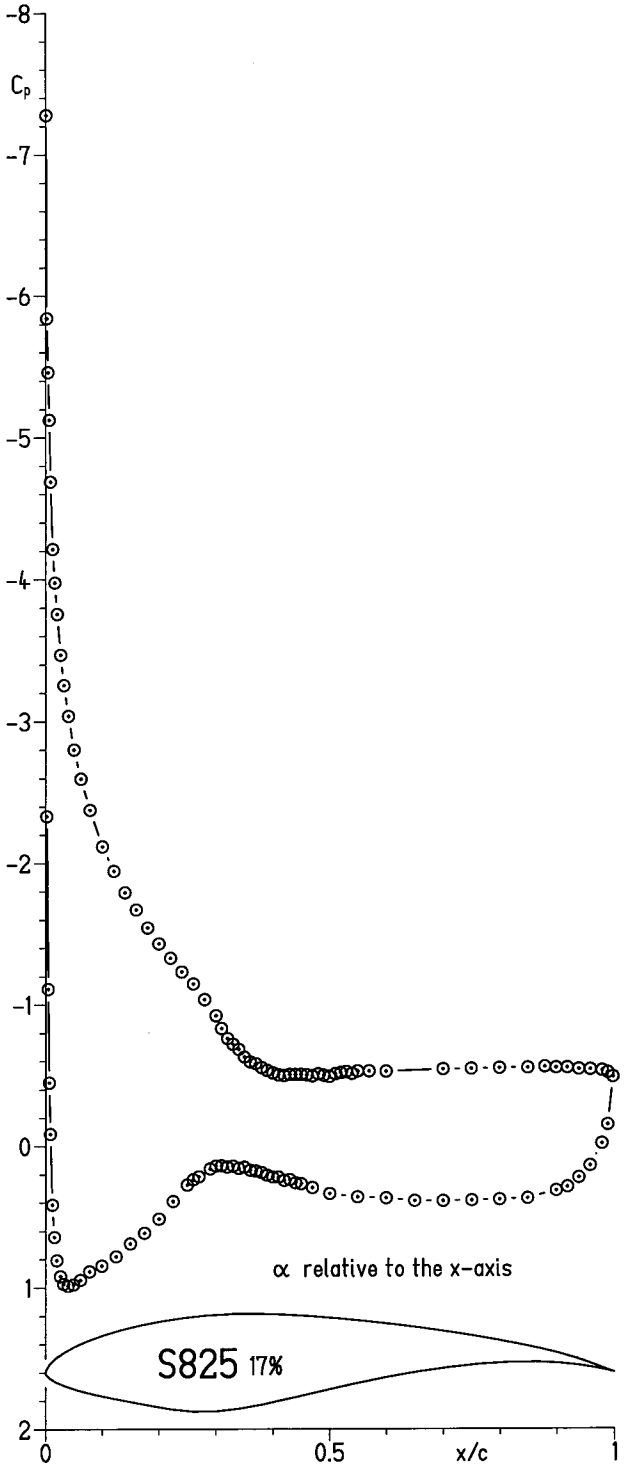

(y) $\alpha = 16.06°$.

Figure 5.- Continued.

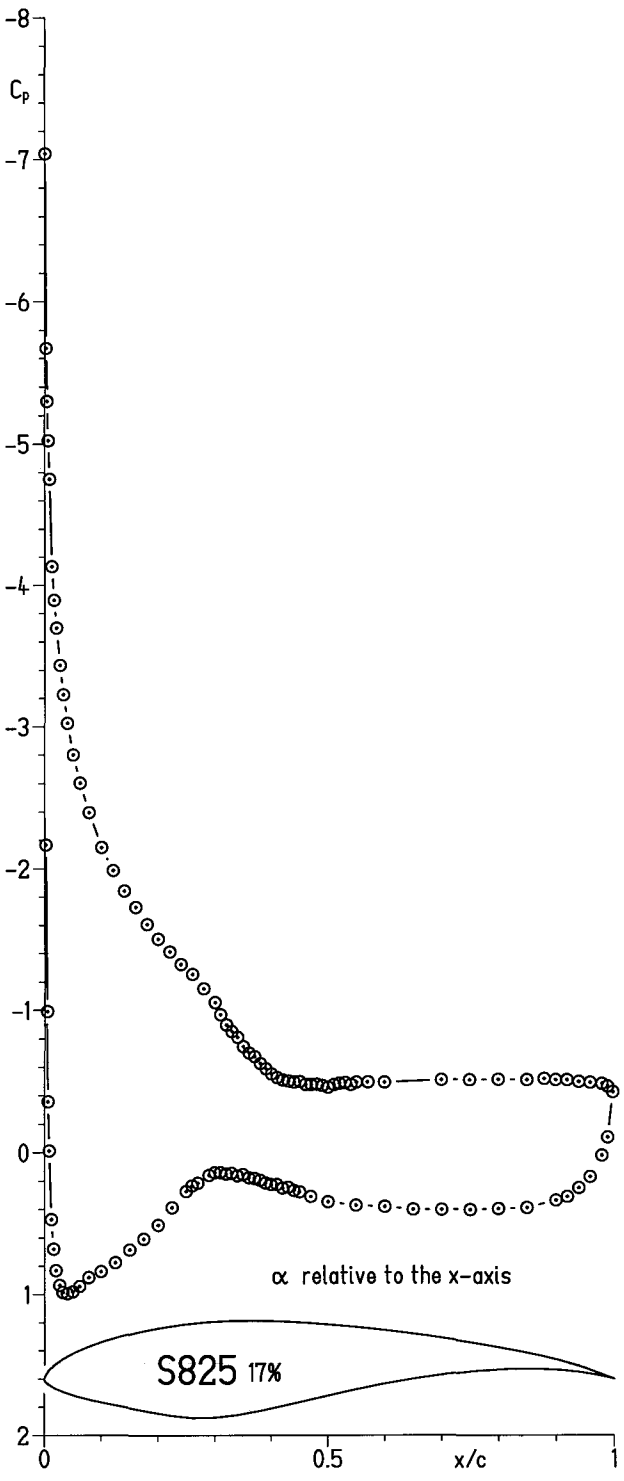

(z) $\alpha = 15.07°$.

Figure 5.- Continued.

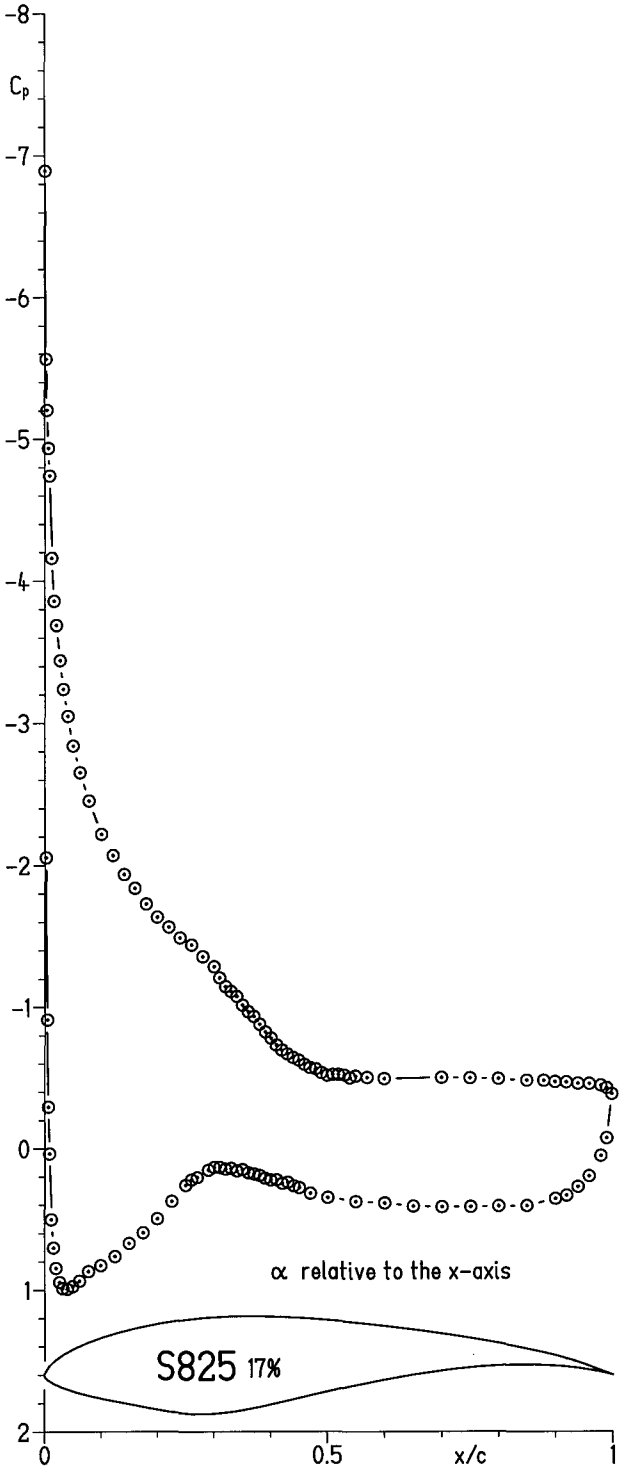

(aa) $\alpha = 14.07°$.

Figure 5.- Continued.

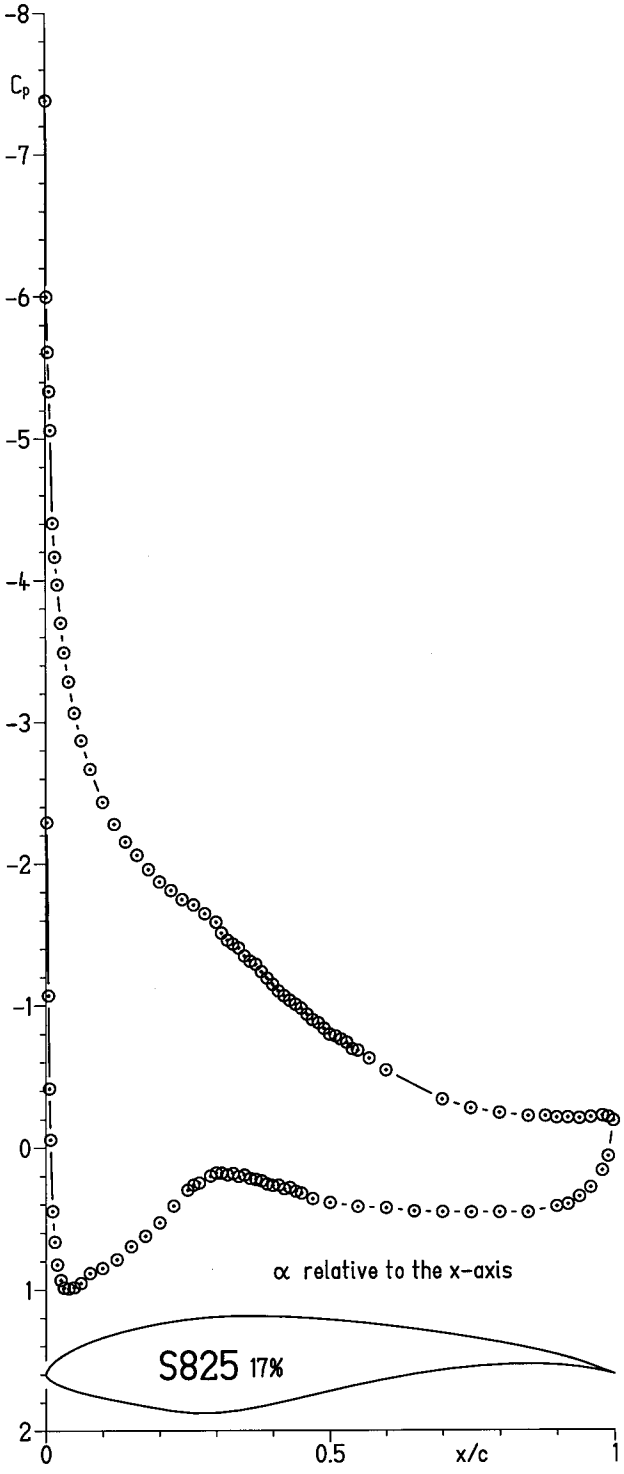

(bb) $\alpha = 13.09°$.

Figure 5.- Continued.

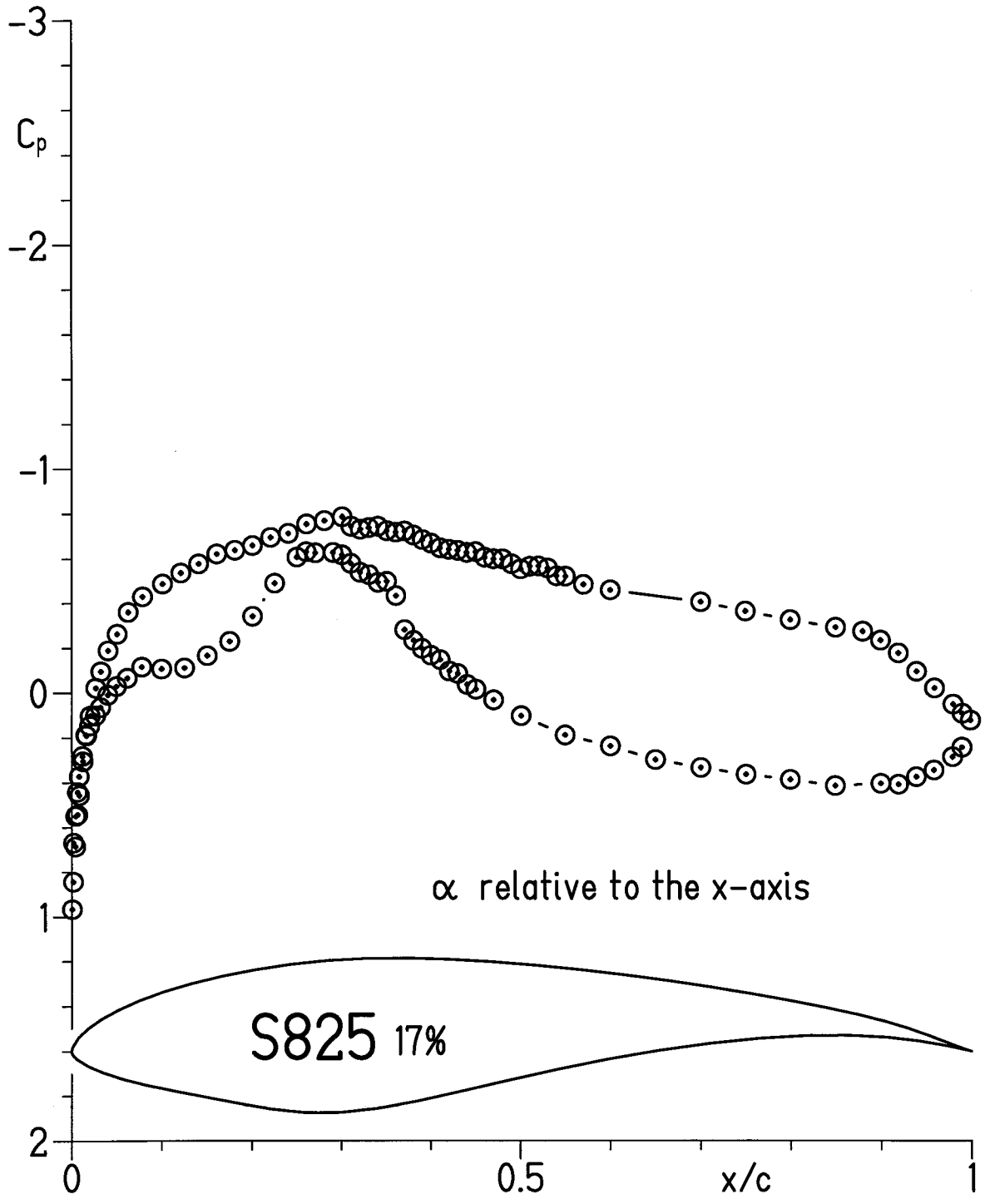

(cc) $\alpha = -1.03°$.

Figure 5.- Continued.

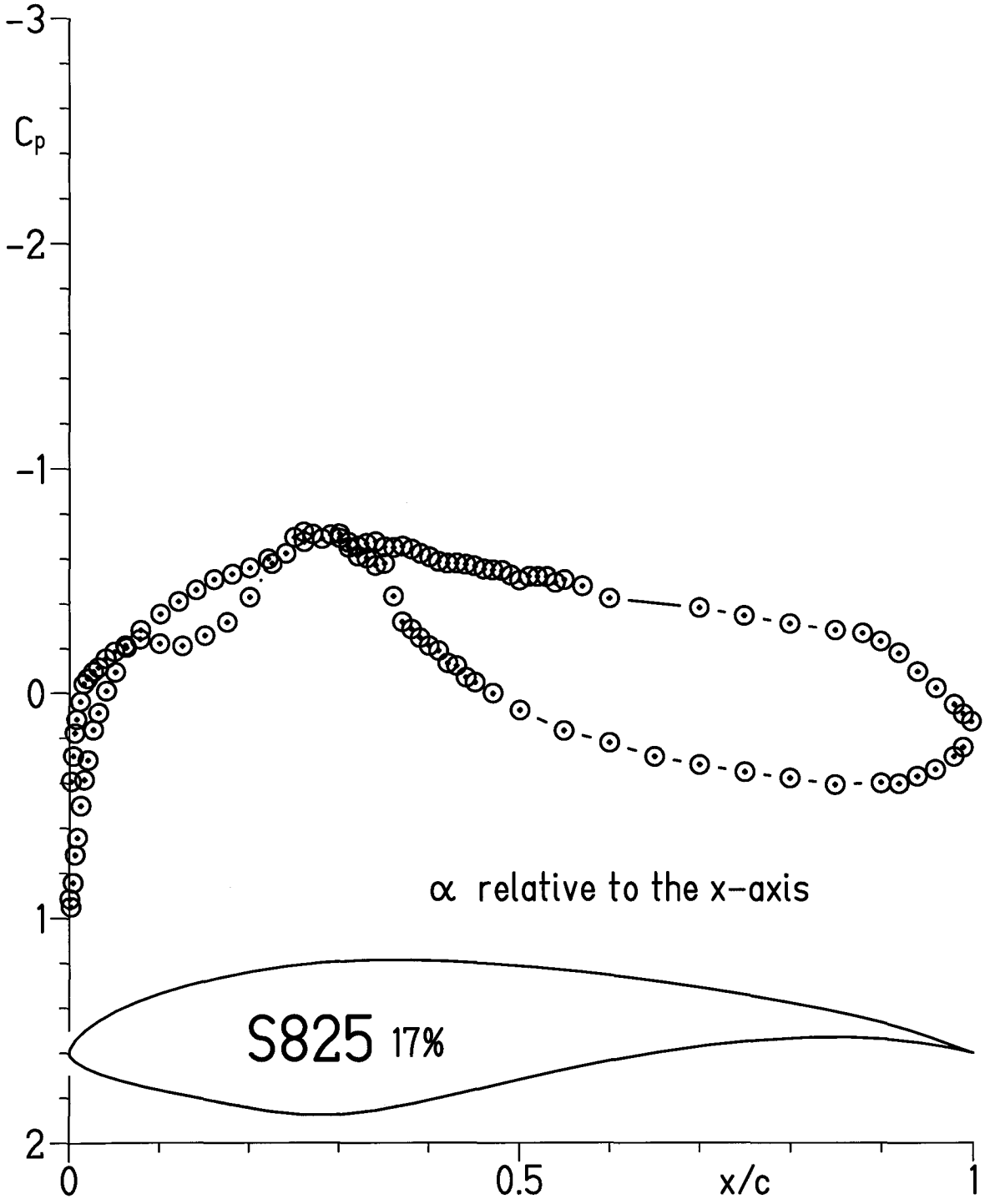

(dd) $\alpha = -2.02°$.

Figure 5.- Continued.

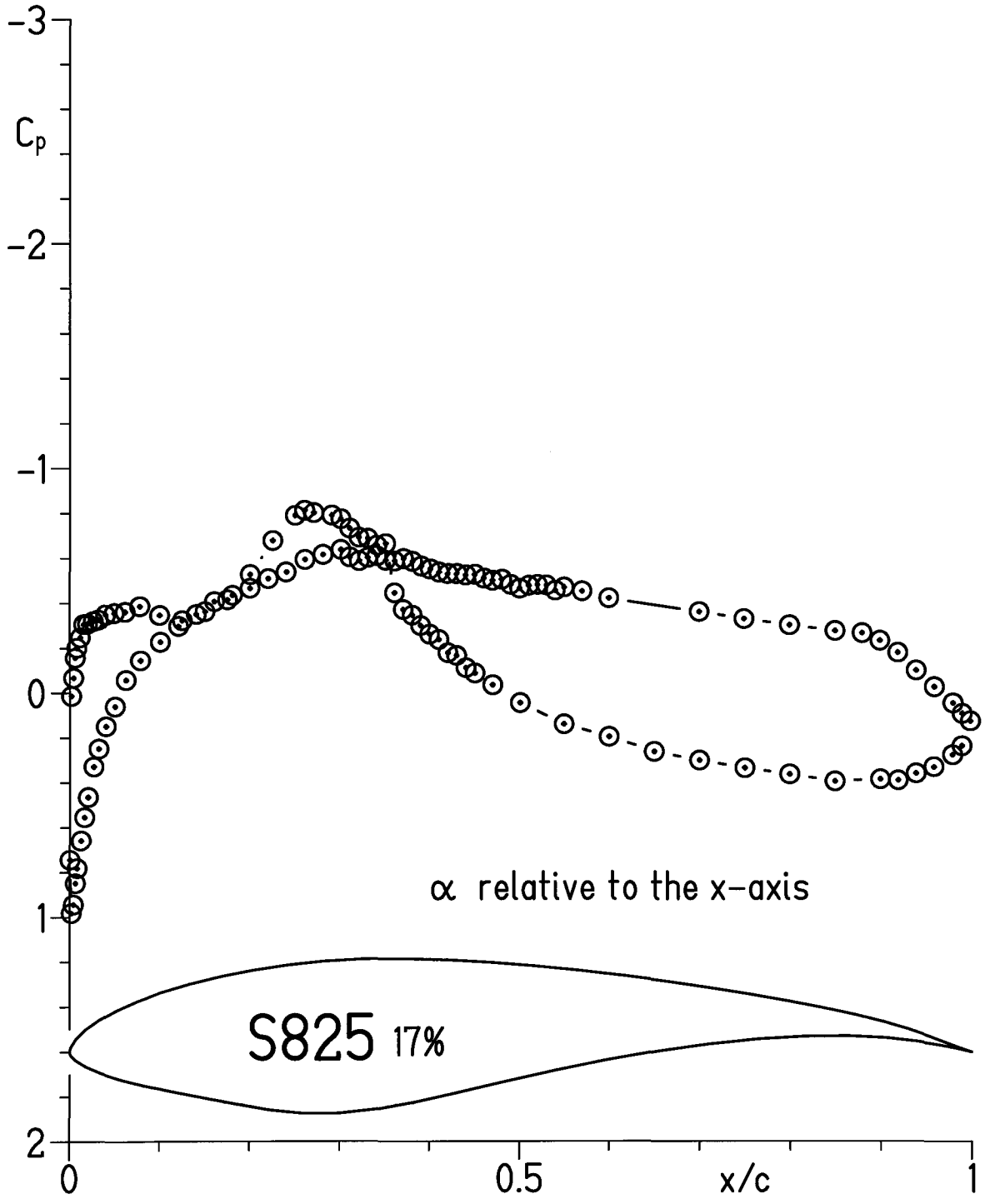

(ee) $\alpha = -3.02°$.

Figure 5.- Continued.

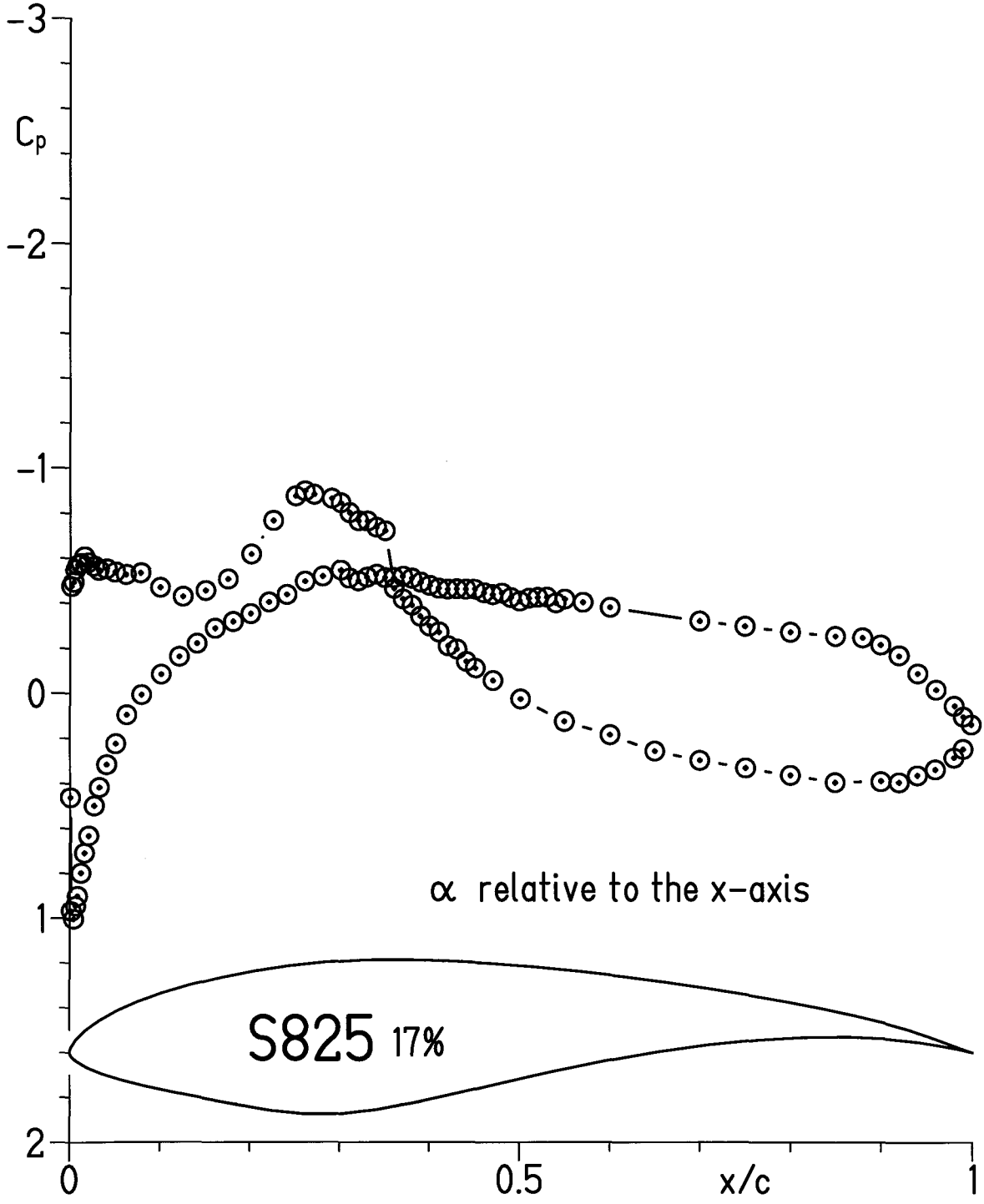

(ff) $\alpha = -4.09°$.

Figure 5.- Continued.

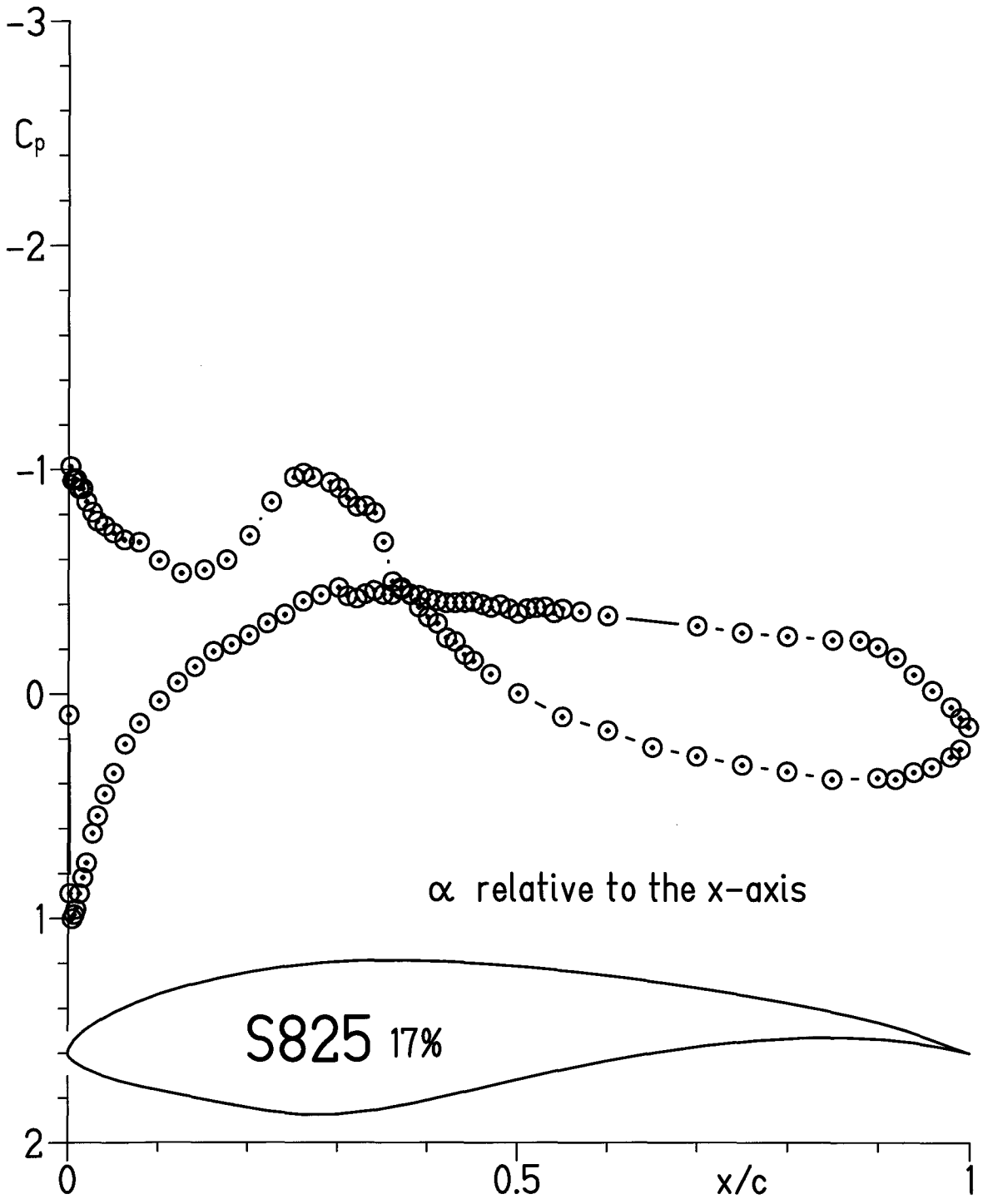

(gg) $\alpha = -5.04°$.

Figure 5.- Continued.

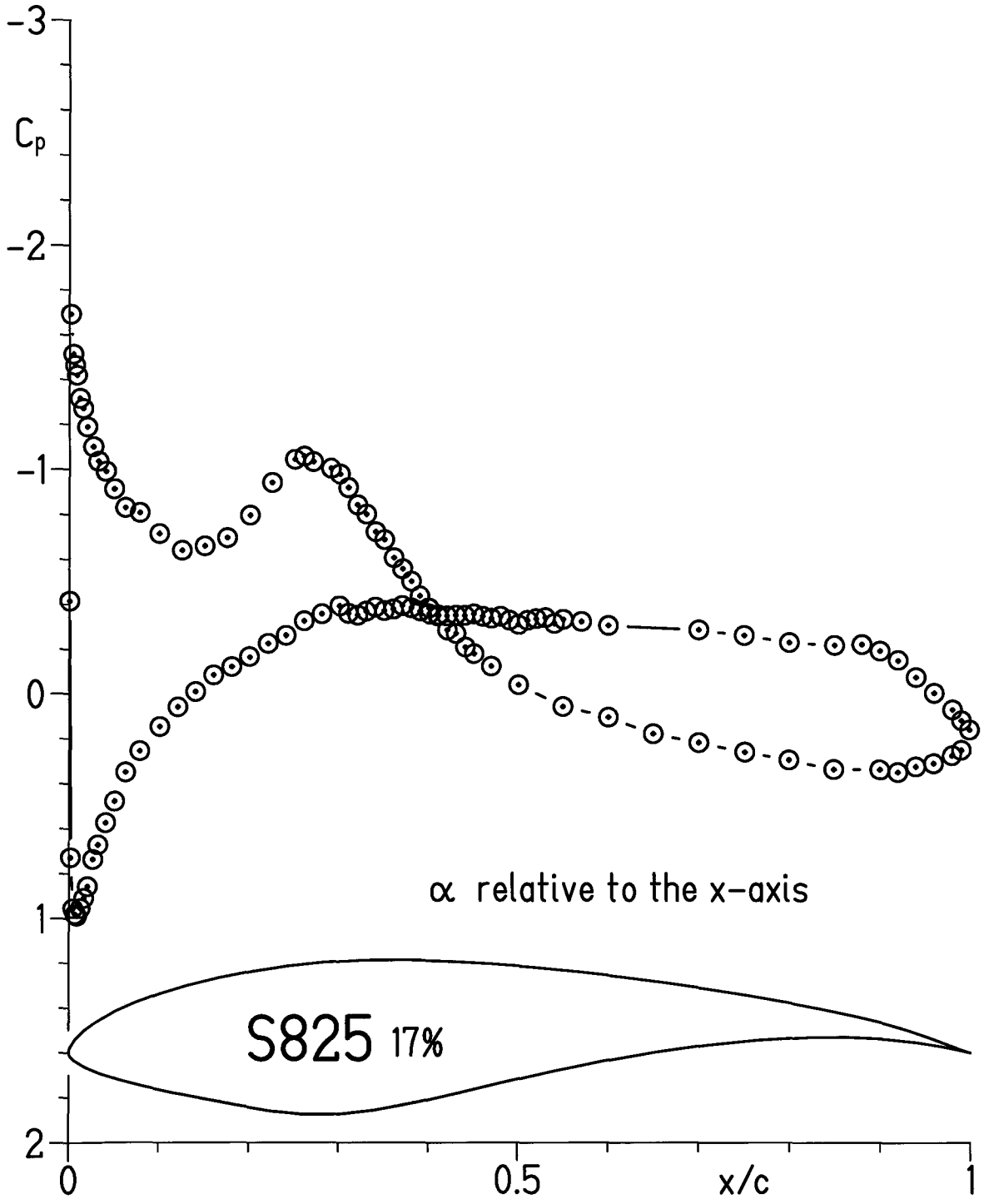

(hh) $\alpha = -6.04°$.

Figure 5.- Concluded.

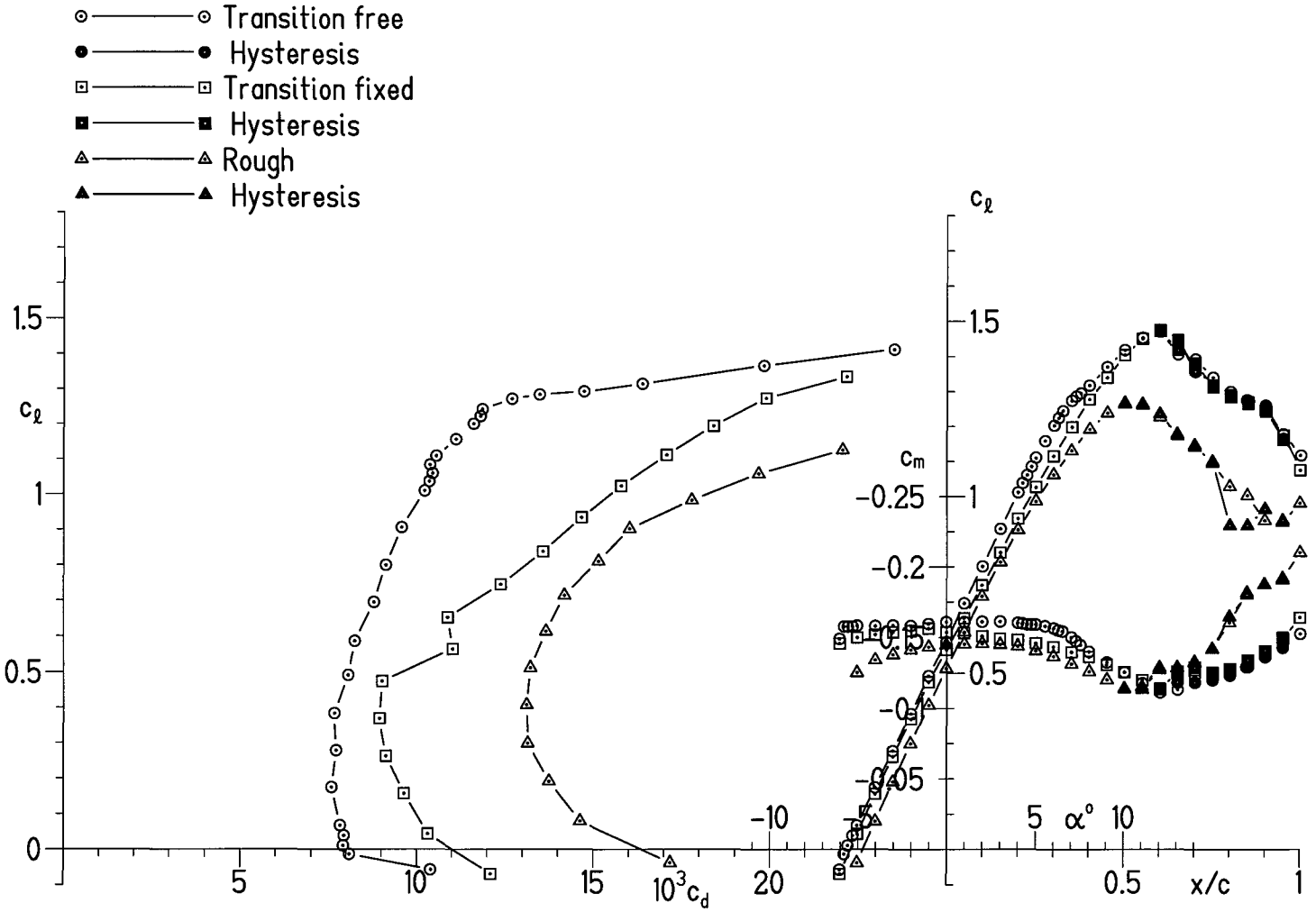

(a) $R = 1 \times 10^6$.

Figure 6.- Section characteristics with transition free, transition fixed, and rough.

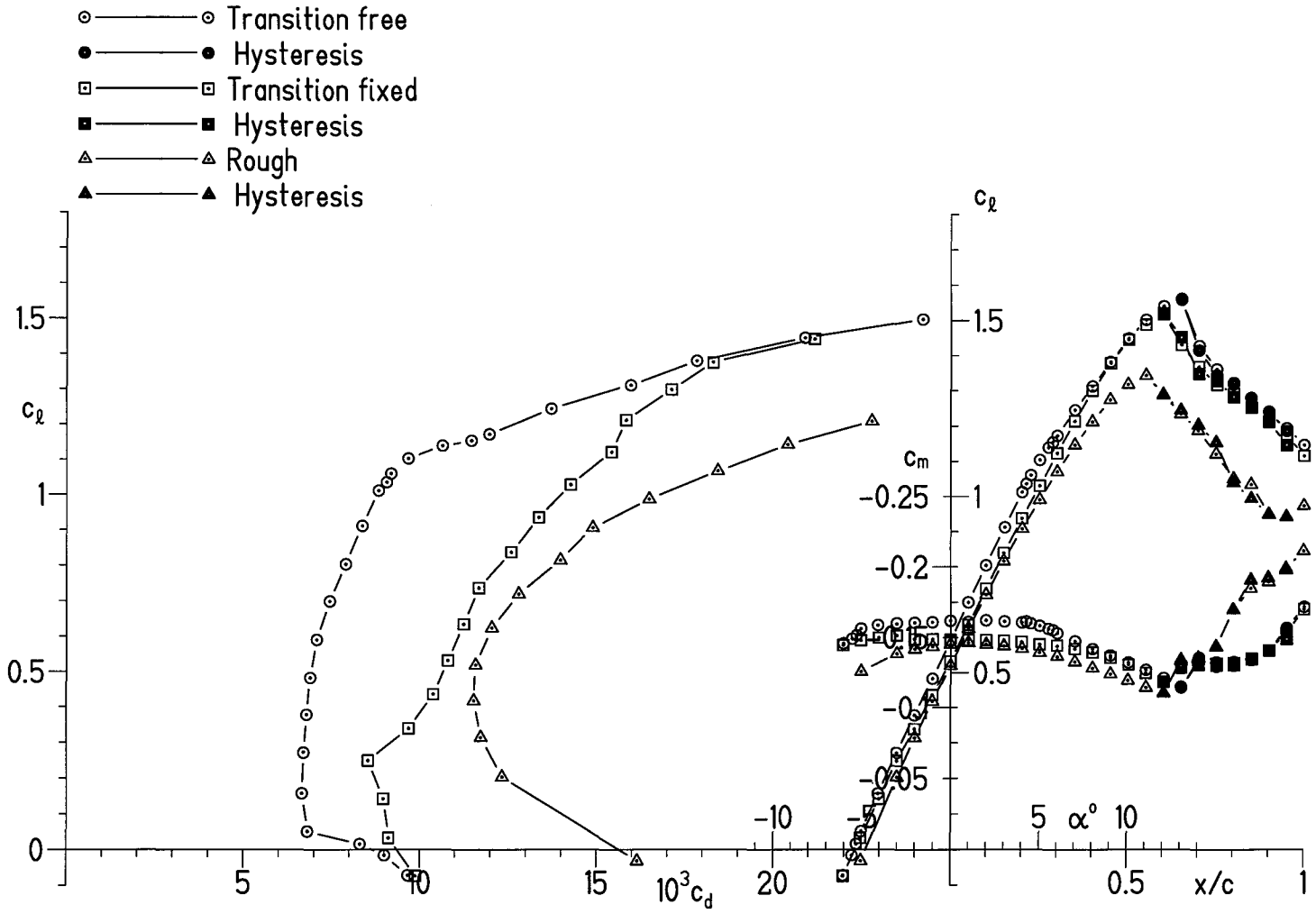

(b) $R = 2 \times 10^6$.

Figure 6.- Continued.

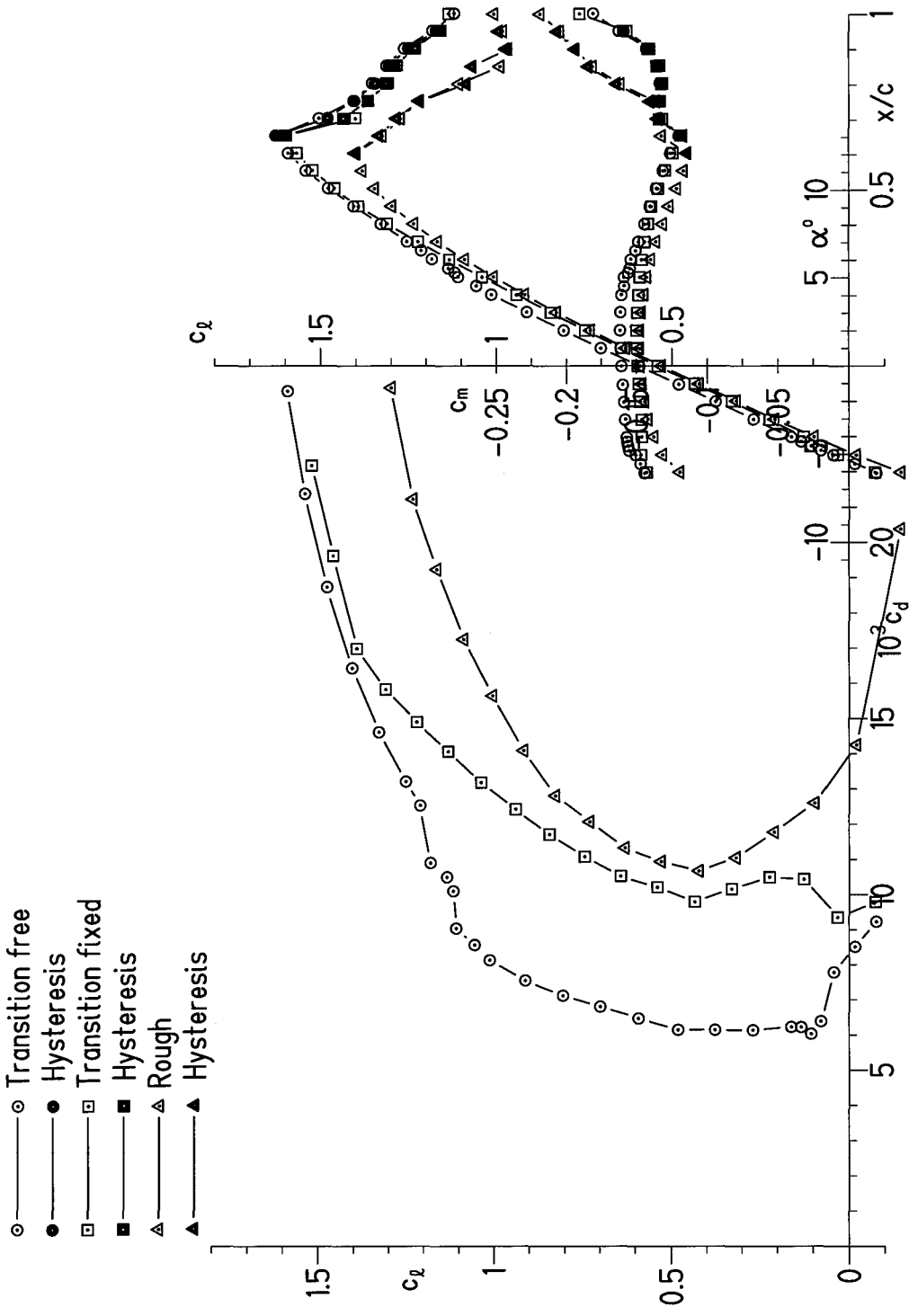

(c) $R = 3 \times 10^6$.

Figure 6.- Continued.

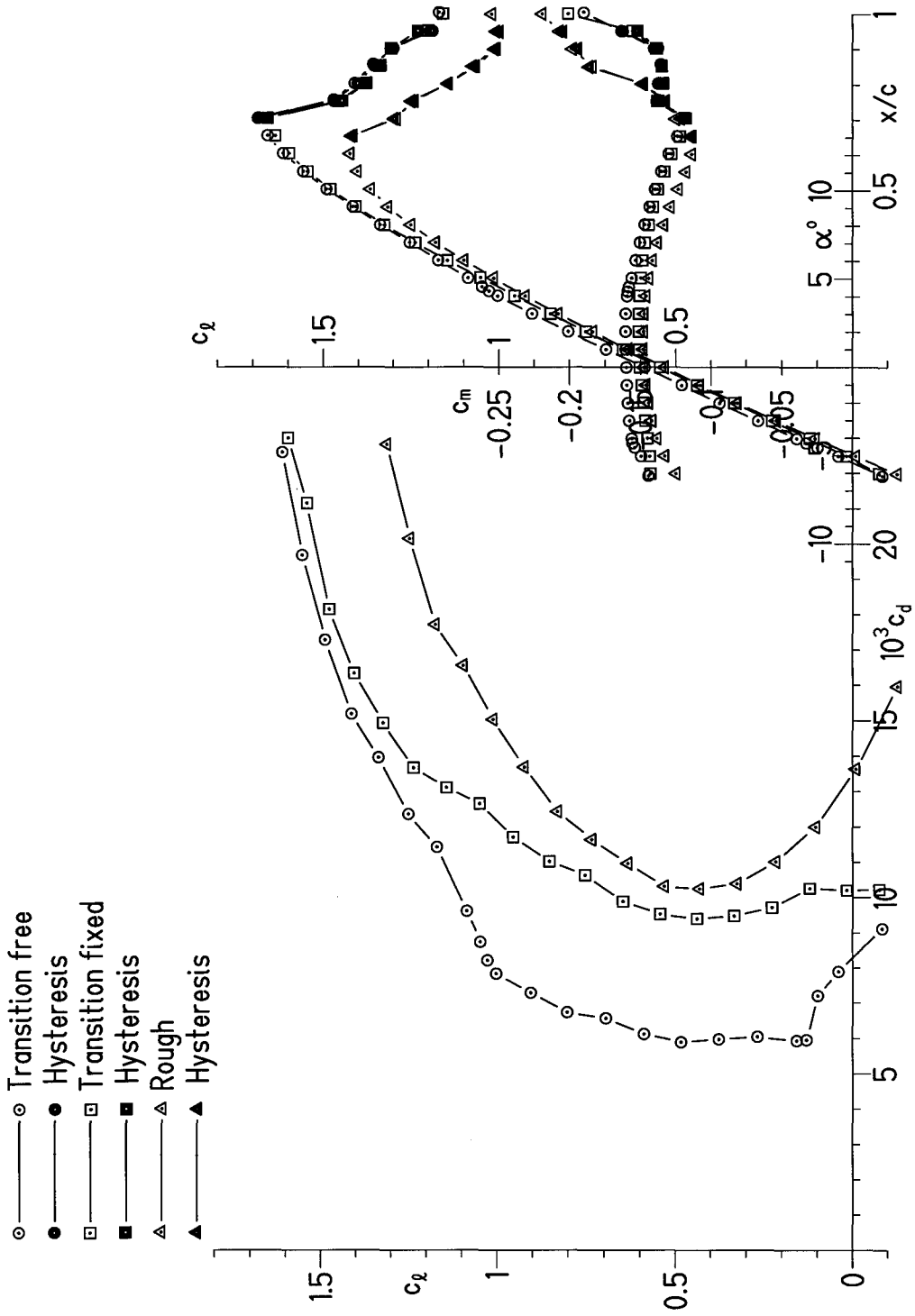

(d) $R = 4 \times 10^6$.

Figure 6.- Continued.

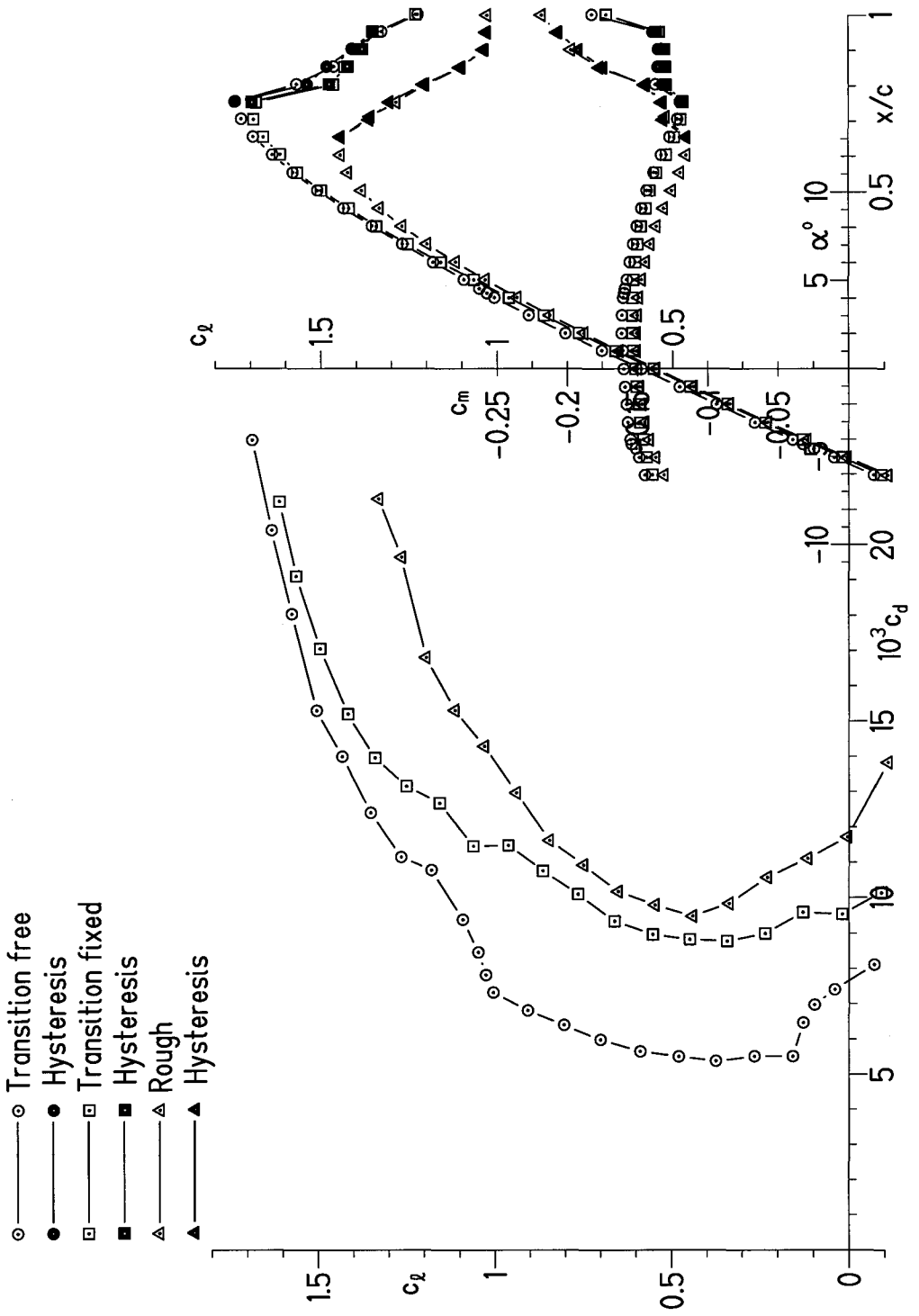

(e) $R = 6 \times 10^6$.

Figure 6.- Concluded.

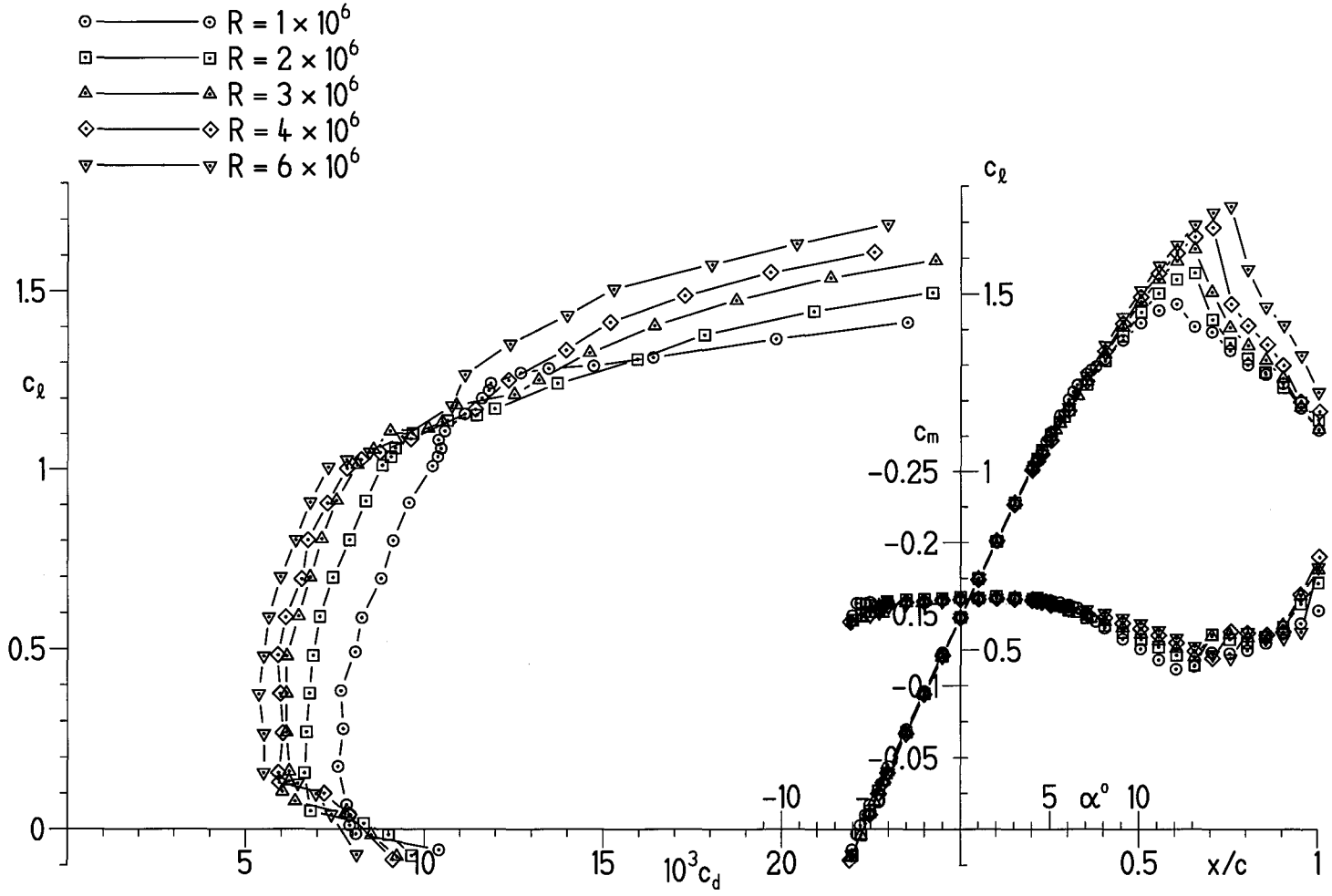

(a) Transition free.

Figure 7.- Effects of Reynolds number on section characteristics.

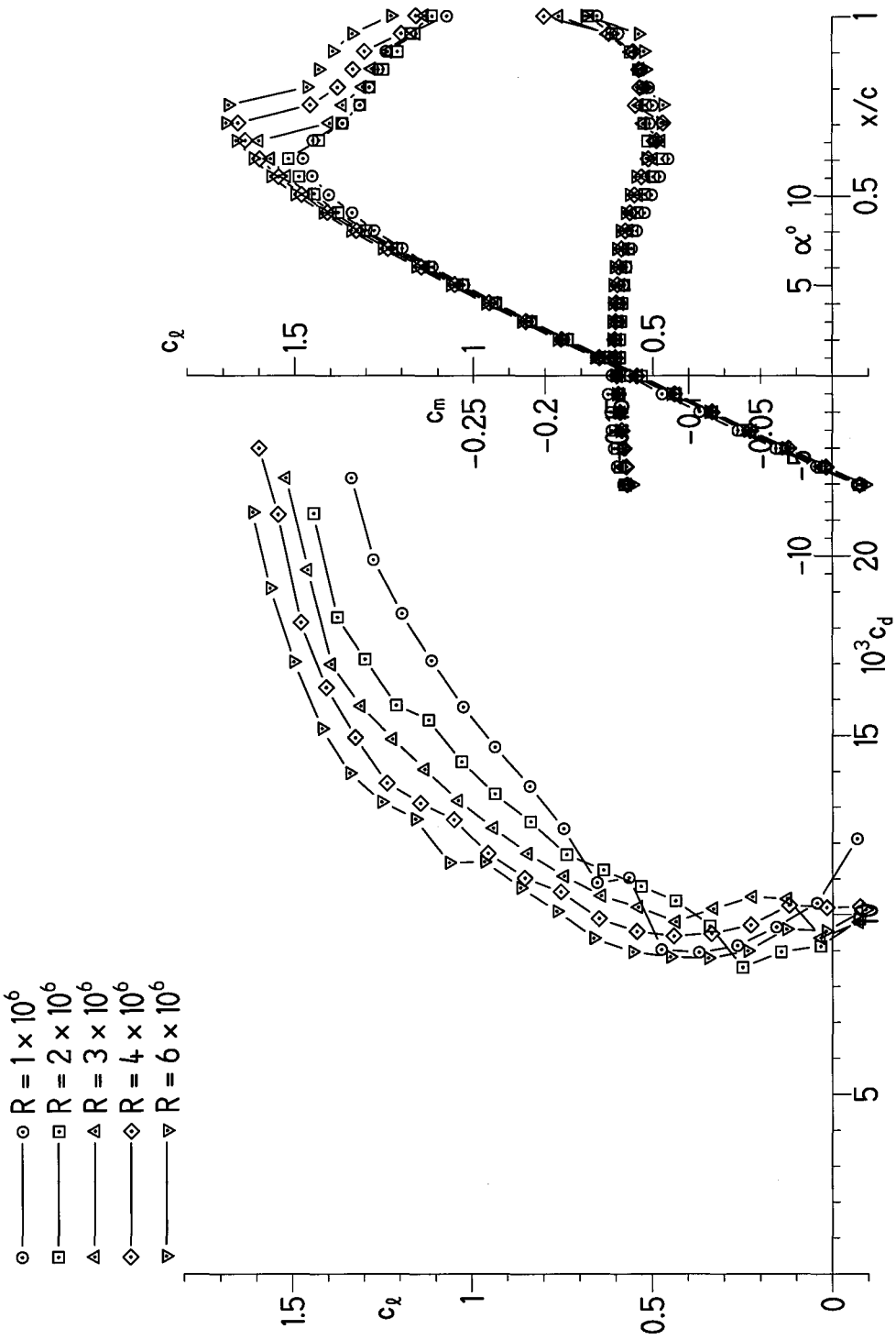

(b) Transition fixed.

Figure 7.- Continued.

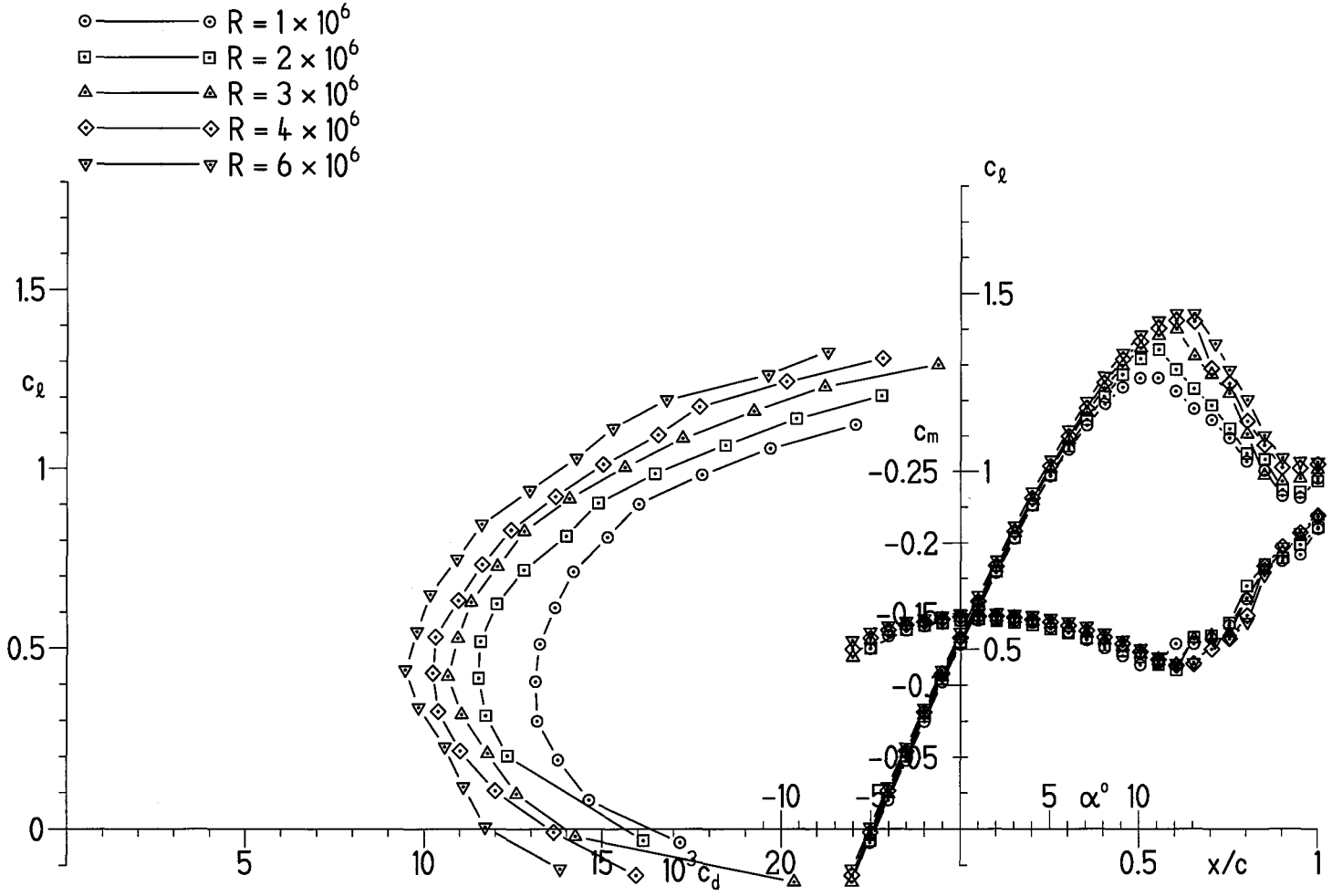

(c) Rough.

Figure 7.- Concluded.

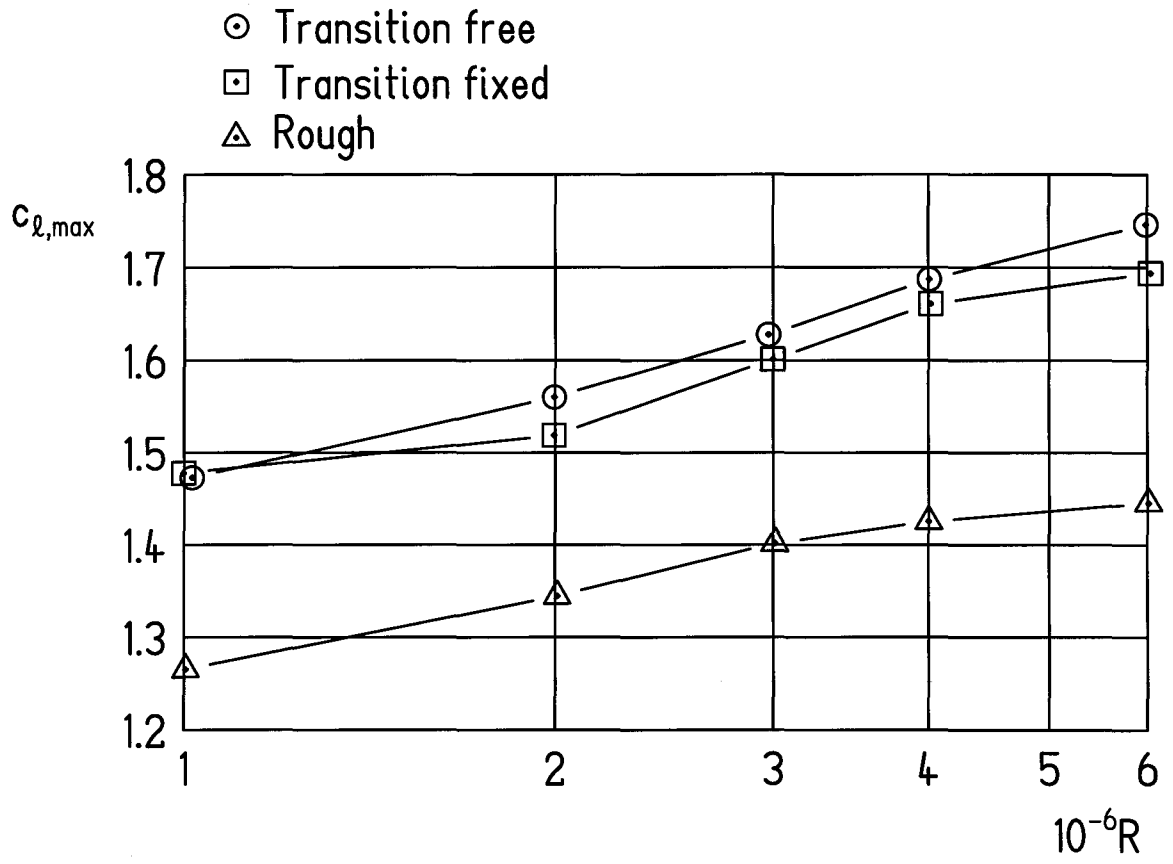

Figure 8.- Variation of maximum lift coefficient with Reynolds number.

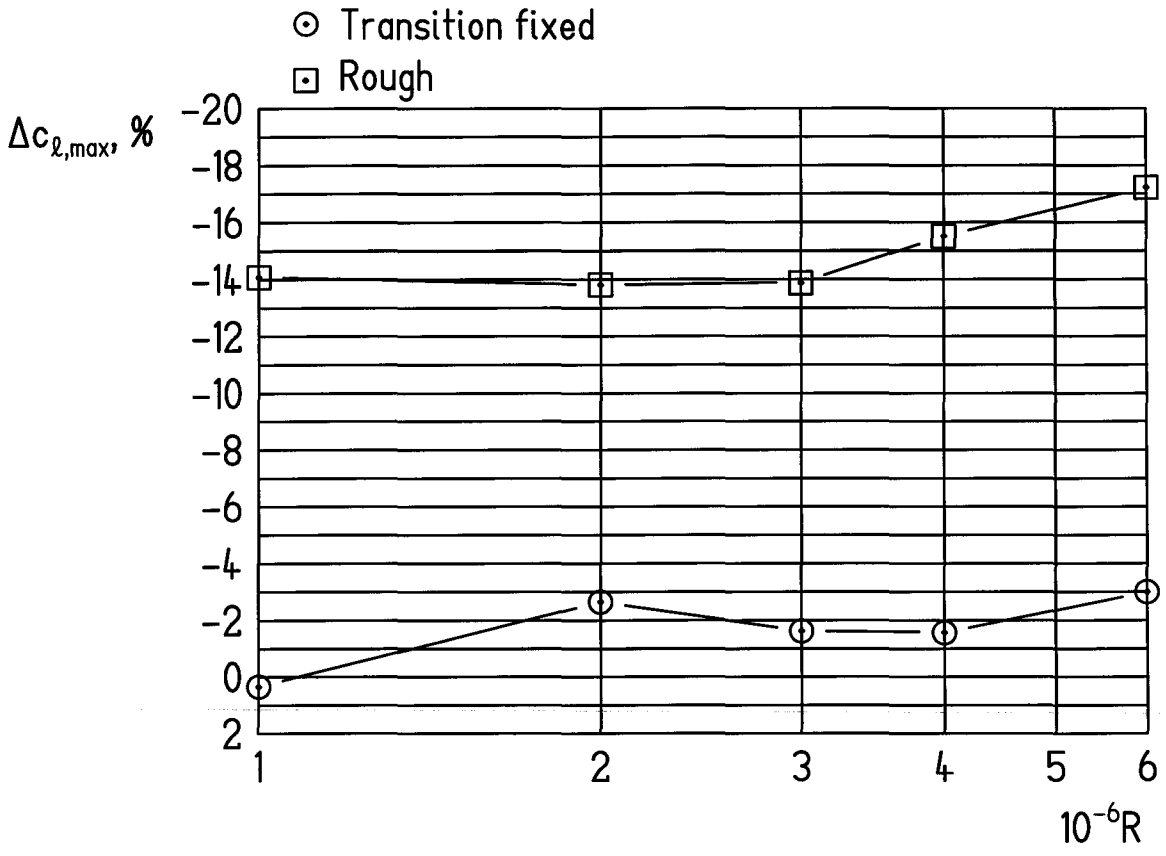

Figure 9.- Variation of change in maximum lift coefficient due to leading-edge roughness with Reynolds number.

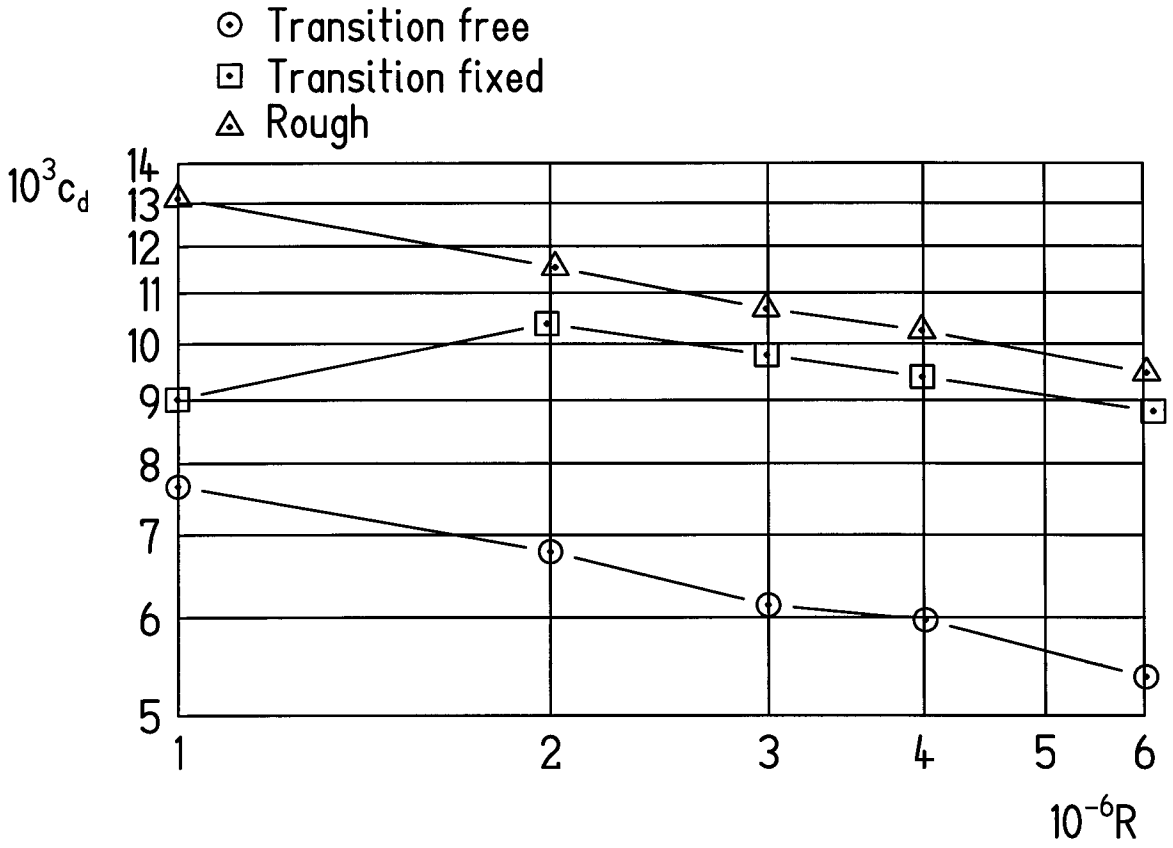

Figure 10.- Variation of profile-drag coefficient at $c_l = 0.4$ with Reynolds number.

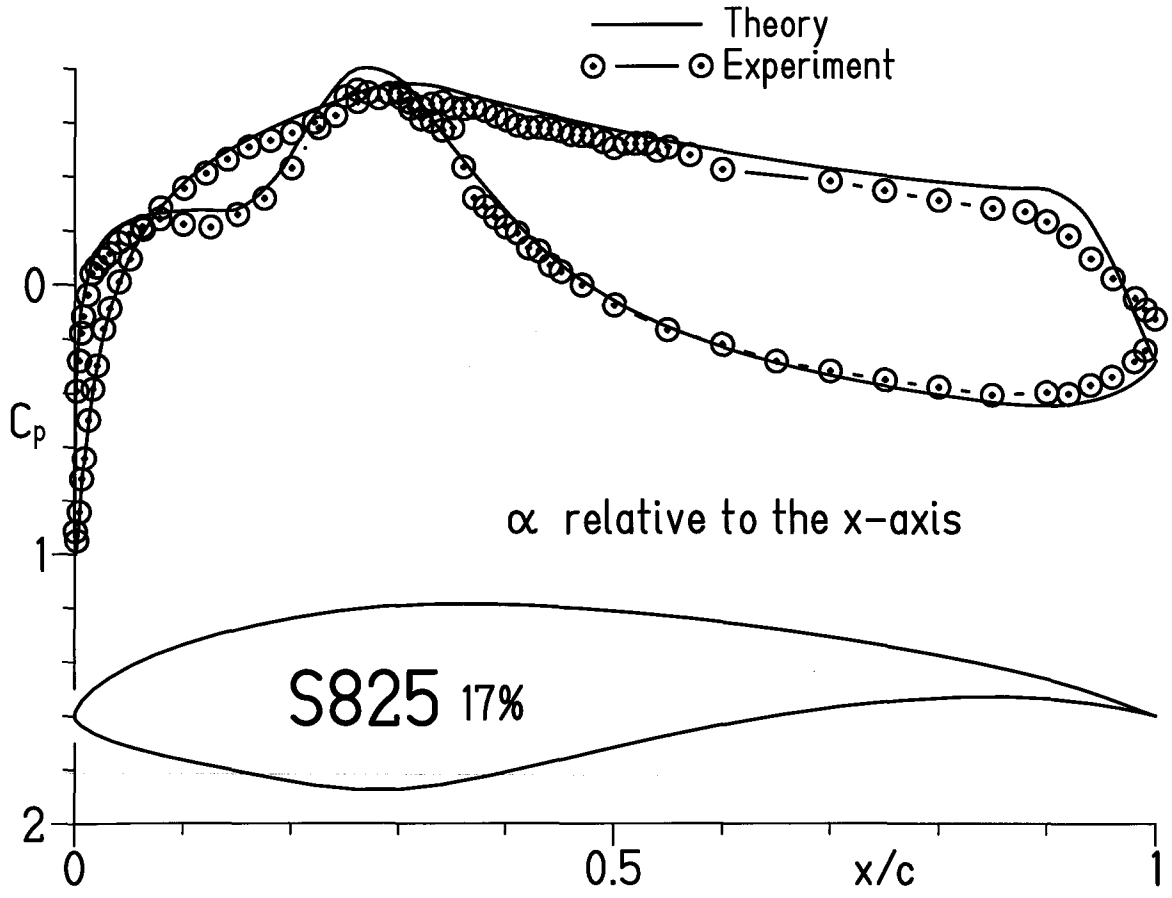

(a) $c_l = 0.38$.

Figure 11.- Comparison of theoretical and experimental pressure distributions.

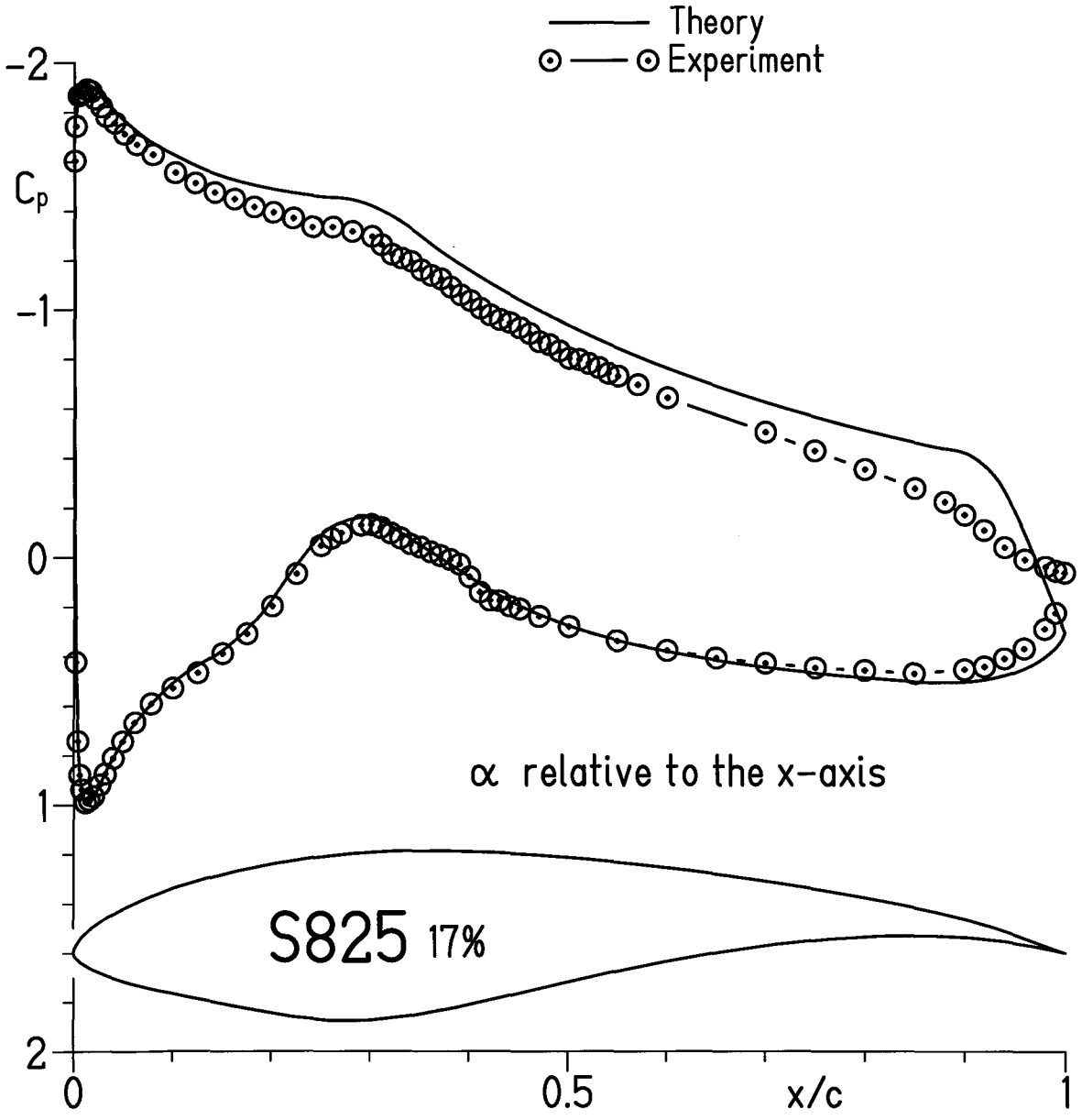

(b) $c_l = 1.17$.

Figure 11.- Continued.

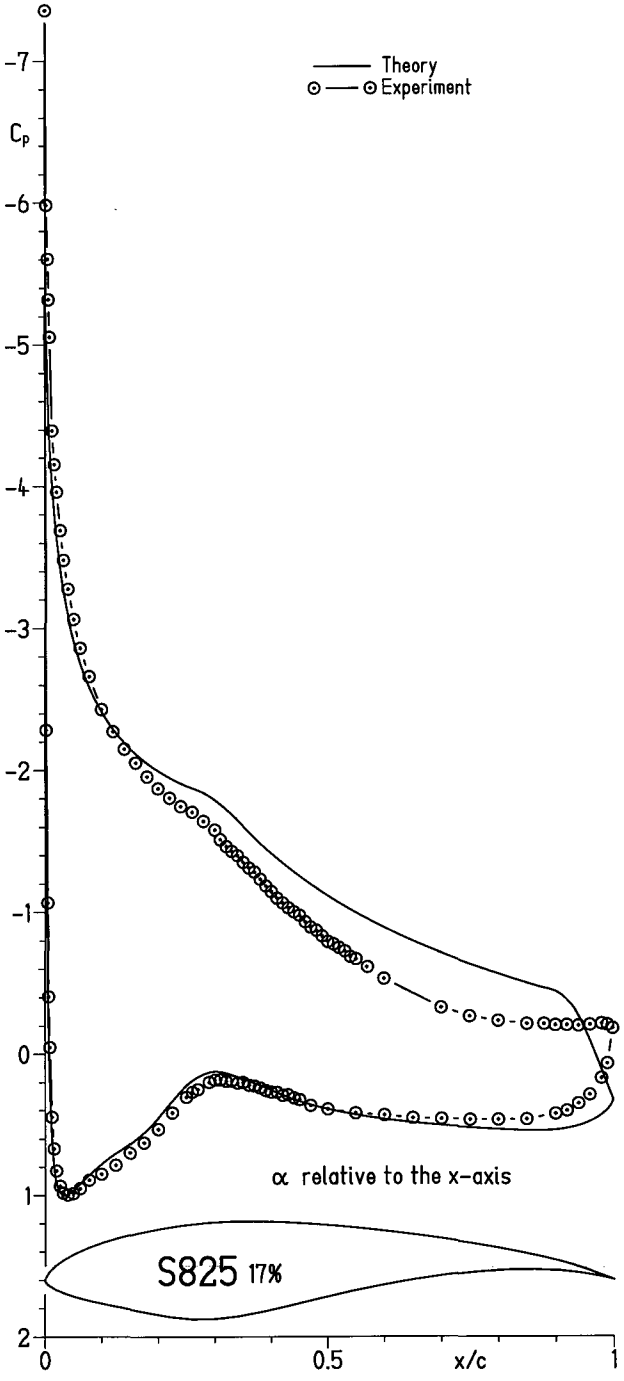

(c) $c_l = 1.56$.

Figure 11.- Concluded.

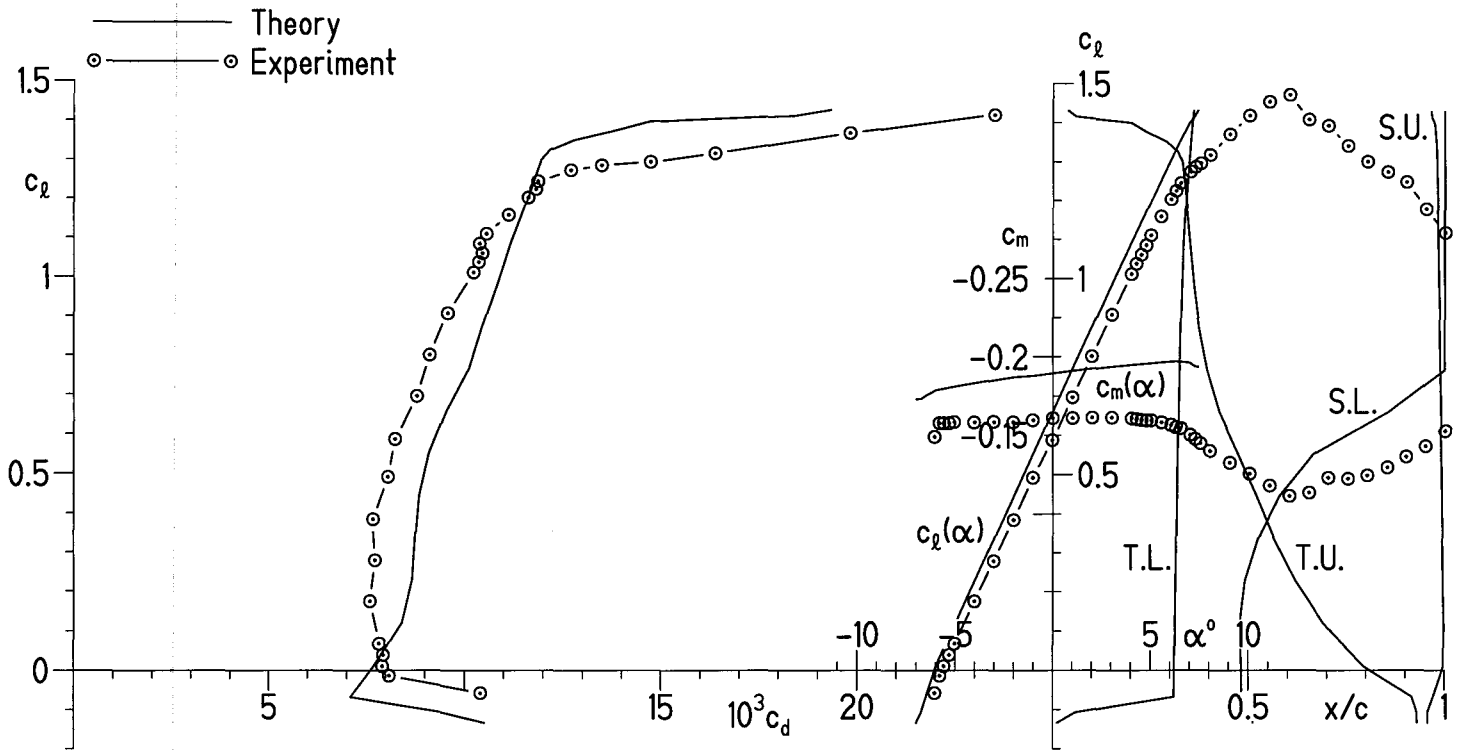

(a) $R = 1 \times 10^6$.

Figure 12.- Comparison of theoretical and experimental section characteristics with transition free.

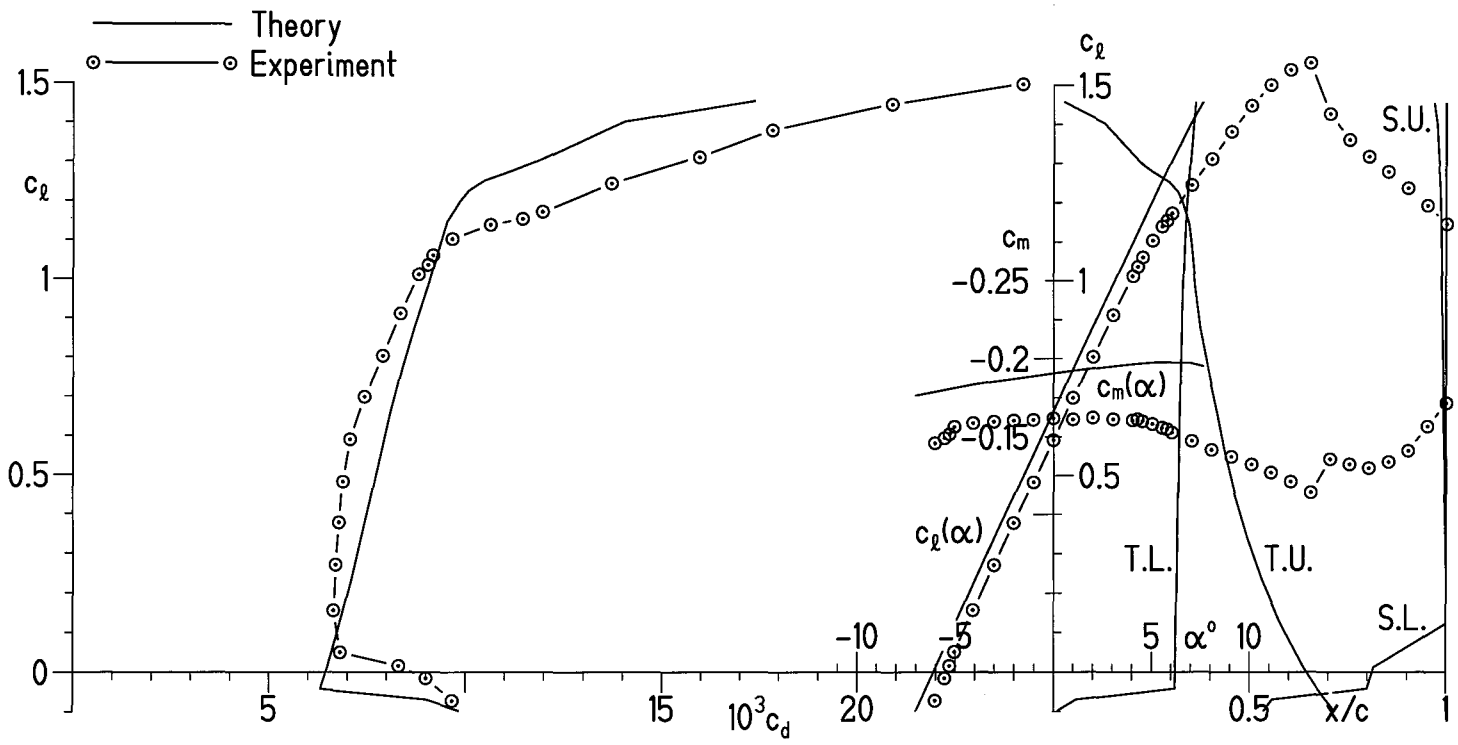

(b) $R = 2 \times 10^6$.

Figure 12.- Continued.

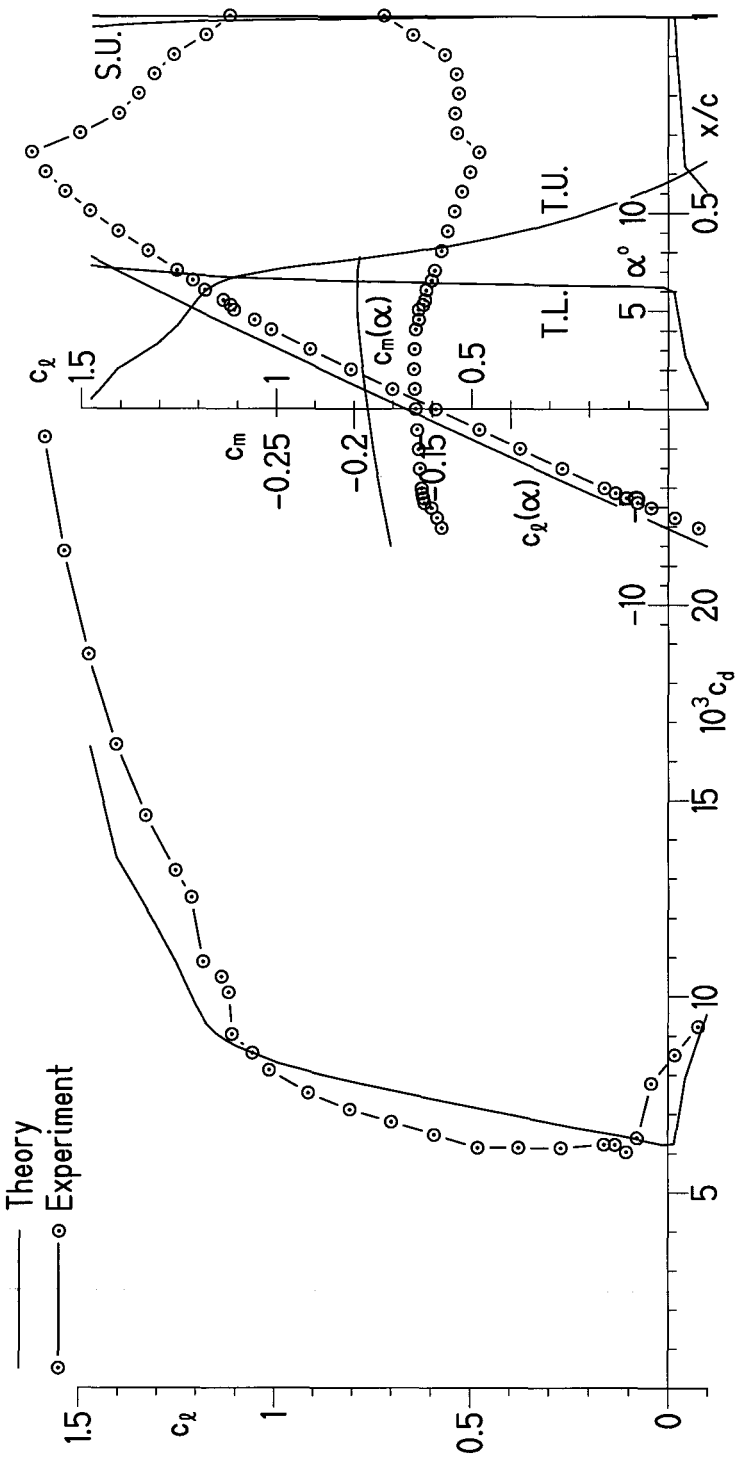

(c) R = 3×10^6.

Figure 12.- Continued.

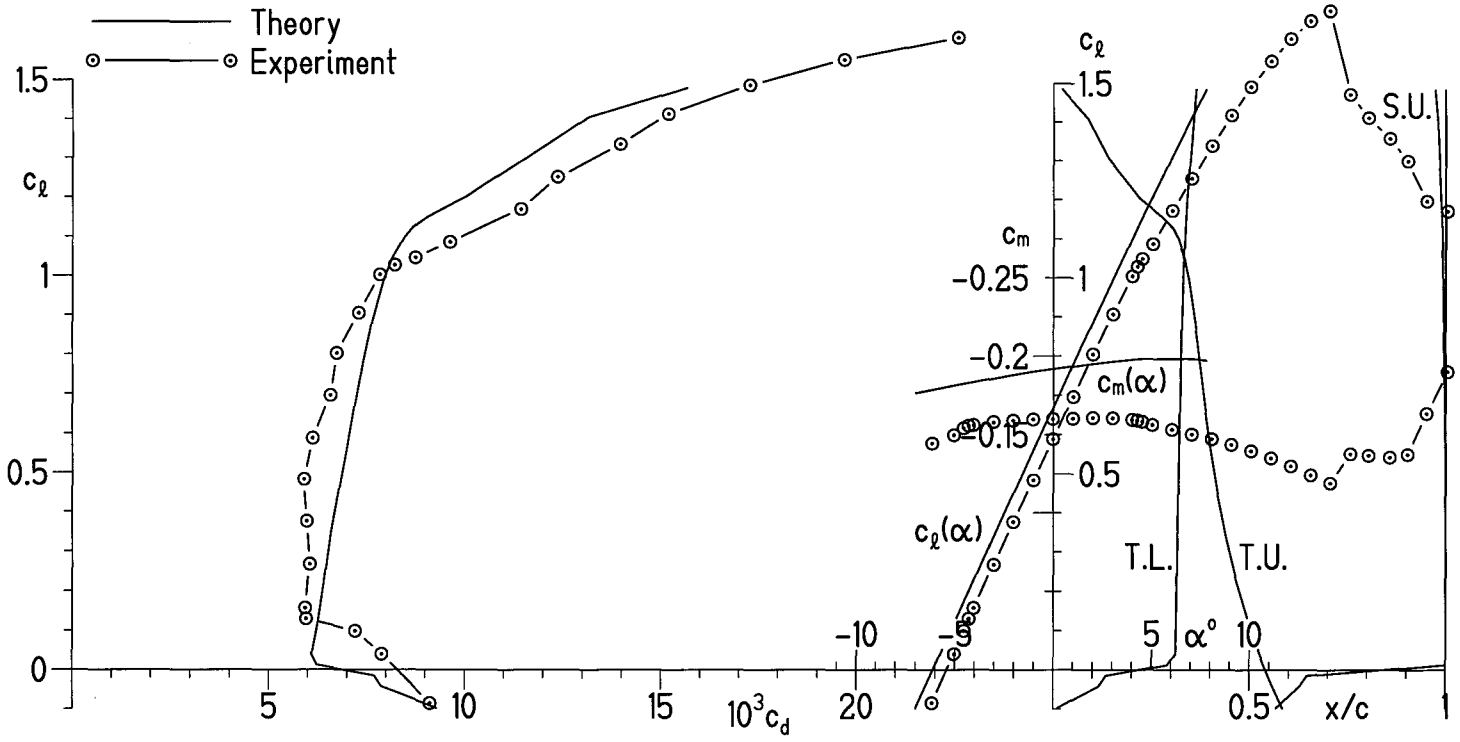

(d) $R = 4 \times 10^6$.

Figure 12.- Continued.

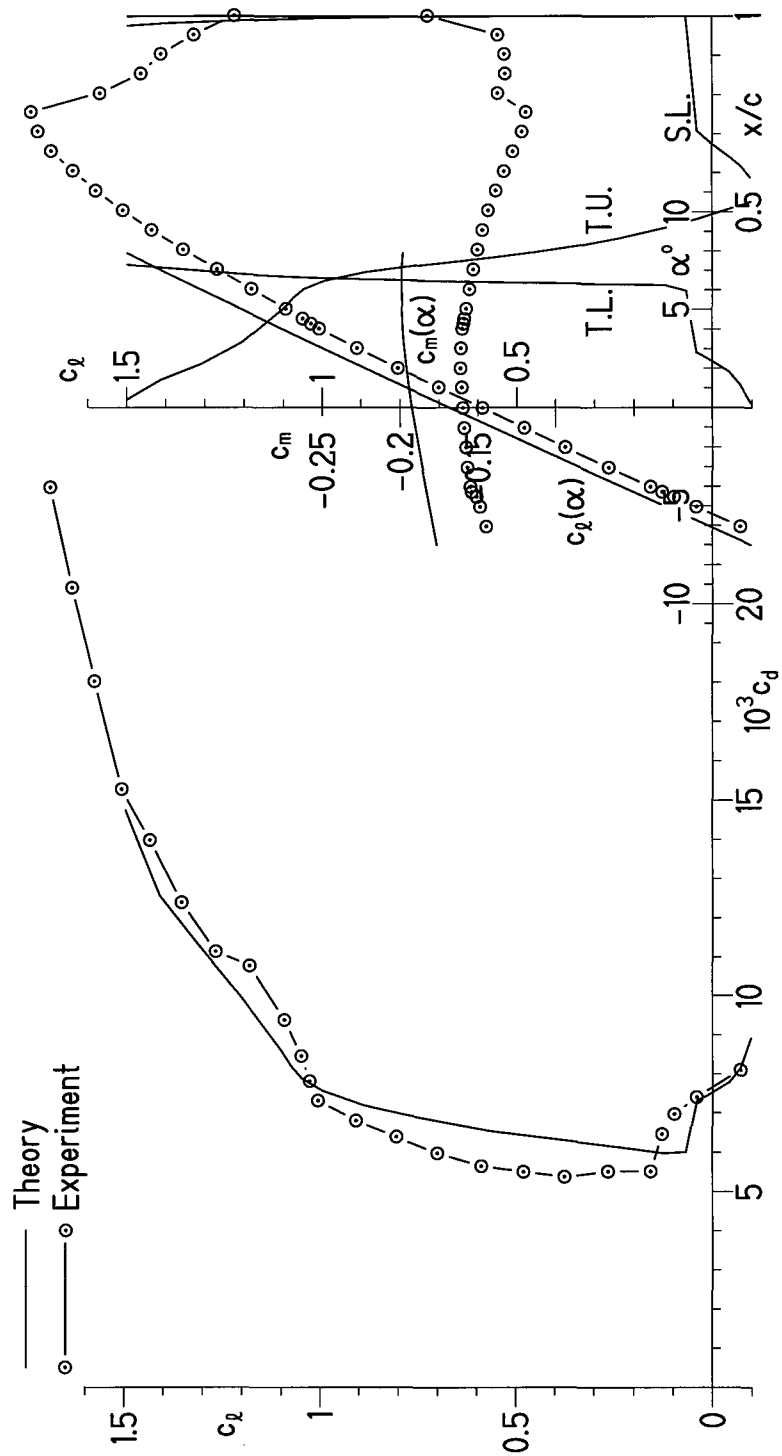

(e) $R = 6 \times 10^6$.

Figure 12.- Concluded.

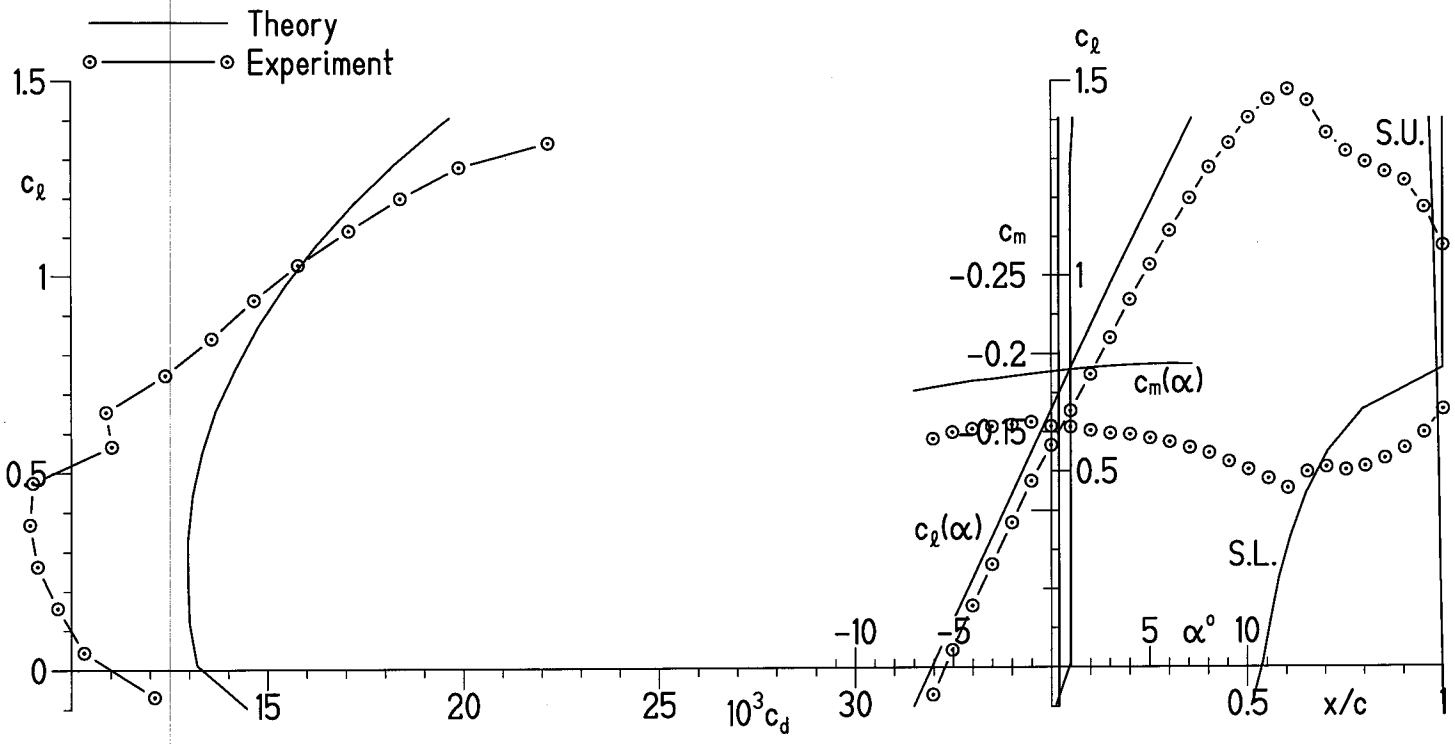

(a) $R = 1 \times 10^6$.

Figure 13.- Comparison of theoretical and experimental section characteristics with transition fixed.

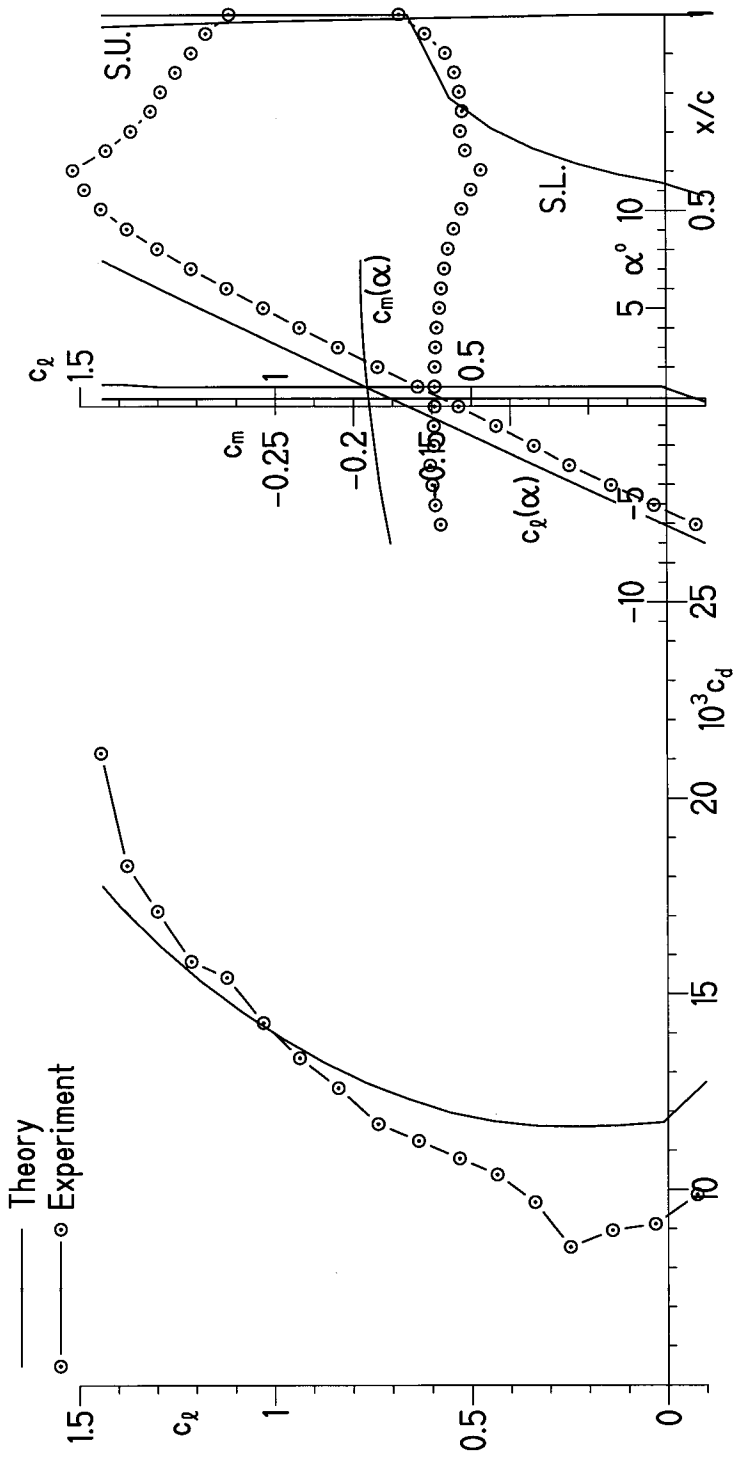

(b) $R = 2 \times 10^6$.

Figure 13.- Continued.

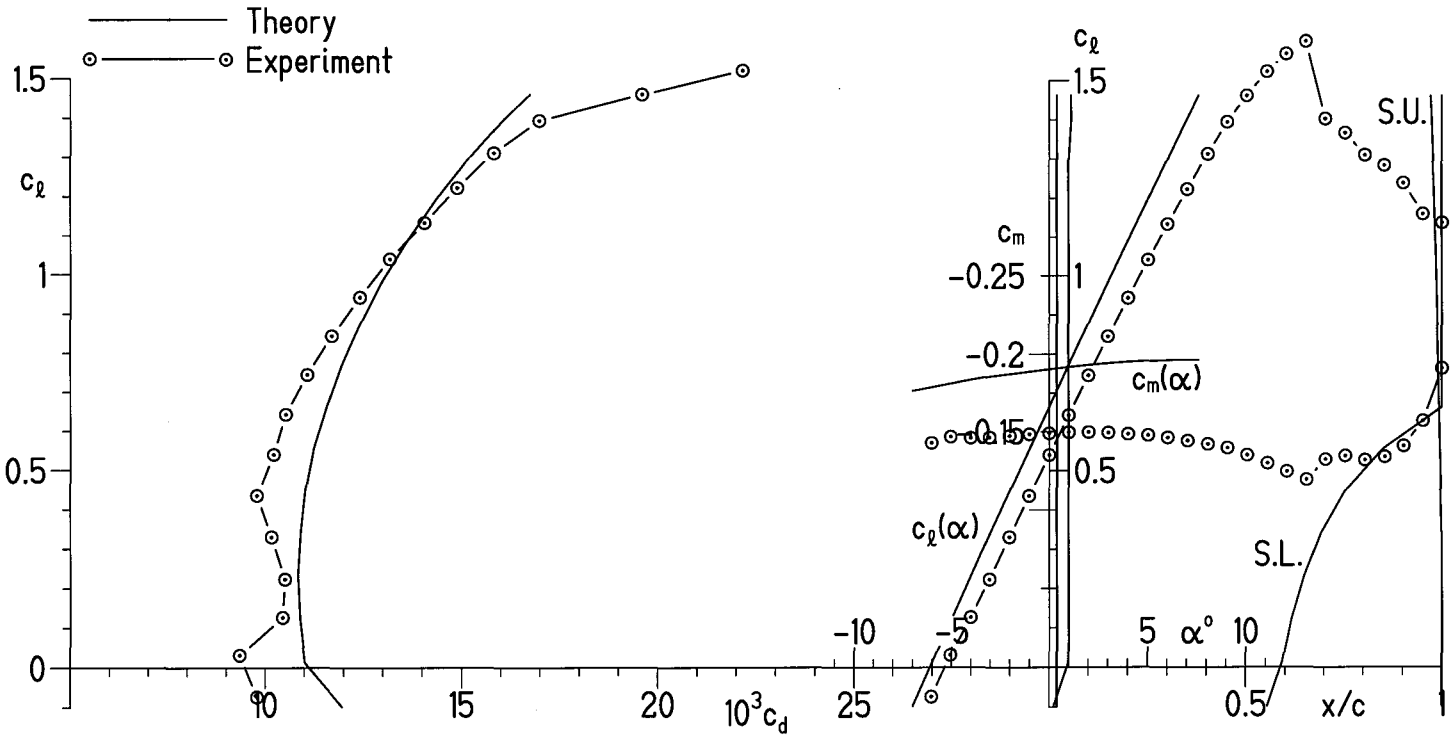

(c) $R = 3 \times 10^6$.

Figure 13.- Continued.

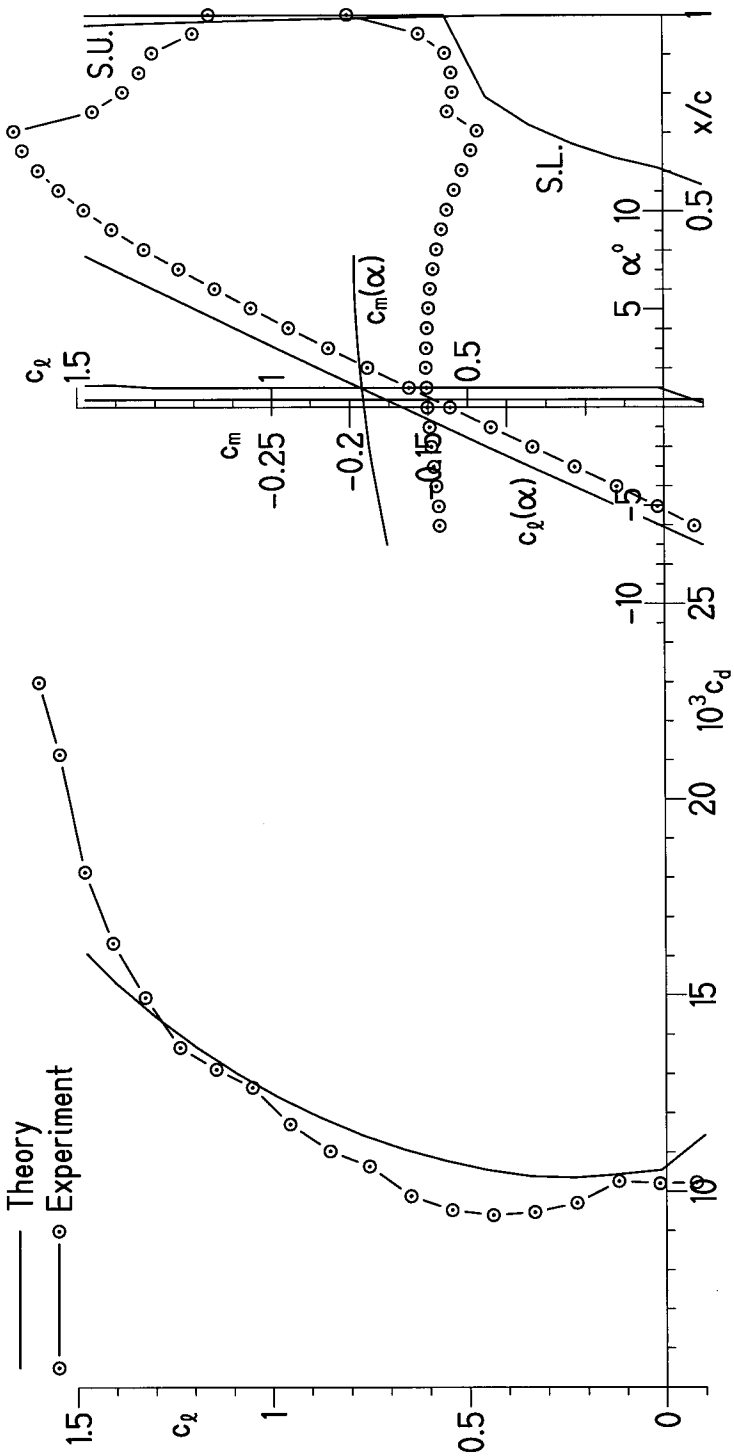

(d) $R = 4 \times 10^6$.

Figure 13.- Continued.

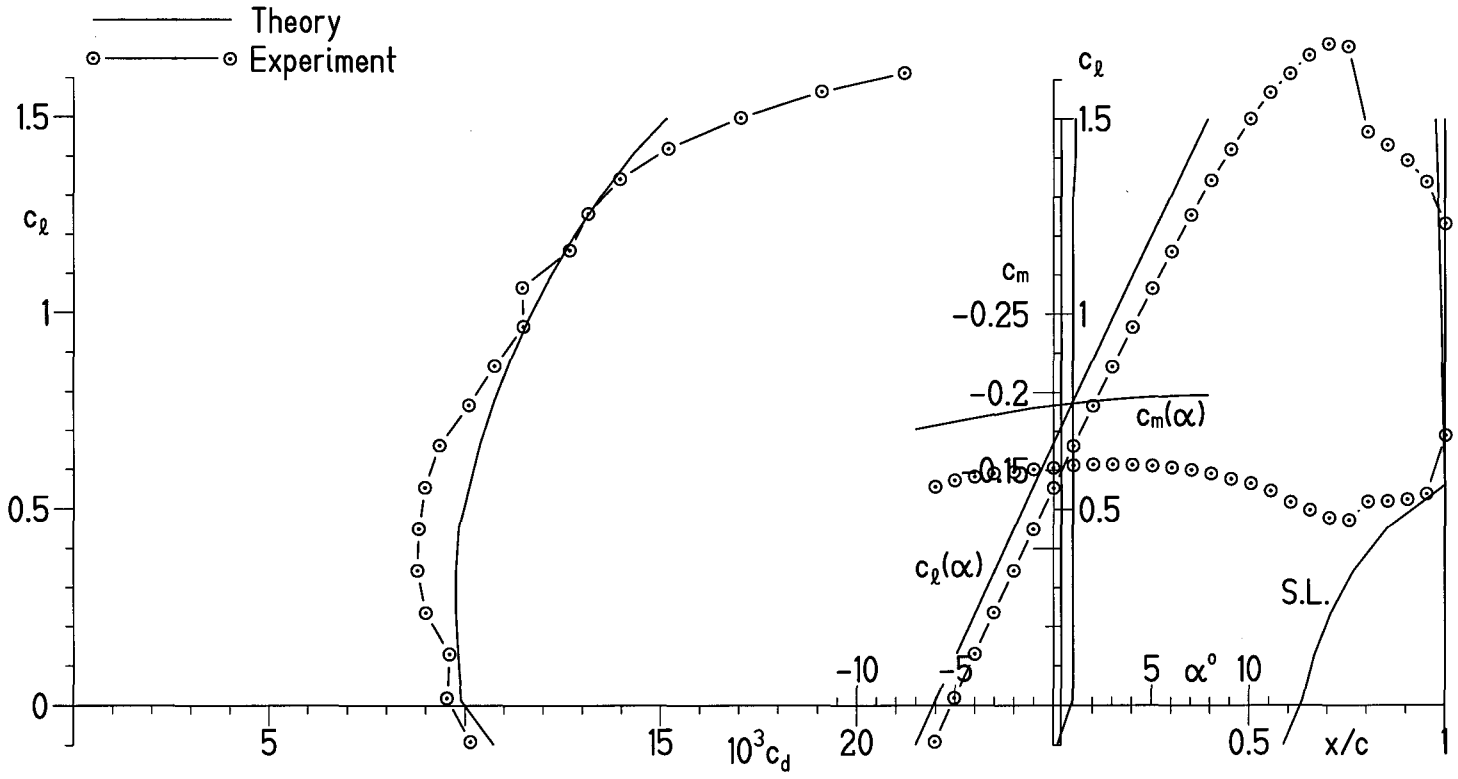

(e) $R = 6 \times 10^6$.

Figure 13.- Concluded.

REPORT DOCUMENTATION PAGE

Form Approved
OMB No. 0704-0188

PLEASE DO NOT RETURN YOUR FORM TO THE ABOVE ORGANIZATION.

1. REPORT DATE *(DD-MM-YYYY)*	2. REPORT TYPE	3. DATES COVERED *(From - To)*
January 2005	Subcontract report	1998 - 1999

4. TITLE AND SUBTITLE
Design and Experimental Results for the S825 Airfoil

5a. CONTRACT NUMBER
DE-AC36-99-GO10337

5b. GRANT NUMBER

5c. PROGRAM ELEMENT NUMBER

6. AUTHOR(S)
D.M. Somers`

5d. PROJECT NUMBER
NREL/SR-500-36346

5e. TASK NUMBER
WER4.3110

5f. WORK UNIT NUMBER

7. PERFORMING ORGANIZATION NAME(S) AND ADDRESS(ES)
Airfoils, Inc.
601 Cricklewood Drive
State College, PA 16083

8. PERFORMING ORGANIZATION REPORT NUMBER
AAF-4-14289-01

9. SPONSORING/MONITORING AGENCY NAME(S) AND ADDRESS(ES)
National Renewable Energy Laboratory
1617 Cole Blvd.
Golden, CO 80401-3393

10. SPONSOR/MONITOR'S ACRONYM(S)
NREL

11. SPONSORING/MONITORING AGENCY REPORT NUMBER
NREL/SR-500-36346

12. DISTRIBUTION AVAILABILITY STATEMENT
National Technical Information Service
U.S. Department of Commerce
5285 Port Royal Road
Springfield, VA 22161

13. SUPPLEMENTARY NOTES
NREL Technical Monitor: J. Tangler

14. ABSTRACT *(Maximum 200 Words)*

A 17% - thick, natural-laminar-flow airfoil, the S825, for the 75% blade radial station of 20- to 40-meter, variable-speed and variable-pitch (toward feather), horizontal-axis wind turbines has been designed and analyzed theoretically and verified experimentally in the NASA Langley Low-Turbulence Pressure Tunnel. The two primary objectives of high maximum lift, relatively insensitive to roughness and low-profile drag have been achieved. The airfoil exhibits a rapid, trailing-edge stall, which does not meet the design goal of a docile stall. The constraints on the pitching moment and the airfoil thickness have been satisfied. Comparisons of the theoretical and experimental results generally show good agreement.

15. SUBJECT TERMS
airfoils; wind turbine; airfoil design; Pennsylvania State University; wind energy

16. SECURITY CLASSIFICATION OF:			17. LIMITATION OF ABSTRACT	18. NUMBER OF PAGES	19a. NAME OF RESPONSIBLE PERSON
a. REPORT	b. ABSTRACT	c. THIS PAGE			19b. TELEPONE NUMBER (*Include area code*)
Unclassified	Unclassified	Unclassified	UL		

Standard Form 298 (Rev. 8/98)
Prescribed by ANSI Std. Z39.18